UNCLASSIFIED

(Title -- Unclassified)

FINAL REPORT

REFRACTORY THRUST CHAMBERS FOR SPACECRAFT ENGINES

Contract NAS 7-262

Project 342

PREPARED BY

J. G. Campbell

C. D. Coulbert

CHECKED BY

C. D. Coulbert
Project Engineer

APPROVED BY

S. J. Minton
Manager, Applied Research

UNCLASSIFIED

THE Marquardt CORPORATION
VAN NUYS, CALIFORNIA

CONTENTS

TMC A673

ILLUSTRATIONS

TMC A673

ILLUSTRATIONS (Continued)

TMC A673

ILLUSTRATIONS (Continued)

TABLES

12874

I. SUMMARY

Pyrolytic graphite and alloys of pyrolytic graphite containing hafnium and zirconium have been investigated experimentally for application to liquid propellant rocket thrust chambers and nozzles.

Although the current level of evolution of production techniques is much further advanced for unalloyed pyrolytic graphite than it is for the alloys studied under this program, the application of both unalloyed and alloyed pyrolytic graphite to free standing thrust chamber design awaits further needed improvement in quality and quality control of these materials.

A study of the maximum structural capability of free standing pyrolytic graphite was conducted using 2-inch diameter thin walled tubes purchased from three different pyrolytic graphite vendors. The effects on tube rupture pressure of heat treatment, microstructure, crystal lattice spacing, surface finish, and maximum nodule size were evaluated. A definite correlation between maximum nodule size and rupture strength was found. Free standing pyrolytic graphite tubes with maximum nodule diameters less than 0.030 inch demonstrated strengths greater than any values previously achieved in this geometry with rupture pressures near 1000 psia.

The fabrication and performance of pyrolytic graphite-hafnium and pyrolytic graphite-zirconium alloys were studied by the Raytheon Company and by Marquardt.

Difficulties in controlling the alloy compositions during deposition were partially overcome, but this control was achieved too late in the program to permit an adequate evaluation of all of the important properties of these alloys.

In motor test firings with gaseous O_2/H_2 propellants, much less erosion was observed with an edge oriented nozzle made with washer shaped sections of pyrolytic graphite-zirconium alloy than with an unalloyed pyrolytic graphite nozzle. The oxidation protection of the zirconium alloy was due to formation of a surface coating of ZrO_2 in the oxidizing environment.

A motor test firing with a free standing hafnium alloy thrust chamber indicated that the oxidation protection afforded by the alloys is probably more effective in the edge oriented designs than in the free standing chamber designs.

Results of this study have yielded several criteria which are recommended for inclusion in specifications for high strength, free standing pyrolytic graphite components.

Author

TMC A673

II. INTRODUCTION

Pyrolytic graphite has found increasing application in rocket thrust chamber designs as its remarkable high temperature strength and resistance to chemical attack have been demonstrated in both liquid and solid propellant motors.

Most of the current applications use pyrolytic graphite in composite designs, especially the edge oriented design, constructed by machining the chamber contour in stacked flat plates.

Another way of using pyrolytic graphite (PG) in thrust chamber construction is as a free standing thin wall shell. Free standing shapes are formed by separation of the PG from the mandrel on which it is deposited through vapor deposition.

Very lightweight thrust chambers using the free standing structure are potentially feasible. Early work at Marquardt, JPL, and elsewhere had shown that free standing PG was marginal in strength and oxidation resistance for liquid rockets using 5000°F class propellants such as the N_2O_4/Hydrazines.

This report describes the work which has been done during a 9-month study of methods of improving both the strength and the oxidation resistance of PG. This work is a continuation of previous studies (Reference 1) which indicated that both the strength and the oxidation resistance might be increased by alloys of PG containing zirconium or hafnium. About a four-fold increase in flexure strength had been achieved with a zirconium alloy, and the oxidation resistance was also much greater, in arc-plasma tests, than that of unalloyed PG due to the formation of the refractory ZrO_2 in an oxidizing environment. Similar behavior was expected of hafnium alloys. Therefore, a subcontract was awarded to Raytheon so that they could continue their previous work on the development of zirconium and hafnium alloys of PG.

The work to be performed by Raytheon included the further study of deposition parameters for the zirconium and hafnium alloys, measurement of thermal and mechanical properties of various alloy compositions, fabrication of free standing tubes for laboratory experimentation, and delivery of six nozzles to Marquardt for rocket test firing. Two of the nozzles were to be edge oriented, and four were to be free standing.

Raytheon was also to deliver samples of various alloy compositions to Marquardt for oxidation testing.

Another avenue of PG strengthening was thought to be heat treating of cylindrical tubes. Therefore, PG tubes were purchased by Marquardt from three vendors to study both the effect of heat treatment and the differences between the PG samples made by different vendors.

Significant improvement was found in the strengths of some of the PG tubes relative to those tested in the previous program (Reference 1). Accordingly, an intensive study was made of the microstructure of the tubes.

The lattice spacing was measured by X-ray diffraction, the residual stresses were measured by strain gage isolation, and the rupture pressure of the tubes under internal pressurization was correlated with nodule size in the PG.

The results of the study of free standing tubes were also correlated with vendor's information regarding the process parameters used in deposition. The surface finishes of sample mandrels were studied for some correlation with PG microstructure and strength.

Rocket test firings of PG and PG alloy nozzles were performed at Marquardt using gaseous O_2/H_2 propellants at a chamber pressure of 100 psia. An item of particular interest in these tests was the demonstration of reduced nozzle erosion for the PG alloys containing hafnium and zirconium.

Finally, the results of the current program were formulated as contributions to a specification for high quality, free standing pyrolytic graphite.

III. STUDIES OF PYROLYTIC GRAPHITE

A. Pyrolytic Graphite Tubes

Forty-six pyrolytic graphite tubes were purchased from three vendors for use in studies of the effect of heat treatment on rupture strength. As the studies progressed, it became evident that the most significant factor in the rupture strength of the tubes was the nodule size and microstructure, evidently caused by variations in mandrel surface finish. Some of the tubes showed rupture strengths about three times greater than those previously found for PG tubes.

1. Description of Tubes

The PG tubes were ordered under specifications which required that the vendor use identical deposition conditions and mandrels for all tube production runs. The deposition temperature was specified as 4000°F. Since there is no agreement as to the optimum deposition conditions (such as pressure, flow rate, and source gas composition), all deposition conditions other than temperature were to be those chosen by the vendor to produce high quality pyrolytic graphite. Therefore although it was known that the deposition conditions would probably vary from vendor to vendor, it was hoped that the tubes produced by each vendor would be of uniform quality.

All tubes delivered by three different vendors had a substrate nucleated microstructure. Recently published data (Reference 2) show about the same room temperature tensile strenght (18,000 psi) for both substrate nucleated and continuously nucleated PG in tensile tests of flat specimens.

Each tube was 4 inches long and each could be cut from longer tubes after discarding the first one inch on each end of the longer tube. The inside diameter was to be 2.0 inches. Tubes were ordered according to two different specifications relative to post-deposition machining, as follows:

a. Machined Tubes

The tube wall thickness was to be 0.060 +0.000, -0.005 inch after machining. The tubes were to be machined on the mandrel side to a depth of 0.003 to 0.005 inch.

b. Unmachined Tubes

The tube wall thickness was to be 0.060 +0.006, -0.006 inch, as deposited with no machining after separation from the mandrel.

Four lots of PG tubes were purchased as shown in Table I. This table also lists the twenty-six tubes (Lot 1) from the previous study (reported in Reference 1).

2. Effective Tensile Strength

The tensile strengths in the a-direction of the flat PG specimens average about 18,000 psi (Reference 2) at room temperature. However, as noted in Reference 1, the effective tensile strength in the a-direction of free standing tubes has usually not exceeded about 8000 psi in the past. The effective tensile strength of tubes or axisymmetric shapes is defined as the total of the residual stress in circumferential direction and the pressure (hoop) stress in the circumferential direction at rupture under internal pressurization.

a. Residual Stress Measurements

Residual stresses were measured by strain gage isolation and the results are listed in Table II. The strain gages were located on the inside and outside and 0.5 inch from one end of each tube.

The circumferential residual stresses in pyrolytic graphite tubes are generally tensile on the inside surface and compressive on the outside surface, and this condition existed in all of the tubes which were tested, although the average residual stress of about 2000 psi was somewhat less than the 3800 psi measured in previous work (Reference 1).

Strain gage isolation consists of installing a biaxial strain gage on the PG tube before rupture and then cutting away the portion of PG around the tube so that the constraint provided by the tube structure is removed. One axis of the strain gage is aligned parallel to the axial direction (z) and the other gage axis is aligned parallel to the circumferential direction (θ).

Stress-strain equations for the surfaces of the tube can be written as follows:

$$\epsilon_{\theta\theta} = s_{11}\,\sigma_{\theta\theta} + s_{12}\,\sigma_{zz} \qquad (1)$$

$$\epsilon_{zz} = s_{12}\,\sigma_{\theta\theta} + s_{11}\,\sigma_{zz} \qquad (2)$$

Where

$\epsilon_{\theta\theta}$ = Circumferential strain

ϵ_{zz} = Axial strain

$\sigma_{\theta\theta}$ = Circumferential stress

σ_{zz} = Axial stress

TMC A673

$s_{11} = 1/E_1$

$s_{12} = -\nu_{12}/E_1$

E_1 = Modulus of elasticity in circumferential direction (i.e., a-direction in PG)

ν_{12} = Poisson's ratio in θ - z plane (i.e., a-b plane in PG)

Equations (1) and (2) can be combined to give another form of the stress-strain equations, as follows:

$$\sigma_{\theta\theta} = \frac{E_1}{1 - \nu_{12}^2}\left[\epsilon_{\theta\theta} + \nu_{12}\ \epsilon_{zz}\right] \qquad (3)$$

$$\sigma_{zz} = \frac{E_1}{1 - \nu_{12}^2}\left[\epsilon_{zz} + \nu_{12}\ \epsilon_{\theta\theta}\right] \qquad (4)$$

The changes in strain due to relief of residual stresses are substituted into Equations (3) and (4) to calculate the residual stresses.

If the residual stresses have a linear gradient across the wall, they in effect provide a bending moment which is completely relieved when the self-restraint of the cylindrical tube is removed. Therefore, strain gage isolation should give an accurate measurement of residual stresses if their distribution across the thickness is approximately linear. A linear gradient of residual stresses is predicted theoretically in PG, and is sometimes approximated in practice (Reference 3). The stresses are generally of the same magnitude, but opposite in sign, on opposite surfaces of a tube. However, different stress magnitudes can also occur, as is shown in Table II.

If the residual stresses are not linear, the strain gage isolation technique will not be exact. As an extreme example, assume a residual stress distribution, after cylindrical restraint is removed, which is tensile at both surfaces but compressive in the center. It would be impossible for any bending of the PG to relieve these residual stresses. If, however, the PG were split in two, the gages on either side would then record an additional strain, and an even better idea of the residual stresses at each surface could be obtained by grinding the PG under the gage thinner and thinner, until finally all restraints on the surface element of PG were removed.

The strain gages on PG Tubes H13 and S19 (See Table II) were used for experimentation to determine whether or not a reduction in the PG wall thickness might relieve further residual stresses. Negligible changes in strain were recorded, indicating that the original residual stress distributions in these PG tubes were approximately linear, and the residual stresses were almost completely relieved by strain gage isolation. Similar experiments at Raytheon (See Section IV below) with carbide-PG alloys showed that reduction of the wall thickness under isolated gages produced very large changes in strain, indicating that unusual residual stress distributions were present. This is consistent with the fact that these carbide-PG alloys had large variations in alloy composition, and hence elastic properties, across the wall.

b. Elastic Constants Measurements

Five PG tubes were instrumented with biaxial strain gages on their outside surfaces for measurement of strain during rupture tests. The tubes were pressurized in a test fixture so that no axial stresses were applied to the tubes (See Figure 1). The ratio between the circumferential pressure stress and the circumferential strain on the outside surface was used to calculate the modulus of elasticity in the a-direction. Values of the elastic modulus were between 3.8×10^6 and 4.9×10^6 psi, as shown in Table III. These values are consistent with the published data for flat PG specimens.

The ratio between the axial strain and the circumferential strain was used to calculate Poisson's ratio in the a-b plane, with results (See Table III) between -0.19 and -0.24. These values are about the same as those reported for PG in the literature. Strain measurements were made at 0.5 inch from one end and at the center of the tube, and very little difference in readings was observed.

Residual stresses on the outside surface were also determined for Tubes H9 and 1S on which the strain gages were not damaged by rupture. The results are listed in Table II.

c. Rupture Strength

Thirty-five PG tubes were ruptured during the study reported herein. The rupture pressure, the circumferential pressure stress, the residual stress on the inside surface, and the effective tensile strength are tabulated in Table IV. The residual stresses for each lot were based on the averages from the residual stress measurements given in Table II.

The rupture pressures and effective tensile strengths of the tubes are much higher than the corresponding values measured in the Lot 1 tubes during the previous work (Reference 1). This comparison is shown in the following tabulation of the average rupture pressure and average tensile strength for all tubes of each of the lots.

Lot No.	Average Rupture Pressure (psig)	Average Tensile Strength (psi)
1	183	6,640
2	295	7,350
3	547	10,780
4	510	11,870

d. Polished Ends

Metallurgical polishing (prior to rupture) was done on both ends of Tubes S17, S9, S1, and S2 of Lot 3, and Tubes 5S and 13S of Lot 4. No improvement in average rupture strength was noted.

3. Microstructure

The large differences in rupture strength of different PG tubes (See Table IV) prompted a study of the microstructure of the tubes. Enlarged (10X) photographs of the inside and outside surfaces and photomicrographs (50X) of the cross section (c-plane) were taken under polarized light.

The PG was found to contain a matrix of fairly small and uniformly sized grains. The matrix grains were often arranged in a pattern of rows, traceable to the machining marks on the mandrel.

Superimposed on the matrix was a random distribution of nodules which were often adjacent to the fracture line. A nodule is defined as an abnormally large grain. The relationship between rupture pressure and the size of the largest nodule on the tube is shown in Figures 2 and 3. Although the absence of large nodules does not guarantee high strength, the presence of large nodules almost certainly precludes a very high strength tube.

The various characteristics of the structure of the PG tubes in each of the lots is discussed below:

a. Lot 1

The Lot 1 tubes were studied previously (Reference 1) and they were found to have a very low average rupture pressure of 183 psig. The mandrels were made from ATJ graphite and they evidently were finished by a rather

heavy lathe cut which left circumferential striations. The mandrel surface finish is evident in the 10X photographs of the outer and inner surfaces of Tube 23 shown in Figure 4. Tube 23 was very weak, rupturing at 70 psig. The width of the striations is about 0.015 inch and this also corresponds to the spacing and size of the matrix grains as shown on the ID surface in Figure 4. Also shown on the ID surface are the randomly distributed nodules of larger sizes.

Although the size of the matrix grains is closely linked with the machine cut spacing, the causes of the random nodules are not known. Possibilities include anomalous size pores, fragments of some contaminant in the ATJ, or large soot particles. The 50X cross section shows some large nodules possibly originating in the interior of the PG rather than on the mandrel surface.

Also shown on the ID surfaces of the Lot 1 tubes are very closely spaced circumferential (horizontal in the photographs) marks which are probably due to post-deposition machining.

b. Lot 2

The Lot 2 tubes were stronger than the Lot 1 tubes, the average rupture pressure being 295 psig.

Circumferential striations visible on the ID and OD surfaces of the Lot 2 tubes are exemplified by Tube H5, shown in Figure 5. Again it is believed that the striations are due to tool marks on the mandrel. The OD striations include both the mandrel machining and the postdeposition machining of the tube. Although the striations on the Lot 1 tubes appear to be wider, the ID surfaces of both the Lot 1 and Lot 2 tubes show the same size and circumferential alignment of the matrix grains. However, the larger random nodules, superimposed on the matrix, are smaller for Lot 2 (Figure 5) than for Lot 1 (Figure 4).

The only feature of the structure which could be well correlated with rupture strength was the size of the largest nodules. Figure 6 shows the ID surface of Tube H11 which ruptured at 110 psig. The 10X photograph shows that the matrix grains were about the same size as those of the stronger Tube H5 (rupture pressure = 420 psig). However, the 2X photograph in Figure 6 shows a large nodule adjacent to the fracture line. Almost half of the tubes which failed at below average pressure showed a similar situation.

c. Lot 3

Both the Lot 3 and Lot 4 PG tubes were produced by the Super-Temp Corporation and they had about the same average tensile strength, near 11,000 psia. However, the two lots were produced in different furnaces and used different finish operations on the ATJ graphite mandrels.

The appearance of the OD and ID surfaces of the Lot 3 tubes is shown by Tube S11 in Figure 7. Again, a circumferential striation is evident on the OD surface, evidently with closer spacing than on the Lot 1 and Lot 2 tubes, since the size of the matrix grains is smaller. The Lot 3 tubes were not machined after deposition, so their OD surfaces should be a good indication of the mandrel surface finishes. However, anomalous random nodules are also present, and again are frequently linked with fracture, as shown in the 2X photograph of the ID surface of Tube S11 (Figure 7).

The strongest Lot 3 tube was S14 which had a rupture pressure of 1020 psig. The matrix grain size (Figure 8) was indistinguishable from that of the weaker Tube S11, but the nodules were smaller and less numerous.

d. Lot 4

The mandrels used for the Lot 4 tubes were finished by polishing them with steel wool. Therefore the circumferential patterns visible on the tubes in the other lots were absent. In addition, a greater spread existed in the size of the matrix grains, which were randomly arranged. The rupture strengths seemed to be dependent on the maximum size of the nodules, as shown in Figure 3.

Figure 9 shows the structure of Tube 1S, which ruptured at 210 psig, despite having a fine sized matrix. However, the maximum nodule diameter was 0.050 inch.

In comparison Tube 3S (Figure 10) had a larger sized matrix but the maximum nodule diameter was only 0.030 inch. Tube 3S ruptured at 810 psig.

4. Surface Finish of Mandrels and Tubes

After study of the correlations between the strengths and structures of the PG tubes, the Super-Temp Corporation and High Temperature Materials, Inc. were requested to supply a sample mandrel made by the same techniques used in filling the orders for Lots 2, 3, and 4.

It was established that different techniques had been used in finishing the deposition surface of the mandrels. The mandrels for Lot 3 had been finished by the Super-Temp Corporation by circumferential machining on a lathe with a machine tool whereas the mandrels for Lot 4 had been polished with steel wool after machining.

The mandrels used for Lot 2 had been finish machined by circumferential machining on a lathe by High Temperature Materials, Inc. (HTM).

The surface finishes of the sample mandrels were measured by a profilometer and the results are given in Table V. There is no apparent correlation with tube strength since Lots 3 and 4, with about the same strength, were made from mandrels of much different rms roughness values. Furthermore, the HTM mandrel, which was representative of those used for Lot 2, had about the same roughness as the sample mandrel for the stronger Lot 3.

The surface roughness was also measured on two unmachined portions of PG tubes and the results are given in Table VI.

Tube 25 from the very weak Lot 1 had a rough ID surface with an rms value of as much as 300 for a 0.100-inch cutoff. The larger cutoff is necessary to record widely spaced surface marks such as those due to the circumferential striations.

Tube S8 from the strong Lot 3 had a lower rms value of about 100. This might indicate that the mandrels used for Lot 1 were very rough, although they were not available for measurement. On the other hand, the Lot 4 tubes had a high average strength despite mandrel surface rms values of 240 to 280.

It is concluded that measurement of the mandrel surface by a profilometer did not yield a worthwhile correlation with rupture strength of PG tubes.

5. Heat Treatment

Pyrolytic graphite tubes from Lot 1 were heat treated in an earlier study (Reference 1) with an apparent strengthening for several heat treatments. The results were not conclusive, because the Lot 1 tubes had such a low average strength. Additional heat treating was done with tubes from Lots 2, 3, and 4 to determine if it would be beneficial for stronger tubes. Early in the present work, however, some of the as-deposited tubes did not rupture until a pressure of about 500 psig had been reached. Since even the strongest heat treated tubes from Lot 1 had not had a rupture pressure above 340 psi, it was evident that the new lots of tubes were much stronger, even without heat treating, than the tubes of Lot 1 which were studied earlier. Therefore the heat treating was curtailed and emphasis was placed on studying the as-deposited tubes.

Examination of the rupture pressures of heat treated tubes (Table IV) does not show any significant improvement over the as-deposited tubes, considering the amount of scatter in the data.

6. Lattice Spacing

Carbon atoms in graphite are arranged in a hexagonal crystal structure of atoms in a plane which is designated as the a-b plane. The spacing between every second plane is designated as the lattice spacing (c_o).

The lattice spacing (c_o) in the c-direction was measured on a number of tubes and tube fragments by Metallurgical Service Laboratories. A complete report of these measurements is given in Appendix B.

The average values of the lattice spacing (c_o), the range of probable error in the measurements, and the condition of the PG samples are listed in Table VII, and the data are shown graphically in Figures 11 and 12.

The lattice spacing (c_o) was measured before and after heat treating Tubes H9, 1S, 3S, 4S, S1, and S2 for 100 hours at 2500°F. The changes in c_o are tabulated below:

Tube No.	Average c_o (Angstroms)		
	Before Heat Treatment	After Heat Treatment	Δc_o
H9-1	6.8709	6.8654	- 0.0055
1S-1	6.8639	6.8591	- 0.0048
3S	6.8613	6.8558	- 0.0055
4S	6.8652	6.8590	- 0.0062
S1-1	6.8654	6.8637	- 0.0017
S2-1	6.8656	6.8636	- 0.0020

These changes in c_o due to the heat treatment are small, about the same size as the probable error in measurement. Heat treatment at higher temperatures produces much greater changes in c_o, as reported in Reference 3.

The lattice spacing was measured before and after rupture on Tubes 2S and H10 in the as-deposited condition and on Tube 4S in the heat treated condition. The changes in c_o are tabulated below:

Tube No.	Average c_o (Angstroms)		
	Before Rupture	After Rupture	Δc_o
2S-1	6.8671 6.8704	 6.8645	- 0.0026 - 0.0059
H10	6.8699	6.8608	- 0.0091
4S	6.8590	6.8608	+ 0.0018

TMC A673

Two different measurements were made on Tube 2S-1 before rupture, as shown above.

The change in c_o due to relief of the residual stresses by rupture was quite small, indicating that measurements of c_o are probably not useful in determining residual stresses in PG tubes.

Two tests were made in which c_o values were measured on the same sample at two different temperatures. The results are tabulated below:

Measurement No.	Tube No.	Temperature (°F)	Average c_o (Angstroms)
37	H10	71	6.8608
38	H10	96	6.8663
39	H12	72	6.8644
40	H12	96	6.8677

An increase in c_o of 0.0055 Angstrom was found for the Tube H10 fragment for a 25°F increase in temperature, whereas an increase of 0.0033 Angstrom was found for Tube H12 for a 24°F increase in temperature. Such a range in room temperature is probably greater than that which occurred during the tests, but it does show that the small changes in c_o caused by heat treatment and residual stress relief were of the same magnitude as the probable error and the effect of room temperature fluctuations.

7. Discussion

In evaluating the tensile strength of PG, a clear distinction must be made between flat plate and free standing shapes.

Residual stresses in PG can be divided into two classes; microstresses, especially around nodules, and macrostresses. Only macroscopic residual stresses can be measured by strain gage techniques, and it is recognized that such macrostresses are really some integrated average of microstresses which may vary considerably on a microscopic scale.

Both microstresses and macrostresses are of different magnitudes in free standing shapes than they are in flat plate, due to the differences in internal restraint. That is, much of the residual stress in a flat plate is relieved by removing the mandrel and allowing the plate to adopt a bowed shape, whereas such residual stress relief is impossible in an internally restrained shape such as a tube.

An attempt is made to account for the difference in strength between flat plate and free standing shapes caused by macrostresses by defining the tensile strength of free standing shapes as the applied stress at rupture plus the residual macrostresses. In comparison, the tensile strength of flat specimens (machined from the bowed plates) is assumed equal to the applied stress at rupture, thus ignoring any residual macrostresses, which are probably small.

It is not possible to make a similar accommodation for the effect of residual microstresses on the tensile strength of flat plates and free standing shapes, since the analysis of microstresses is difficult or impossible. For example, no adequate analysis has yet been made of the microstresses around a nodule. It is hypothesized that the magnitude of microstresses increases with nodule size, so that failure occurs under less applied load in the presence of large nodules. This hypothesis is consistent with the relationship between tube rupture pressure and maximum nodule size (See Figures 2 and 3).

Previous studies of nodules in flat PG during bend tests (Reference 4) showed that the nodules had no effect on bend strength if the nodule diameter was less than one-third the sample width. However, the bend tests reported in Reference 4 were made by loading specimens in the a-direction. Nodules near the neutral axis of such a bend sample would not be in the region of high tensile stress on the lower surface. On the other hand, bend tests with c-direction loading would always result in a superposition of bending stresses with the microstresses around nodules.

The effect of such microstresses would probably be much more pronounced if the last deposited surface of the PG, where the nodule diameter is maximum, were on the bottom of the bend test samples, where the maximum tensile loading occurs. The bending tensile strength of PG is consistently higher than the tensile strength from pull tests, but a quantitative correlation of strength with nodule size is not available for either bend or pull tests.

It is probable that a large portion of the difference between the literature values for room temperature tensile strength of flat plate PG from pull tests (18,000 psi, Reference 2) and the tensile strength of free standing shapes (6,600 to 11,800 psi in this report) is due to the fact that the flat plate data have been obtained with small tensile test specimens (a-b plane surface area of 0.3 square inches) carefully selected to avoid nodules, whereas the data for tubes presented in this report are for large specimens (with an a-b plane surface area of about 25 square inches) which includes nodules. The occurrence of nodules is directly proportional to the a-b plane surface area, and microstresses around nodules are always superimposed on applied stress during pull tests.

At the same time, other factors in the deposition process may be equally important in defining the strength of PG, as is indicated by the tubes with small nodules and small residual macrostress which failed at very low rupture pressure.

A reference to residual stresses throughout this report means macrostresses unless otherwise specified.

The causes of nodule growth are not completely understood but possible causes are mandrel surface flaws or impurities, sooting, or unfavorable deposition conditions.

It would probably not be practicable to inspect the mandrel surface to detect minute flaws or impurities which may be responsible for large nodules. However, it does seem that a study of rupture strength of PG tubes produced with different grades and surface finishing of graphite mandrels might establish a production procedure for increasing the yield of tubes and thrust chambers free of large nodules.

A specification for pyrolytic graphite in free standing shapes would ideally reflect knowledge of the interactions of PG structure and deposition conditions with the ability of the part to withstand all of the mechanical and thermal stresses which will be applied in service. Naturally, such a complete understanding of the required PG quality is not yet possible. However, the results of the tube rupture tests strongly suggest that it will be necessary to eliminate large nodules in order for the PG shapes to withstand high internal pressure. The probability of a large nodule is probably directly proportional to total surface area, indicating some difficulty in producing large thrust chambers. Despite all of the unknowns which remain, a specification for free standing pyrolytic graphite is urgently needed, and the contributions of the present study to such a specification are given in Appendix A.

B. Pyroid

One form of free standing pyrolytic graphite evaluated for thrust chamber application was "Pyroid", produced by Pyrogenics, Inc. (Formerly Space Age Materials Corporation). This form of PG is deposited by a plasma deposition technique which facilitiates very rapid deposition rates and very thick sections for unusual geometries and property orientation. During last year's program (Reference 1) a 100-pound thrust chamber of Pyroid was designed and built with a wall thickness in excess of 1/2 inch. Inspection made visually and by X-ray photographs revealed the presence of numerous internal delaminations (See Figure 13). The occurrence of these delaminations is an expected inherent characteristic of any thick walled sections of PG in which the critical ratio of wall thickness to radius of curvature is exceeded (i.e., $t/r > 0.10$). For some applications, the presence of the delaminations themselves is not detrimental. However, they should be predictable and controlled if the part is to be machined or if it expected to carry structural or pressure loads.

The Pyroid chamber which was evaluated did not appear to meet these requirements. However, this was only the second chamber of this configuration which had been fabricated. To evaluate further this material, a machining study followed by a proof pressure test was conducted on this chamber.

1. Machining Study

The Pyroid thrust chamber was machined on both the inner and outer surfaces in several stages with intermediate inspections to check the propagation of additional internal delaminations. The following cutting techniques were used during machining:

1. Standard carbide cutting tools with both sharp and rounded points were used at different feeds and rotational speeds.

2. Spherical and cylindrical files were held against the rotating part.

3. Spherical and cylindrical files, driven by an air motor, were used at different speeds and feed rates.

4. Abrasive cloth, wrapped on a suitable shape, was used against the rotating part.

Chipping and peeling was present in all of the above cutting techniques. As the tool cut into any one of the numerous delaminations, the crack would open and layers of the graphite would be peeled away by the tool. The abrasive cloth, while much slower than the other techniques, did minimize peeling. Examination of X-ray photographs of the finished parts indicated that machining did not increase the size or number of delaminations. The Pyroid chamber after machining is shown in Figure 14.

The finished chamber was pressure tested between the attached flange and the exit cone. The setup is shown in Figure 15. A preliminary leak-check was made using air. Leakage began at 5 psig and it was severe at 25 psig. The air appeared to be entering the chamber wall through cracks and delaminations and escaping at the edge of the attach flange and the end of the exit cone, where the layers were cut. The only leak through the outside layer existed at the large growth nodule, in the convergent section.

A proof pressure test of the Pyroid chamber was made using water. The same leakage paths were noted with water as were noted with air. Water flowed out of the delamination openings at both ends of the chamber, and it was evident that pressurized water had filled the gaps within the chamber walls, so that the internal pressure was being contained only by the outer shell of the chamber.

The Pyroid chamber failed at 105 psig. The failure appeared as a longitudinal crack on the outside of the chamber running from the attach flange radius to the throat. There was no corresponding crack on the inside of the chamber. The failure, rather than indicating the strength of a delamination free chamber, indicated the strength of the outer shell alone.

The results of the machining study and the pressurization test of the Pyroid chamber indicated that machining of Pyroid chambers should be avoided if possible. Delaminations within the chamber wall, if exposed by machining, will provide leakage paths and greatly reduce the strength of the chamber. If the concentricity of the delaminations could be more closely controlled it might be possible to do a limited amount of machining without exposing delaminations at the inner surface.

2. Pyroid Tube Rupture Tests

During the heat treatment and tube evaluation phase of the program, four Pyroid tubes fabricated by the plasma process were ordered from Pyrogenics, Inc. using the specification for unmachined tubes. Difficulty was experienced in fabricating the tubes with a wall thickness greater than 0.050 inch without delaminations. Only one tube was delivered under this phase. The tube which was delivered unmachined had flaws on the external surface due to mandrel adherence. In addition, the wall thickness was not uniform. The wall thickness varied from a maximum of 0.055 to a minimum of 0.030 inch.

The microstructure and nodule size were comparable to those of tubes made by the conventional furnace process and the burst pressure at tube rupture was 220 psig. The rupture crack passes beside a 0.035 inch diameter nodule.

It was concluded from these studies that the Pyrogenics process for fabricating PG may have some advantages in the manufacture of special geometries but the process does not appear to be suitable for thin walled, nondelaminated, free standing components.

IV. STUDIES OF PYROLYTIC CARBIDE-GRAPHITE ALLOYS

A. Background

Several promising alloys of pyrolytic graphite are formed by co-deposition of metals such as hafnium, zirconium, and tantalum which form a refractory carbide phase within the PG matrix.

Previous study (References 1 and 5) showed that zirconium alloy had two important advantages over unalloyed PG: (1) increased tensile strength, and (2) lower oxidation rates, due to formation of the refractory oxide ZrO_2 when exposed to an oxidizing environment. Some important properties of the refractory carbide- PG alloys are summarized below:

1. Melting Point

The melting points of the five most refractory carbides, their carbide-graphite eutectics, and their oxides are listed in Table VIII.

The phase diagram of zirconium carbide and graphite (shown in Figure 16) is typical of the other carbide systems. The carbon rich alloys of carbide and graphite all are susceptible to melting at an eutectic point which is at a lower temperature than those for either the pure carbide or graphite. Metal rich compositions and pure carbides are not of interest because of their very brittle behavior. Considerations of strength and ductility show that alloys of large excess carbon content are most promising.

All of the carbides oxidize rapidly in rocket combustion gases containing water vapor, and their resistance to oxidation depends on the formation of an oxide layer which may deter further oxidation. On this basis, the carbides of hafnium and zirconium are preferred because of the high melting temperatures of their oxides.

The propellant combination O_2/H_2 and storable hypergolic combinations such as $N_2O_4/0.5\ N_2H_4$ - 0.5 UDMH all produce combustion temperatures near 5000°F, the exact temperature depending on mixture ratio, combustion efficiency, and chamber pressure. Free standing chambers of low radial conductivity, such as pyrolytic graphite, encounter inner wall temperatures very close to the combustion temperature. Therefore, the hafnium carbide-graphite alloy may be much superior to the zirconium carbide-graphite alloy, since its oxide melting temperature is slightly higher, and its carbide-graphite eutectic temperature is much higher, based on data recently obtained from Reference 6. Melting temperatures for HfC-C and ZrC-C eutectics were reported as 5882° ± 90°F and 5288° ±90°F, respectively. Recent data on the Hf-HfC system (i.e., metal rich) are presented in Reference 7. The melting temperature of 5250°F for HfO_2 was taken from Reference 8.

As a specific example, the combustion temperature of O_2/H_2 at 100 psia with C* efficiency of 95% is 4750°F. The pertinent melting temperatures for the ZrC-C system are 4868°F for the oxide and 5288°F for the carbon rich eutectic, indicating a small margin in both cases. For HfC-C, the same temperatures are 5252°F and 5882°F, indicating what may be an important advantage for steady state operation.

None of the other refractory carbides listed in Table VIII were considered further in this study because of their lower oxide melting temperatures, although a viscous molten oxide is sometimes very resistant to erosion, as in the case of SiO_2.

2. Oxidation Resistance

As already indicated, the oxidation resistance of the carbide-graphite alloys depends on the production of an oxide coating. The oxidation protection afforded by the carbide-graphite alloys is potentially much superior to that of a single surface coating, since the alloys provide a continuously regenerated oxide coating. Experimental evidence of oxidation protection which was available at the beginning of the present study included the following:

1. Flat samples of ZrC-C alloy were tested (See Reference 1) in a plasma gun containing H_2O vapor, with the plasma impinging on the sample at a 45° angle. The static pressure was atmospheric and the plasma velocity was subsonic. Erosion of the ZrC-C alloy, at a surface temperature of 4000°F, was about 20 percent of pure pyrolytic graphite. Whether the erosive force was greater or less than that which would be encountered in a rocket motor nozzle was not known.

2. Edge oriented nozzle inserts were tested in a solid rocket as reported in Reference 5. A combustion temperature of 6550°F, an initial combustion pressure of about 1000 psia, and a throat diameter of 0.525 inch were used. The HfC-C alloy was much superior to the ZrC-C alloy for the first 20 seconds of firing, although erosion occurred thereafter in both cases.

3. Brittleness

Stoichiometric HfC and ZrC are very brittle and have a high modulus of elasticity. On the other hand, small concentration alloys of the carbides in PG are not significantly more brittle than PG which has been shown to be sufficiently resistant to the mechanical shocks in motor ignition and operation.

4. Strength

The data which were available on tensile (i.e., flexure) strength of carbide alloys at the beginning of this program are shown in Figure 17, all for ZrC-PG taken from Reference 5. The flexural strength of unalloyed PG is about twice the tensile strength in the a-direction. The optimum composition for flexural strength is not known although the strength of almost pure ZrC was only 10,000 to 20,000 psi, indicating a maximum strength for some intermediate ZrC-PG composition. A very large increase of strength over that of PG (100 weight % carbon) was shown for about 20% zirconium by weight.

5. Thermal Shock

Calculations made by Raytheon (Reference 5) showed that the thermal shock resistance of the ZrC-PG alloy was higher than that of PG, which itself has demonstrated more than adequate thermal shock resistance for thrust chamber applications.

B. Raytheon Subcontract

Although previous studies indicated that the increased strength and oxidation resistance of the ZrC-PG alloy appeared to provide important advantages over unalloyed PG for free standing or edge oriented thrust chambers, tubular shapes had never been produced and only limited information was available regarding the variation of material properties with alloy composition. Therefore, a subcontract was awarded to Raytheon for further study of the hafnium and zirconium alloys of PG.

1. Work Items

The work items under the Raytheon subcontract were as follows:

1. Study process control of composition and microstructure of ZrC-PG and HfC-PG through fabrication and analysis of tubular shapes.

2. Determine thermal expansion, flexural strength and modulus of elasticity for various alloy compositions.

3. Fabricate 15 to 20 cylindrical tubes (OD = 2.375 in., wall thickness $\simeq$ 0.050 in.) of several compositions of ZrC-PG and HfC-PG with evaluation of hoop tensile strength and residual stresses.

4. Deliver two edge oriented nozzles (See Figure 18) to Marquardt for motor firing tests.

5. Deliver four free standing thrust chambers (See Figure 19) to Marquardt for motor firing tests.

6. Deliver samples of various alloy compositions to Marquardt for oxidation testing.

2. Materials and Experimental Procedure

a. Materials

The carbide-graphite composites were derived from the reaction between a metal chloride and methane in the presence of a hot substrate - a commercial graphite in this case. Pertinent chemical reactions are as follows:

$$CH_4 \longrightarrow C + 2H_2$$

$$MeCl_4 \longrightarrow Me + 2\ Cl_2 \qquad (Me = Zr \text{ or } Hf)$$

$$C + Me \longrightarrow MeC$$

$$H_2 + Cl_2 \longrightarrow 2HCl$$

An excess of the methane with respect to the metal chloride results in formation of a two-phase pyrolytic carbide-graphite material.

The zirconium and hafnium tetrachloride powders used were of reactor grade, and they were purchased from the Wah Chang Corporation, Albany Division, Albany, Oregon. Table IX lists the impurity content of these powders as determined by spectrographic analysis. The methane was supplied by the Matheson Company and is their C.P. grade. Table X is an analysis of this gas. Substrates were machined from ATJ grade graphite.

b. Apparatus

The furnace used by Raytheon could produce samples as large as 8 inches in diameter with a hot zone 20 inches long. In operation, the furnace is maintained automatically at ± 1.0 mm Hg by the pressure regulating system. Pressure and temperature are also controlled in the chloride vaporizer, and feed line temperature is maintained at 10° to 20°C over that of the vaporizer to prevent condensation of the chloride and the resultant constriction of the inlet lines. The gas panel has flowrator meters to control the flow of nitrogen, helium, and methane.

c. Sample Preparation

Three types of pyrolytic carbide-graphite samples were prepared in the course of the program. Plate stock was prepared for the edge oriented nozzle inserts. In some cases, bars were cut from the plates for flexural strength test specimens. Coupons, approximately 2 by 2 inches also were cut from plate stock for oxidation tests by Marquardt. Rings were obtained from cylinders of the test material to determine burst strength, residual stress, and elastic modulus. Finally, the tapered thrust chambers were made to specifications supplied by Marquardt.

(1). Plate Stock

The carbide-graphite material was co-deposited, for the most part, onto graphite plates 4 inches wide by 17 inches long. Four plates were used in each firing. Run times ranged from 12 to 36 hours with the majority lasting about 24 hours. Because of the delay in receiving precontoured substrate plates, some deposits were made onto flat plates. These tended to bow when they were released from the substrate due to growth and anisotropic stresses as well as to non-homogeneous carbide contents.

Plate stock containing 18 weight % ZrC-PG was used to produce edge oriented nozzle inserts. The plates were approximately 300 mils thick and they were cut into squares 2.5 inches on edge and ground flat. The squares were joined into a solid block by means of a thin film of epoxy resin. Then a 0.5 inch hole was drilled into the center of the block and secured with a long bolt. The exterior and ends of the block were rough machined to shape while they were chucked to the bolt. A similar procedure was used for form the PG in the forward insert. Finally, the two parts were joined with epoxy resin and the nozzle insert was finish machined to specifications.

The same procedure was used to fabricate the 18 weight % HfC-PG nozzle insert except that the thinner, more bowed plates could not be ground flat prior to joining them. Therefore, plates having a similar bow were bonded together into the block required to make the nozzle.

From some of the other tests, coupons of varying zirconium and hafnium carbide contents were cut and submitted to Marquardt for oxidation resistance testing.

(2). Tubes

Pyrolytic carbide-graphite tubes were deposited in graphite mandrels 2 3/8 inches ID and 13 inches long. Rings cut from the tubes with a wall thickness of approximately 50 mils fit over a tubular bladder used in the burst strength determinations. Special care was taken to produce tubes with

uniform wall thickness as well as uniform composition and microstructure. Since any machining would result in minute notches which might weaken the material, only the "as deposited" rings were measured and the calculations were based on the wall thickness of the thinnest section.

(3). Thrust Chambers

Thin walled, free standing thrust chambers of the same carbide--graphite composite materials were also fabricated for test firing. For these specimens, the wall thickness was to be in the 40 to 50 mil range with a maximum of 70 mils at the throat. The only machining which was necessary was at the inlet section in order that the chamber could fit into a holder on the test engine.

The graphite mandrel was removed from the exterior of the thrust chamber by weakening it to the point where it split off the deposit due to stresses created by thermal expansion mismatch. Then the ends of the oversized thrust chamber were faced off to the print dimensions and the "turnings" were used for chemical analysis. Finally, the inlet section was machined and the completed chamber was radiographed to show any cracks or delaminations.

(4). Samples for Measurement

The stress tube mandrels usually shattered in tension prior to removal from the furnace. In the cases wherein the mandrel was still intact, a few axial saw cuts were sufficient to initiate separation. Sound stress tubes had strain gages attached at positions 3, 6 1/2, and 10 inches from the bottom of the tube. Standard techniques were utilized to apply the strain gages. Single element, paper backed foil gages, mounted tangentially, were used at positions 3 and 10, whereas double element bakelite backed rosettes were used for the center gage. Rings one-half inch in width were hand cut from the tube after zero strain readings were noted. The ring edges were sanded on microcut cloth prior to burst testing.

Microstructural specimens were obtained from areas most representative of the material. Normal polishing procedures, using 600 grit paper, silk, and felt cloth with Linde A abrasive, were employed.

Thermal expansion specimens were obtained from the area adjacent to the burst test specimen at position 6 1/2. These specimens were 1 inch long and approximately 0.080 x 0.040 inch in cross section. In thick deposits, samples were taken from both the substrate and the deposition sides. Light sanding with microcut cloth preceded testing.

In some cases, flexural samples could be obtained from tubes where the size permitted several 0.080 by 0.080 x 1 1/8 inch beams to be machined. After light sanding with microcut cloth, these specimens were tested in the perpendicular orientation.

d. Testing Procedure

(1). Burst Strength

When material condition permitted, three burst tests were performed on each stress tube. Internal pressure was applied to the test ring by a tubular bladder. The test rings were cycled once to 200 psig prior to testing to check zero strain readings. A plot of pressure versus strain yielded the modulus of elasticity. The stress calculation was based on thin wall theory and assumed that the tangential stress was uniaxial. The modulus of elasticity calculations involved determining the slope of the pressure versus strain curve and multiplying by the radius-to-thickness ratio.

Failure usually occurred near the strain gage, since these gages were intentionally mounted at the thinnest cross section to record the maximum strains. If the strain gage remained intact subsequent to ring failure, it was then isolated from the remaining material. A final strain reading at this point was compared with the original reading taken before the cutting of the rings to determine the total residual stress.

(2). Flexural Strength and Other Properties

The room temperature flexural tests were performed over a 1 1/2 inch span on an Instron Model TT-C-M1 tensile tester. The deflection rate was 0.020 inch per minute and single point loading was used. When modulus of elasticity measurements were made, a strain gage was mounted on the tensile side of a beam. The beam was then subjected to double point loading and the strain was recorded as a function of load. The strain gage preamplifier and X-Y recorder of the Instron tester were used to record the strain gage output and load simultaneously.

Elevated temperature flexural tests were performed in a graphite resistance furnace in a nitrogen atmosphere. A deflection rate of 0.020 inch per minute was also used in these tests. No modulus measurements were made at elevated temperatures.

The density was determined by the toluene submersion method after suitable drying and evacuating.

The photographs of the microstructure were obtained with a Bausch & Lomb metallograph. All photomicrographs were of unetched polished material at 100X magnification in polarized light with the sample oriented 15° from extinction.

Polished sections of the co-deposited, carbide-graphite were similar in appearance to PG; that is, no second phase was visible with the microscope. However, the carbide was readily observed by X-ray diffraction and chemical analysis. The anomaly was clarified by investigating the broadening of the X-ray absorption line as a means of measuring particle size. It showed that the carbide particles were in the range of 100 to 200 Angstroms and, therefore, they were beyond the resolving power of the optical microscope.

The thermal expansion tests were performed in a Lietz dilatometer. This apparatus records expansion photographically. A series of levered prisms magnify the expansion up to 800 times by directing a light source through these prisms to a photographic plate.

(3). Chemical Analysis

The test carbide-graphite material was pulverized in a porcelain mill. The powder was placed in a previously weighed porcelain crucible and then reweighed. Next the crucible and its contents were placed in a furnace and heated to 1000°C in circulating air for over 12 hours. When the cooled sample reached room temperature, it was weighed once more. From these data, it was possible to compute the weight of residual metal oxide, the weight of metal in the oxide, and the weight percent of metal (in the form of carbide) that existed in the composite.

The above technique is predicated on the fact that the vapor deposited carbides and graphite are extremely pure and that the composite is readily converted to the metal oxide. The validity of this method was checked out against wet chemical analysis and it was found to give almost identical results.

All weighings were made on a Mettler electronic balance which weighs automatically to 10^{-5} gm.

The convention has been adopted throughout this report that alloy compositions will be described by the weight percent of metal (i.e., zirconium or hafnium).

3. Observations

a. Processing and Products

The following process runs were made during this program:

	Plates	Tubes	Chambers
ZrC-PG	10	20	12
HfC-PG	5	5	4

TMC A673

Because of experience gained under a previous project, relatively little difficulty was experienced in fabricating the pyrolytic carbide-graphite plates. The dense ATJ graphite substrate was highly polished and then coated with a thin layer of PG prior to the final deposition. The PG acted as a mold partant and allowed the free standing plates to be easily separated from the substrate.

Doubling the width and length of plates over those previously made (Reference 5) introduced a longitudinal compositional gradient problem. This could be overcome largely by increasing the total gas flow so as to "smear out" the gradient. However, the higher flow rates lowered the efficiency of deposition by decreasing the gas residence time. Also the net carbide content of the material was less. To compensate for the latter, the vaporizer temperature was increased but, surprisingly, no real benefit was noted.

The transverse bowing of plates, normal to the gas flow direction, was nullified by pre-contouring the substrate plates with a reverse bow, just as has been done for PG. A longitudinal bow was also observed but it was not compensated because it was less severe than in the opposite direction.

Plates containing various carbide-graphite ratios were deposited where the composition varied from almost pure PG to stoichiometric carbide. Most of the runs were made under conditions required to produce the lower carbide contents, since it is in this composition range that the most promising materials have been found to date.

Tubes and thrust chambers turned out to be much more difficult to produce as compared to plates because of residual stresses. In addition, the separation from the substrate was more of a problem for these shapes. Especially where the deposits were thin, the tubes had a tendency to pull out-of-round. This was also true for thicker tubes in which the substrate failed prior to removal from the furnace. Substrates were intentionally made thin and heavily scored so that they could be broken apart readily after the run, leaving only the free standing tube.

A special effort was made to produce tubes with uniform wall thickness, since this is a critical factor in burst tests. Unless the stream of reacting gases entered the graphite tube on dead center during the firing, the result was an uneven build-up. This condition could be greatly relieved by rotating the substrate or the gas inlet tube during the run.

Control of compositional variation in tubes through their thickness as well as along the length was desirable in order to attain either lower or controlled residual stresses. This proved virtually impossible with a simple vaporizer as the means of producing metal halide gas. The vapors came off strongly at first and then decreased with time. Changing the vaporizer temperature

did not eliminate this effect. It became apparent that the only way to obtain a uniform carbide composition through the thickness, i.e., with time, was to feed the halide into the vaporizer at a constant rate rather than having the entire halide charge sitting in the vaporizer for the entire run.

Much of the cut-and-try work to produce thrust chambers was avoided by a study of gas flow conditions during a simulated run. Measurements taken with a hot wire anemometer apparatus indicated the optimum flow rate and sample position for the most uniform linear flow velocities over the surface of the thrust chamber. A test run with PG proved that the predicted conditions were indeed very accurate. The throat and outlet sections were almost identical in thickness and the inlet was somewhat thinner. With thickness uniformity under control, it took only a few firings to find the process time required to give a total thickness to meet specifications without any machining except at the inlet or holder end.

The tendency to form cracks was greater in the thrust chambers than in the other shapes, although not nearly as much as was found previously with vapor deposited carbides in test nozzles. The cracks run longitudinally at the ends and circumferentially near the throat. Their path was followed in the case of one chamber that had no cracks when removed from the furnace. The following day, it developed a crack (while still in the mandrel) which traveled slowly to the throat where it turned and circled. Crack-free chambers that had the mandrel removed shortly after the run did not develop cracks.

Two types of graphite mandrels were tried as thrust chamber substrates. One was thin walled and scored to assist in obtaining a free standing piece. These proved easy to remove but they were unsatisfactory because they were ruptured by the stronger deposit and then pulled out-of-round. Mandrels with a heavy wall (over 1/4 inch thick) were better since they did not break on cool-down and could be removed afterward by scoring until they ruptured due to expansion mismatch with the stronger composite material.

Perhaps the most difficult problem associated with producing thrust chambers was making them to size. Chambers that withstood all operations up to this final process broke with an audible snap when the machine tool cut into it. It is believed that if the material were ground rather than turned to shape, the susceptibility to cracking would have been greatly reduced.

b. Tube Tests

The tubes produced by Raytheon were 13 inches long and they were deposited inside a female graphite mandrel with an ID of 2 3/8 inches. Rupture test data for specimens taken from the center station of the first two usable tubes are shown in Table XI. The data listed in Table XI were obtained by cutting a 1 inch long ring from the center of the tube, cementing strain gages on the

outside surface, and then pressurizing the ring by hydraulic pressure. The elastic modulus in the a-b plane is determined from a plot of the recorded strain and the hoop stress. Residual hoop stress is calculated from the change in strain gage readings after the sample is ruptured and residual stresses are relieved.

Previous Raytheon work (Reference 5) with flat samples had shown increasing strength with increasing zirconium content at least up to 22 weight percent, and the data in Table XI show that a similar strengthening has been achieved in tubular shapes. The tensile strength of 17,400 psi achieved with Tube MZ-4 is much higher than that usually obtainable with pyrolytic graphite tubes (See Section III-A).

Two other tubes (MZ-9 and HR-63Z) were cut into a number of rings which were individually tested. The data for these two tubes are given in Table XII.

The residual stresses in Tube MZ-9 were determined by isolating rosette strain gages on the inside and outside and at the thickest and thinnest sections of a ring cut from location 4, four inches from the bottom of the cylinder.

The results of the tangential residual stress tests were as follows:

At maximum thickness (0.078 inch)

σ = -1250 psi (Outside)

σ = 1500 psi (Inside)

At minimum thickness (0.037 inch)

σ = -3360 psi (Outside)

σ = 3520 psi (Inside)

The residual stresses listed for Tube MZ-9 in Table XII were determined by assuming that the residual loading of location 4 was typical of the distribution along the length of the tube. The residual stresses reported in Table XII were thus calculated by a thickness ratio relative to location 4. The residual stress data are anomalous in that the residual stress is smaller for the thicker section of the tube.

The elastic moduli for locations 5, 6 1/2, 8, and 10 of Tube MZ-9 were reproducible at 5.3×10^6 psi. The elastic modulus for location 3, however, was 7.2×10^6 psi. Analysis of the experimental data for this location showed an excessive, nonlinear longitudinal strain indicating a tensile axial stress. This stress caused errors in the tangential strain and, hence, a high modulus. Since this modulus is used to determine the tensile strength from the strain gage reading, this value for this location is also in error.

As can be seen in Table XII, a considerable increase in tensile strength is realized for Tube MZ-9 over previously reported values for tubular PG (Reference 1) of less than 9000 psi. No explanation can be given at this time for the apparent low strength at location 6 1/2 of Tube HR-63Z, although the module size at this thicker location appeared larger than average for this tube.

Burst tests were also performed on Tube HR-64H (4 weight percent hafnium). Rings were taken from positions 3, 6 1/2, and 10. The tensile strengths determined were 2200, 4800, and 2300 psi, respectively. A fourth ring (position 5) yielded a strength of 7900 psi. Residual stress measurements by the gap method yielded a 3000 psi tangential tension on the outside surface. On the basis of the hafnium content, the magnitude of these strengths, as in the previous tube, is much lower than anticipated. However, the anomaly of tensile residual stress on the outside surface suggests that unfavorable metal concentration gradients existed through the thickness.

The burst results from Tube MZ-20 are presented in Table XIII. Chemical analysis of this material showed very little zirconium content. The data of Table XIII confirm the chemical analysis. The strength, modulus of elasticity, Poisson's ratio, and density are similar to those of unalloyed material. Examination of the deposition data indicated very little zirconium pickup, hence the material tested was essentially pyrographite. The tensile strength at locations 6 1/2 and 10 was very high for PG, but the tube length was only 1 inch. It is probable that longer tubes would have greater probability of containing an excessively large module, with a lower average tensile strength.

It was originally thought that the burst strength plus the residual stress would yield values approaching the flexural strength. Since the data do not show this trend, the isolation method of measuring residual stress came under closer scrutiny. Tests were initiated to determine the amount of residual stress remaining after isolation from the test ring. Two rings from Tube MZ-16 (3.0 weight % Zr) and one ring from Tube MH-4 (3.5 weight % Zr) were tested. The tests consisted of mounting rosette strain gages on the tubes and cutting rings. These rings were then cut and the gages were isolated on the original thickness. The data at this point would normally be used for the residual stress. However, the isolation was carried one step further in these tests. The material on the back of the gage was reduced to a minimum by a cleaving technique. In addition, Tube MH-4 was instrumented with a three-gage rosette in an effort to determine if the principal stresses are truly axial and transverse. The results of these tests are presented in Table XIV.

It can be seen from these data that there is a considerable difference in residual stress between the original isolated thickness and the cleaved thickness. The data from MZ-16 position 4 showed a decrease in tangential stress and hence is not a serious case. MH-4 position 6 1/2 showed a 127% increase in residual stress with an 82% decrease in thickness. The data from MZ-16 position 9 1/2 showed a stress reversal from 3580 psi tension to 6300 psi compression for a 77 1/2% decrease in thickness. Chemical analysis of this section showed a concentration gradient from 4.0% Zr on the outside surface to 1.6% on the inside with 11.7% Zr at the center.

The three-gage rosette analyses of MH-4 showed the principal stresses to be 12.4° from the axial and transverse directions. This condition results in errors of less than 5% when calculations are based on two-gage rosette analysis.

In general, the quality of the stress tubes after removal from the furnace was poor and only a few could be tested completely. Most of the tubes that were discarded were considered not testable because of cracks that propagated along their length. There was no preferential crack direction. All would start at a free end in an axial direction but there the consistency ended. Some would continue axially whereas others would propagate tangentially. Occasionally tubes were removed from the furnace with a conchoidal crack which would spiral around the circumference. The sign of the crack-causing stress was also inconsistent although most tubes opened on failure indicated that the outside surface was in tension. The reason for the high failure rate is believed to be the serious alloy concentration gradient that exists in these tubes.

Of the tubes that were tested, Tube MZ-9 indicated the highest strength. Position 10 of this tube yielded a tensile strength of 23,200 psi. The zirconium content at this position was 9.7%. The microstructure of this tube showed a fine grained regenerative structure which was essentially crack free. The coefficient of expansion was as expected and showed a 20% increase over that for pyrographite at 1075°C.

Delaminations were observed in Tubes MZ-2 and MZ-4. Since the microstructure sample was taken from an area close to the burst test ring, these delaminations were not realized until after the testing. It should be noted that Tube MZ-4 with the delamination showed an increase in strength of 25% over the strength of pyrolytic graphite.

The very low strength values of Tube HR-63Z was surprising at this alloy content. The microstructure showed no serious faults. Re-examination of the process conditions revealed that the gas inlet tube was not straight and that the resultant circumferential wall thickness varied up to 60 percent. Although the residual loadings on a continuous ring must be equal at every point on the circumference, the stress will vary according to thickness. The stress

variation along the periphery of this run was apparently sufficient to cause the originally circular cross section to become elliptical. When testing an elliptical section in the burst apparatus, serious bending stresses arise and lower the resultant tensile strength. Since the microstructure and density of this run showed little deviation from normal, the low apparent strength of this material is attributed to either the excessive variation of thickness or to incomplete strain gage isolation technique.

By necessity, the chemical analysis of Tube MZ-20 was not done until after the burst tests were performed (the failed ring is used for analysis). It was not known during testing that the material was of low concentration. Being of low concentration, however, the concentration gradient across the thickness also was correspondingly low. This fact is reflected in the low residual stress. Even isolation down to a 0.026-inch thickness showed only a 2600 psi residual stress.

Another factor that may be affecting the burst results is a biaxial stress field in the burst apparatus. In order to investigate this effect, three element rosette gages were used. These data indicated that although the tangential stress applied by the diaphragm was principal, a second compressive principal stress of approximately 5% was being applied at higher pressures due to the flexible diaphragm restraints at the edges of the rings. Because of the small Poisson's effect, this error was considered negligible.

It should be mentioned that the residual stresses measured in Raytheon's study are those existing on the outside surface of the ring and they give no indications to stress distribution or inside surface stress. The residual stress was always added to the burst stress to obtain ultimate strength. In the cases wherein the measured residual stresses were compressive, it was assumed that a linear stress distribution existed across the thickness and an inside tensile surface stress of equal magnitude was added to the burst stress.

c. Flexural Tests

Flexural tests were performed on zirconium and hafnium plate materials as well as on stoichiometric zirconium carbide and some stress tube runs. These results are presented in Tables XV through XVIII. The specimens were cut from the tubes in such a manner that the beam axis coincided with the tube axis. The test span varied from 1/2 to 2 inches depending on the material. All tests were performed in the perpendicular orientation to minimize interlaminar failures.

The stoichiometric zirconium carbide (Table XV) gave a flexural strength of 46,500 psi at room temperature. The density, thermal expansion, and composition are essentially those which would be predicted from X-ray data. The flexural strength, however, was much higher than previously measured values.

A possible explanation is the small crystallites observed in this material as compared with the large columnar crystals observed in previously prepared ZrC by the same chemical vapor deposition process. The strength value reported above is an average of twelve tests. Strength values between 38,200 and 54,000 psi were observed.

On the other end of the concentration scale, plates of 3 weight percent zirconium (MZ-11) were tested in flexure at room temperature. The average of six beams was 35,500 psi. These beams contained a slight delamination crack. Hence the results are believed lower than those for sound material of the same concentration.

Another run with plates of 6 weight percent zirconium content (MZ-7) was examined and the results are listed in Table XVI. For this material, the density and room temperature strength are in the anticipated range. The elevated flexural strength is lower than the room temperature value. This is unusual since most graphitic materials tested to date show an increase in strength with an increasing testing temperature. Possibly the many small delaminations seen in this material open up at elevated temperatures causing a reversal of the normal trend in strength with temperature. This too can possibly explain the increase in elastic modulus. The opening of these microcracks fits with the strong hysteresis observed in the stress-strain curve when sample beams were tested.

Table XVII presents the flexural strengths at room temperature and 1800°C for hafnium Run MH-3 (22 weight % Hf). These data show a substantial increase in strength over that for unalloyed material. The flexural strengths of unalloyed material at 20°C and 1800°C were 26,000 psi and 35,000 psi, respectively.

The results of flexural tests on tube material for Runs MZ-9, (6 weight % Zr), MZ-16 (3.0 weight % Zr), MZ-17 (3.5 weight % Zr), and MH-4 (3.5 weight % Hf) are presented in Table XVIII. The low flexural strength of MZ-9 was attributed to the location from which the specimens were taken. The beams were cut from a position near the low burst strength position (6 1/2) reported in Table XII. It has been empirically determined that a 2:1 ratio exists between results of flexural and burst tests.

Table XVIII shows that the material of MZ-17 is only slightly stronger than that of MZ-16. These results indicate, however, the improvement possibilities over pyrolytic graphite with only a small zirconium carbide addition.

The only flexural tests performed on a hafnium carbide tube are also presented in Table XVIII for Run MH-4. These data show only a slight increase in strength over the strength of pyrolytic graphite, but the hafnium content was only 3.5 weight percent.

d. Thermal Expansion

The thermal expansion curves for Runs MZ-9, MZ-11, MZ-17, MH-3, and MH-4 are plotted against temperatures up to 1100°C in Figures 20 and 21. The expansion of unalloyed pyrolygic graphite is superimposed on these curves for comparison purposes. It can be seen from these curves that both the zirconium and hafnium alloys at these concentrations show only a slight increase in thermal expansion. All of these data were obtained from samples of the complete thickness. Figure 22 is the thermal expansion of samples taken from the substrate and deposition side of MZ-16 (3.0 Weight % Zr). The material used in this investigation was taken from the same position (9 1/2) that yielded the residual stress reversal mentioned earlier in this report.

It can be seen from Figure 22 that a considerable difference in expansion is realized between the inside and outside surfaces of the stress tube. The deposition surface has an expansion 2 1/3 times greater than the substrate surface at 1075°C. Subsequent chemical analysis showed the deposition surface to have 11 weight % Zr whereas the substrate surface only has 4 weight % Zr. It should be noted that the substrate surface expansion is less than that of unalloyed material. More than any other factor, this compositional gradient and its effect on the expansion coefficients, and thus on the residual stresses, was the cause of the premature tube failures.

e. Microstructure

Photomicrographs of sections taken from Tubes MZ-9, MZ-11, HR-63Z, and MH-3 are shown in Figures 23 and 24. Although an occasional large or misoriented nodule is observed, these photomicrographs are representative of the material. Microcracks were observed in all of the samples. These cracks were approximately 0.02 to 0.15 inch in length and they were rarely propagated beyond a tilt boundary. Tube HR-63Z showed a delamination at the center of the thicker section which probably accounts for the lower apparent burst strength.

f. Chemical Analysis

The simplified method of determining carbide (or metal in the form of carbide) in the composite made it possible to do many more analyses than were thought possible within the allocated funds. One hundred sixty-six were made in this laboratory and two by the Jarrell-Ash Company, Newtonville, Mass. There was about a 5% difference between the values obtained by oxidation and those by wet chemical analysis (Jarrell-Ash Co.). Since the reproducibility of the former was even better than that of the latter no further tests were made by the wet chemical technique.

The improvement in compositional uniformity with higher flow rates can be seen in the following tabulation taken from two ZrC-PG plate runs:

Total Flow (liters/min)	Weight % Zr versus Distance (inches) from Bottom End			
3	20.8 (3)	16.0 (6)	13.8 (9)	5.9 (12)
6	7.3 (2)	5.5 (8)	5.6 (12)	4.9 (14)

High flow rates also gave good uniformity in the case of stress tubes as well as plates.

Tube MZ-16	Composition versus Location		
	Bottom	Middle	Top
Weight % Zr	6.9	5.1	4.6

The same uniformity lengthwise, however, did not hold true through the thickness. An analysis of the middle section for MZ-16 showed the following:

	Initial Deposit	Middle	Final Deposit
Weight % Zr	4.0	11.7	1.6

4. Delivered Parts

a. Oxidation Samples

The samples of ZrC-PG delivered to Marquardt for oxidation testing are illustrated in Figure 25 which shows the last deposited surface. Numerous large nodules and growths are evident.

The microstructure of a 20 weight % Zr-C alloy sample produced under the current contract is shown in Figure 26-A. Many microcracks and delaminations are present.

The microstructure of a similar alloy (20 weight % Zr-C) produced under a previous contract (about two years ago) is shown in Figure 26-B. A very fine microstructure was deposited until about half way through the run, when some event caused large growth cones to form.

TMC A673

At the beginning of this program, the deposition techniques used by Raytheon were found to be unsatisfactory for making large pieces with uniform composition controlled both radially and axially. A number of variations in deposition conditions were studied but the results were not encouraging. These early parts were made by charging the chloride vaporizer with a large amount of hafnium or zirconium chloride powder at the beginning of the run, with only an indirect control of the rate of metal pickup by varying the methane flow or the temperature.

The last deposited surface of the HfC-PG samples delivered for oxidation testing are shown in Figure 27. Very large growth nodules are present, evidently caused by chunks of unvaporized chloride powder reaching the deposition zone.

b. Edge Oriented Nozzles

The edge oriented ZrC-PG nozzle insert delivered for motor testing is shown in Figure 28. The zirconium content was about 18% by weight. The ZrC-PG plates used to make the insert were curved so that they had to be matched before machining the insert. As a result, some gaps between plates existed, which were filled with an epoxy cement. The convergent section of the nozzle (forefront in the photograph) was made of unalloyed PG.

A side view of the edge oriented HfC-PG nozzle insert is shown in Figure 29. The curvature and epoxy between the hafnium alloy plates (left side of photograph) are evidence that the structural integrity of the nozzle was inadequate.

c. Tapered Nozzles

The four tapered nozzles delivered by Raytheon are shown in Figure 30. It was not possible within the time and funds available to produce four completely satisfactory free standing nozzles. Therefore, one of the nozzles (MTC-XVI-H) was tested on the mandrel. A total of 16 deposition runs were made while attempting to produce tapered nozzles, and most of the nozzles cracked during machining to final dimensions. One such nozzle, MTC-XVII-H, was used to obtain the following chemical analysis:

	Inlet	Throat	Outlet
Weight % Hf	6.2	10.8	1.9 (Initial deposit) 9.0 (Final deposit)

TMC A 673

The metal content also varied through the thickness in tapered thrust chamber MTC-XVI-H, which was test fired by Marquardt while still on the mandrel. A sample of the throat after test showed the following:

	Throat
Weight % Hf	15.8 (Average) 7.5 (Initial deposit) 19.1 (Final deposit)

The alloy composition of Chamber 28 VI was not determined exactly but it was probably about 20% Zr by weight. The other ZrC-PG nozzle (MTC-XV-Z) was not test fired because of visible delaminations.

The quality of the carbide alloys improved near the end of the program, as can be seen by comparing the tapered nozzle (Figure 30) with the oxidation samples produced earlier (Figures 25 and 27). Improvement was also evident in the microstructure, as can be seen by comparing the first tapered nozzle (28 VI, Figure 31-A) with one of the last tapered nozzles produced (MTC-XVI-H, Figure 31-B). The latter nozzle was made using a new vaporizer which controlled the rate of chloride powder fed into the vaporizer by a screw feed system. However, the time available was not sufficient to determine the full capability of the screw feed system for controlling alloy composition.

5. Discussion and Conclusions

Many more tubes and chambers were made than were originally projected. The reason was that no experience had been gained previously on fabricating tubular shapes of these pyrolytic graphite-carbide materials. As it turned out, they proved to be much more difficult than the flat pieces. There is reason to believe that the trouble stems from the fact that this process involves two different reacting gases rather than the single one used to make PG. In the compositional range of interest, a small change in the ratio of carbide-to-graphite causes a relatively large change in the coefficient of thermal expansion. Thus, if the gas ratios change in the course of a run strong stresses are built into the piece. These tend to relieve themselves by bowing longitudinally as well as transversely in the case of plates. Tubular shapes, however, are constrained by their shape from bending and they therefore are highly stressed.

Uniformity of composition along the length of the object being fabricated was obtained by increasing the total flow rate of gases through the female mandrel of deposition. This, however, reduced the deposition rate and the ratio of carbide to graphite. Apparently, the metal halide is more sensitive to a decrease in gas residence time than is methane under the same temperature and pressure.

To compensate for the decreased carbide content, the temperature of the vaporizer was increased. This caused the fine halide powder to sinter, thereby reducing the surface area exposed for evaporation. Thus, the only method available to increase the ratio of carbide to graphite with this apparatus, was to reduce the methane flow and thus reduce the deposition rate.

The direct, screw feed vaporizer became available near the end of this program. It is hoped that this vaporizer will make it possible to deliver a fixed amount of halide vapor into the furnace and also vary the amount at will. High carbide content materials could be made as easily as low content material. Even more interesting is the possibility of producing any desired compositional variation through the thickness of the wall with this feed system, and thereby to control residual stress. Also, an effect similar to the tempering of glass could be made by high carbide content at both surfaces and low content in the interior. Further experience with the screw feed vaporizer is required to evaluate its capabilities.

6. Suggestions for Future Work

A refinement in the processing technique worthy of future investigation is the further development of the chloride feed mechanism to the state where it is possible to produce a material with a controlled gradient of carbide through its thickness. By this means one might negate the residual stress that occurs normally in anisotropic materials. Also, it would be possible to make a sandwich type structure high in carbide at the surface and low in the interior. The benefit would be twofold. Oxidation resistance should be greater due to more carbide available to form the oxide. The material should be even stronger due to the compressive force exerted by the higher coefficient of thermal expansion of the surface layer. Any bending stress would have to overcome this compressive force before a tensile force could be exerted. Since these materials are stronger in compression than in tension, the net effect would be an increase in strength.

Isotropic, higher expansion graphites have recently been developed for coating with silicon carbide. The substitution of this graphite for the ATJ grade, used as a substrate for the pyrolytic carbide-graphite, might largely eliminate the cracking problem previously encountered due to thermal expansion mismatch between substrate and deposit.

The final machining of test pieces would be improved by grinding rather than by using a metal cutting tool. Apparently, the latter method creates notches that lead to cracks where the material is highly stressed. Any ground surfaces would of course also require fine polishing for increased strength.

The mechanical properties should be redetermined for the various carbide content materials where there is a uniform carbide distribution through the thickness. These data would be more meaningful than those previously obtained with specimens highly stressed because of severe carbide gradients. This would help to resolve the question as to whether there is a composition that produces maximum strength.

With the availability of fine grained, delamination free specimens one might determine how the introduction of finely dispersed carbide into pyrolytic graphite effects the normally anistropic thermal conductivity.

Finally, the mechanical and thermal properties should be investigated for controlled carbide gradient materials such as the graded and the sandwich structures previously mentioned.

V. OXIDATION TESTS

Oxidation rates of PG, ZrC-PG, and HfC-PG were measured during tests in which air heated by an arc plasma was passed through an 0.25-inch orifice and impinged on small (1 by 1 inch) samples of the pyrolytic materials. The surface temperature was determined from pyrometer readings and erosion rates were calculated from the change in sample thickness. The jet impingement was on the a-b plane at an angle of 45°.

The objective of the oxidation testing program was to determine the effect of zirconium and hafnium contents on the oxidation resistance of the carbide alloys. However, this objective was not met due to delaminations and mechanical failure of most of the carbide alloy samples, which were produced before Raytheon had put a new vaporizer system into operation.

The most useful erosion rate data obtained during the oxidation testing are shown in Figure 32. The straight line which is drawn to average the erosion rates for pyrolytic graphite shows that the chemical erosion of PG in air increases from about 3 mils/sec at 4400°F to about 5 mils/sec at 5400°F, for the conditions of air jet impingement used in these tests.

Test data for the points plotted in Figure 32 are tabulated in Table XIX.

An alloy of about 20% zirconium in PG showed a lower erosion rate of about 0.6 mil/sec at 4400°F and 4660°F, but at 5060°F (about the melting point of ZrO_2) the erosion rate of 5 mils/sec was about the same as that for PG. The erosion data shown in Figure 32 for the zirconium alloy of PG were obtained using samples of ZrC-PG produced by Raytheon for an earlier program (Reference 1). None of the zirconium alloy specimens provided by Raytheon under the current subcontract were able to withstand the plasma tests without delaminations or mechanical failures.

A sample of HfC-PG containing 78.6% hafnium by weight was tested at 4400°F and it experienced an erosion rate of about 0.6 mil/sec, the same as that for the ZrC-PG sample at the same temperature.

A fragment of the tapered motor chamber MTC-XVII-H was tested at 4700°F and it had an erosion rate of 1.8 mil/sec, about half the erosion rate of PG, but about 3 times that of the 20% ZrC-PG at a similar temperature.

Another sample of 78.6% HfC-PG was tested at 5270°F (about the melting point of HfO_2) and it experienced melting and a fast erosion rate of 13 mils/sec which was worse than that of PG at that temperature.

On the other hand, two tests of 75% HfC-PG at 4930°F and 5240°F resulted in a low erosion rate of 0.6 mil/sec.

The probable reason for the high erosion rates during Runs 34 and 37 is that the melting temperature of the oxide had been exceeded in each case. Some uncertainty exists regarding the emissivity of the oxide coatings, and hence the surface temperatures during the oxidation tests are uncertain. The emissivities of ZrO_2 and HfO_2 are low at room temperature, but they rise to 0.8 at 4000°F (References 9 and 10).

The emissivity of HfO_2 was evaluated at Marquardt during propane torch tests and a value near 0.4 was obtained by comparing Ray-O-Tube and optical pyrometer readings. At a brightness temperature of 4500°F, the difference between emissivities of 0.4 and 0.8 would mean a difference of 490°F in determining the true surface temperature during the oxidation tests.

The propane torch was directed perpendicularly to the a-b plane of a ZrC-PG sample, and no surface erosion occurred during a 10 minute run at a surface temperature of 3700°F. The flame curled around the edges and seemed to cause more damage to the c-plane edges, producing a finely serrated effect.

There is a possibility that the HfO_2 formed on oxidized samples of HfC-PG may also contain some ZrO_2 because of the 3% impurity of Zr in the $HfCl_4$ (See Table IX). The melting point of a mixture of HfO_2 and ZrO_2 might be lower than the melting point of either pure oxide, but data on the melting point of such a mixture could not be found in the literature.

VI. MOTOR FIRING TESTS

Nozzles and thrust chambers made of pyrolytic graphite and the carbide alloys were tested with a hot gas generator purchased from Astrosystems International, Inc., which consisted of four water cooled combustion chamber sections and an uncooled propellant injector. The injector is shown in Figure 33. Water cooled sections made by Marquardt were used to connect the pyrolytic nozzles and thrust chambers to the gas generator.

Pyrolytic nozzles tested during this program had nominal thrust diameters of either 0.60 inch or 0.868 inch, and both sizes were tested with the same injector.

Motor firing tests were made with gaseous O_2/H_2 at a nominal chamber pressure of 100 psia and an O/F ratio of 5.0.

Circumferential distribution of the heating pattern in the steel nozzle (Figure 34) was obtained by short duration runs. Sixteen thermocouples were evenly spaced on the outside of the 0.10-inch thick steel nozzle at a point (just upstream from the throat) where maximum heating rates usually occur. Two thermocouples were also placed at the throat.

The heating pattern at 2.5 seconds after ignition is shown in Figure 35. The C* efficiency was 93.2 percent of theoretical shifting equilibrium C*, the chamber pressure was 101.2 psia, and the O/F ratio was 5.04. The temperatures are plotted as ratios of each individual temperature divided by the minimum temperature, which was 1610°F. The hottest locations showed heating rates about 9 percent greater than the minimum.

An ATJ graphite nozzle of the geometrical configuration shown in Figure 18 was tested for 60 seconds to determine the distribution of erosion in the nozzle when using the Astrosystems injector. The ATJ graphite occupied the positions of both the forward and aft inserts in Figure 18. Figure 36 shows the uniformity of erosion of this nozzle.

A. Edge Oriented Nozzles

Edge oriented nozzles of the design shown in Figure 18 were tested by attachment to the gas generator as shown in Figure 37.

1. Pyrolytic Graphite

The erosion during a 300 second test of a PG nozzle was quite uniform as shown by the postrun photograph of the nozzle shown in Figure 38. The chamber pressure history (Figure 39) for the pyrolytic graphite nozzle indicates that the steady state temperature and erosion rate were reached after about 60 seconds.

2. Pyrolytic Zirconium Carbide-PG

An edge oriented ZrC-PG nozzle made by Raytheon was tested for 300 seconds. The appearance of the insert before testing is shown in Figure 28. The ZrC-PG plates were about 1/8-inch thick. The convergent section of the nozzle after the run is shown in Figure 40 and the exit end is shown in Figure 41. The decrease in chamber pressure of the ZrC-PG nozzle was much slower than that of the PG nozzle as shown in Figure 38. In addition, the contours of the two nozzles after testing for 300 seconds were also much different, as shown in Figure 42.

The principal mode of failure of the ZrC-PG nozzle was mechanical in nature, particularly during the last 60 seconds of testing, during which small chunks of the ZrC-PG nozzle were ejected. Surprisingly enough, however, the nominal diameter near the throat of the ZrC-PG nozzle was still close to 0.60 inch after the run, although chunks of the nozzle at the throat had been removed.

The superior oxidation resistance of the ZrC-PG material is quite evident in the convergent section at the juncture between ZrC-PG and the PG forward insert, as shown in Figure 40.

This test showed that the oxide formed on edge oriented ZrC-PG nozzles is sufficiently resistant to the fluid dynamic shear forces at the throat to act as an effective oxidation barrier. It is quite likely that much greater mechanical integrity is possible with ZrC-PG than that observed with the nozzle which was tested. Raytheon had considerable difficulty producing good quality carbide-PG alloys, but much better quality material was being produced by the end of the program than that used in this nozzle test.

3. Pyrolytic Hafnium Carbide-PG

An edge oriented HfC-PG nozzle made by Raytheon was tested for 120 seconds. The convergent and divergent sections of the nozzle after the test are shown in Figures 43 and 44, respectively. The HfC-PG nozzle was made of thin curved plates because of the difficulties Raytheon encountered in making flat plates. The hafnium content was about 18%. A side view of the HfC-PG nozzle before testing is shown in Figure 29 which shows that curved plates were used and it was obviously not a good quality nozzle. The plates of both Raytheon nozzles were joined by epoxy cement in order to facilitate fabrication and early pyrolysis of the epoxy undoubtedly left gaps between disks and contributed to the poor mechanical strength of both the HfC-PG and ZrC-PG nozzles. Furthermore, voids were almost certainly present between disks in the HfC-PG nozzle before firing because of the use of curved plates.

At motor ignition, nozzle particles were ejected and the chamber pressure dropped rapidly, as shown in Figure 39.

B. Tapered Nozzles

Tapered nozzles of the design shown in Figure 19 were tested by attachment to the gas generator as shown in Figure 45. This configuration was intended to investigate the feasibility of free standing thrust chambers made of carbide-PG alloys, and to measure the relative erosion rates of PG alloys and unalloyed PG on the a-b plane.

1. Pyrolytic Graphite

Tapered pyrolytic graphite thrust chambers were available from previous studies (Reference 1). These PG chambers were produced by Berylco. Three additional tapered chambers were later purchased from Berylco which had a wall thickness of about 0.030 inch instead of the 0.040 to 0.050-inch wall thickness of the nozzles of the original order. The proof tests, wall thickness, and motor test experience of each of the tapered nozzles purchased for both this and the previous program are listed in Table XX.

Motor firings of Nozzles Nos. 1 and 2 under the previous program used N_2O_4/0.5 N_2H_4-0.5 UDMH, but the results were inconclusive because of very low C* efficiency.

Motor firing during this program used gaseous O_2/H_2 at a chamber pressure of 100 psia. Five tapered pyrolytic graphite nozzles were tested with the gas generator as shown in Figure 46. Four of the five nozzles ruptured shortly after ignition (See Table XX). Nozzle No. 4 was test fired for two 3-second runs (Figure 47). The throat erosion was not measurable, but a fine longitudinal crack was found on the inner surface after the second run. The nozzle ruptured at ignition for the third run. Therefore, no chemical erosion data were obtained from the test firing of tapered PG nozzles because of failure of all five tapered nozzles.

The microstructures of the ruptured tapered PG nozzles were found to contain large nodules, which, based on the strength--nodule size correlation for PG (Figures 2 and 3), would indicate low strength.

An extreme example was tapered PG Nozzle No. 3. The 10X view of the ID and OD surfaces of Nozzle No. 3 are shown in Figure 48. This nozzle ruptured during a proof test at 90 psig. There is no evidence of any systematic mandrel marks affecting the size or distribution of the matrix grains, which are comparatively small. There are some large nodules, however, the largest being 0.060 inch.

A more typical tapered PG nozzle was No. 4 which had two successful 3-second test firings but ruptured at the third ignition, with a nominal chamber pressure of 100 psia. The ID surface is shown in Figure 49.

Tapered nozzle No. 7 had the finest matrix grains of any pyrolytic graphite specimen examined under this program, as is shown in Figure 50. Only one or two nodules with a diameter of about 0.020 inch were observed on the inside surface. The nozzle shattered at motor ignition, and the cause of the failure is not known. Only fragments of the nozzle were available for examination. It is possible that a large nodule was responsible for the failure but the evidence was lost.

The maximum nodule diameter (on the inside surface) observable on the broken tapered PG nozzles are listed below:

Tapered Nozzle No.	t (in.)	d_{max} (in.)	d_{max}/t (in.)
1	0.050	0.050	1.0
2	0.050	0.060	1.2
3	0.050	0.070	1.4
4	0.050	0.060	1.2
5	0.030	0.040	1.33
7	0.030	None	--

It is concluded that most of the failures of the tapered PG nozzles were caused by excessive nodule size.

2. Pyrolytic Zirconium Carbide-PG

A free standing pyrolytic ZrC-PG nozzle made by Raytheon and designated as Nozzle 28VI (Figure 30) was test fired but it ruptured at ignition. X-ray photographs of Nozzle 28VI before firing revealed delaminations and a 50X photomicrograph (Figure 31) of the cross section before firing also shows a major delamination. In addition, Figure 31 shows that there was at least one change in the deposition conditions during manufacture. It is probable that the zirconium content was not controlled adequately during deposition, contributing to the poor microstructure of Nozzle 28VI.

3. Pyrolytic Hafnium Carbide-PG

Because of the difficulty which Raytheon had encountered in producing free standing tapered nozzles, it was decided to test one nozzle without removing it from the mandrel. This nozzle (MTC-XVI-H) is shown before testing in Figure 30. A 50X photomicrograph of the cross section after firing is shown in Figure 31.

The nozzle was test fired for 30 seconds. After the test, the graphite mandrel had a longitudinal crack, and smaller cracks were observed in the HfC-PG although they did not extend to the throat. The test data are as follows:

C* Efficiency	= 96.8%
Chamber pressure at beginning of run	= 105.3 psia
Chamber pressure at end of run	= 100.3 psia
D_* before run	= 0.837 inch
D_* after run	= 0.849 inch
Average erosion rate	= 0.20 mil/sec

Photographs of tapered nozzle MTC-XVI-H are shown during firing in Figure 51 and after firing in Figure 52.

A light oxide film was observed after the run, but the adherence of the oxide during the run was evidently poor. No erosion data for pure PG are available for direct comparison. An indirect comparison is possible from the throat erosion rate of 0.46 mil/sec of the edge oriented PG nozzle. However, the erosion rate on the c-plane, as in an edge oriented nozzle, is often higher than that on the a-b plane, as in a tapered nozzle. Therefore, it must be concluded that the hafnium oxide film formed on the a-b plane of this free standing HfC-PG nozzle did not greatly reduce the erosion rate at the throat.

C. Discussion

The adherence of the HfO_2 or ZrO_2 to the thrust chamber is undoubtedly very sensitive to the fluid dynamic shear stresses of the combustion gas, as well as the orientation of the PG. Although the motor test results from Nozzle MTC-XVI-H discourage the idea that zero erosion can be achieved on the a-b plane

of hafnium alloys of PG, it is possible that the alloys are still better than PG by some small factor. The possibility exists that the oxide might gain better adherence during a longer test (this effect was noted in plasma tests) or that pre-oxidation of the chamber might be beneficial. More oxidation protection might also be afforded by larger concentrations of Hf or Zr.

The oxide adherence on edge oriented nozzles appears very promising, based on the test of the ZrC-PG nozzle. It is probable that the better adherence of the oxide in the test of the edge oriented ZrC-PG nozzle than was observed in the test of the MTC-XVI-H nozzle was due to the formation of fine serrations on the c-plane edges which held the oxide in place, rather than to any difference between HfO_2 and ZrO_2.

VII. CONCLUSIONS AND RECOMMENDATIONS

1. The principal conclusion from this study is the realization that the evaluation of pyrolytic graphite and its alloys for thrust chamber applications is being delayed by the unsatisfactory quality and inconsistency of the pyrolytic materials being produced under the present state of the art.

In this regard, it must be recognized that the production of carbide alloys of PG, although closely related to pyrolytic graphite, is in a much earlier stage of evolution than is the production of PG, and a separate assessment must be made of the current status of either unalloyed PG or the carbide alloys.

2. The current status of free standing PG is that cylindrical tubes can now be produced with sufficient rupture strength (say an average of 500 psig) so that if a similar strength can be achieved in the future with thrust chamber shapes, the structural limitations of free standing PG chambers will be overcome for some applications.

3. The results of this study give strong evidence that a large increase in rupture strength of free standing PG may be achieved by reducing the size of nodules. A systematic study should be made of techniques by which nodules can be eliminated. Techniques which might be considered include mandrel surface cleaning and the use of graphite mandrels with greater purity, density, uniformity, and smaller particles than ATJ graphite.

4. The effect of deposition parameters on the rupture strength of PG tubes should be evaluated systematically.

5. The status of free standing carbide-PG alloys made with zirconium or hafnium is that the nonuniformity of alloy composition throughout the length and thickness of tubes produced with current techniques is so severe that the potentialitites of these carbide-PG alloys could not be properly evaluated under the current program.

6. In spite of the current nonuniformity of composition of the carbide-PG alloy, some evidence was obtained that the strengthening expected from the addition of zirconium and hafnium can significantly improve the strength of free standing shapes. One tube made of ZrC-PG had a tensile strength of 23,200 psi. The maximum strength of an unalloyed PG tube was 18,500 psi.

7. Evidence was also obtained that the carbide alloys will have oxidation resistance superior to that of unalloyed PG in the edge oriented configuration, for liquid propellants such as O_2/H_2 and N_2O_4/hydrazine.

8. There was no indication (based on one 30-second test firing) of superior oxidation resistance of the carbide alloys in free standing configurations. Further motor testing is required in order to more adequately evaluate the oxidation rates of free standing carbide alloys.

9. Pyroid, a pyrolytic graphite made by a proprietary technique, does not appear to be suitable for free standing thrust chambers.

VIII. REFERENCES

1. Marquardt Report 5992, "(Title -- Unclassified) Pyrolytic Refractory Thrust Chamber Development", Contract NAS7-54, 20 May 1963. UNCLASSIFIED.

2. Gebhardt, J. J. and J. M. Berry, "Mechanical Properties of Pyrolytic Graphite", AIAA Journal, Vol. 3, No. 2, February 1965, pp 302-308.

3. Lockheed Missiles and Space Division Report LMSC-80 1376, "Pyrolytic Graphite Final Report", Volumes I and II, 1 June 1962. AD No.'s 329784, 329785. CONFIDENTIAL.

4. Smith, W. H., "Quality Control Procedures and Results for Pyrolytic Graphite", Pyrolytic Graphite Symposium of American Society for Testing and Materials, 30-31 March 1964, Palm Springs, California. UNCLASSIFIED.

5. Raytheon Co., "(Title -- Unclassified) Pyrofiber, Free Standing Pyrographite and Pyrocarbide", Task III, Contract NOrd 19135 (FBM), Final Report, 14 November 1959 to 13 January 1963. UNCLASSIFIED.

6. AEC TR 4871, "On the Character of the Reaction of Certain Refractory Carbides and Their Solid Solutions with Carbon", K. I. Portnoi, et al, Proceedings of the Academy of Science of the USSR, Div. of Tech. Science, Metallurgy and Fuel, No. 2, pp 147-149, 1961. UNCLASSIFIED.

7. AEC TR 5645, "Phase Diagram of the Hf-HfC System", R. G. Avarbe, et al, Zhurnal Prikladnoi Khimii, Vol. 35, pp 1976-1980, 1962. UNCLASSIFIED.

8. Curtis, C. E., L. M. Doney, and J. R. Johnson, "Some Properties of Hafnium Oxide, Hafnium Silicate, Calcium Hafnate, and Hafnium Carbide", J. Am. Ceramic Soc., Vol. 37, p 458, 1954.

9. Cox, R. L., "A Technique for Measuring Thermal Radiation Properties of Translucent Materials at High Temperature", pp 469-481, NASA SP31, "Measurement of Thermal Radiation Properties of Solids", 1963. UNCLASSIFIED.

10. Moore, V. S., A. R. Stetson, and A. G. Metcalfe, "Emittance Measurements of Refractory Oxide Coatings up to 2900°K", pp 527-533, NASA SP 31, "Measurement of Thermal Radiation Properties of Solids", 1963. UNCLASSIFIED.

TABLE I

PYROLYTIC GRAPHITE TUBES PROCURED FOR HEAT TREATMENT STUDY

Lot No.	Vendor and No. of Tubes	Type	Wall Thickness (in.)	Tube Nos.
1	High Temperature Materials, Inc. (26 tubes)	Machined after deposition	0.060 + 0.000 - 0.005	1 through 26
2	High Temperature Materials, Inc. (15 tubes)	Machined after deposition	0.060 + 0.000 - 0.005	H1 through H15
3	Super-Temp Corp. (15 tubes)	Unmachined	0.060 ± 0.006	S1, S2, S5, S7, S8, S9, S10, S11, S14, S15, S16, S17, S19, S20, S22
4	Super-Temp Corp. (15 tubes)	Machined after deposition	0.060 + 0.000 - 0.005	1S through 15S
5	Pyrogenics, Inc. (1 tube)	Unmachined, Pyroid	0.060 ± 0.006	P1

TMC A673

TABLE II

RESIDUAL STRESSES IN PYROLYTIC GRAPHITE TUBES

Lot No.	Tube No.	Circumferential		Axial	
		Inside (psi)	Outside (psi)	Inside (psi)	Outside (psi)
2	H3	1500	-3300	1360	24
2	H13	2100	-2080	- 160	1200
3	S5	2410	-3760	-1360	450
3	S19	1200	-1910	- 800	850
4	6S	1810	-3360	- 620	500
4	11S	3100	-3170	- 880	68
2	H9	N.A.	-3040	N.A.	500
4	1S	N.A.	-3060	N.A.	500

N.A. = Not available

TABLE III

OBSERVED ELASTIC CONSTANTS FROM RUPTURE TESTS OF PYROLYTIC GRAPHITE TUBES

Tube No.	Elastic Modulus E_1 (psi)	Poisson's Ratio ν_{12}
H9	4.9×10^6	- 0.19
1S	4.1×10^6	- 0.19
14S	4.5×10^6	- 0.23
H15	3.8×10^6	- 0.24
S1	3.8×10^6	- 0.22

TABLE IV

RUPTURE TEST DATA FOR PYROLYTIC GRAPHITE TUBES

Lot No.	Tube No.	Heat Treatment at 2500°F (hours)	Rupture Pressure (psig)	Circumferential Stress on Inside Surface		Effective Tensile Strength (psi)
				Pressure Stress at Rupture (psi)	Residual Stress (Estimated) (psi)	
2	H1	100	295	5,750	1800	7,550
2	H2	100	340	6,400	1800	8,200
2	H4	--	420	8,200	1800	10,000
2	H5	--	420	7,770	1800	9,570
2	H6	30	295	5,450	1800	7,250
2	H7	30	300	5,450	1800	7,250
2	H8	--	550	10,520	1800	12,320
2	H9	100	400	7,500	1800	9,300
2	H10	--	80	1,450	1800	3,250
2	H11	--	110	2,000	1800	3,800
2	H12	--	80	1,560	1800	3,360
2	H15		260	4,720	1800	6,520
2	Average:		295	--	--	7,350
3	S1	100	620	10,200	1800	12,000
3	S2	100	980	16,700	1800	18,500
3	S7		350	5,950	1800	7,750
3	S8		580	10,000	1800	11,800
3	S9		580	9,740	1800	11,540
3	S10		780	12,500	1800	14,300
3	S11		250	4,180	1800	5,980
3	S14		1020	16,100	1800	17,900
3	S15		490	7,750	1800	9,550
3	S16		270	4,320	1800	6,120
3	S17		100	1,530	1800	3,330
3	Average		547	--	--	10,780

TMC A673

TABLE IV (Continued)

Lot No.	Tube No.	Heat Treatment at 2500°F (hours)	Rupture Pressure (psig)	Circumferential Stress on Inside Surface		Effective Tensile Strength (psi)
				Pressure Stress at Rupture (psi)	Residual Stress (Estimated) (psi)	
4	1S	100	210	3,880	2450	6,330
4	2S		520	9,450	2450	11,900
4	3S	100	810	14,700	2450	17,150
4	4S	100	610	11,100	2450	13,550
4	5S		420	7,760	2450	10,210
4	7S		300	5,650	2450	8,100
4	8S		300	5,650	2450	8,100
4	9S		610	11,300	2450	13,750
4	10S		415	7,680	2450	10,130
4	12S		695	13,100	2450	15,550
4	13S		550	10,200	2450	12,650
4	14S		690	12,800	2450	15,250
4	Average		510	--	--	11,870
5	P1		220	7,000	2000	9,000

TMC A673

TABLE V

SURFACE FINISHES OF GRAPHITE MANDRELS

(All readings in rms)

Lot No.	Sample No.	Vendor	Finish	0.030 Cutoff	0.100 Cutoff
2	1-A	HTM	Machined	60 to 100	80 to 120
	2-A	HTM	Machined	60 to 80	70 to 100
	1-B	HTM	Machined	50 to 80	70 to 100
	2-B	HTM	Machined	60 to 140	80 to 150
3	2-C	Super-Temp	Steel Wool	90 to 100	100 to 110
	2-D	Super-Temp	Steel Wool	75 to 85	100 to 120
4	1-C	Super-Temp	Machined	200 to 240	240 to 280
	1-D	Super-Temp	Machined	200 to 230	240 to 280

TABLE VI

SURFACE FINISHES OF PYROLYTIC GRAPHITE TUBES

(All readings in rms)

Lot No.	Tube No.	Vendor	Location	0.030 Cutoff	0.100 Cutoff
1	25	HTM	Inside, as deposited	110 to 140	180 to 300
3	S8	Super-Temp	Inside, as deposited	65 to 80	90 to 110

TABLE VII

SUMMARY OF LATTICE SPACING MEASUREMENTS
IN PYROLYTIC GRAPHITE TUBES

Measurement No.	Sample No.	Condition of Sample	Lattice Spacing (c_o) (Average) (Angstroms)	Probable Error (Angstroms, ±)
1	11	Fragment	6.8708	0.0067
2	12	Fragment	6.8673	0.0083
3	24	Fragment	6.8656	0.0075
4	25-1	Fragment	6.8716	0.0071
5	25-2	Fragment	6.8715	0.0068
6	26	Fragment	6.8712	0.0057
7	H9-1	As-deposited tube	6.8709	0.0064
8	H9-2	As-deposited tube	6.8712	0.0066
9	H9-3	As-deposited tube	6.8722	0.0075
10	H10	As-deposited tube	6.8699	0.0066
11	H11	As-deposited tube	6.8721	0.0071
12	H12	As-deposited tube	6.8713	0.0065
13	H13	As-deposited tube	6.8704	0.0072
14	1S-1	As-deposited tube	6.8639	0.0063
15	1S-2	As-deposited tube	6.8642	0.0065
16	1S-3	As-deposited tube	6.8603	0.0044
17	2S-1	As-deposited tube	6.8704	0.0077
18	3S	As-deposited tube	6.8613	0.0044
19	4S	As-deposited tube	6.8652	0.0062
20	5S	As-deposited tube	6.8634	0.0067
21	H9-1	Heat treated tube	6.8653	0.0059
22	1S-1	Heat treated tube	6.8591	0.0053
23	3S	Heat treated tube	6.8558	0.0054
24	4S	Heat treated tube	6.8590	0.0058
25	S1-1	As-deposited tube	6.8654	0.0069

TMC A673

TABLE VII (Continued)

Measurement No.	Sample No.	Condition of Sample	Lattice Spacing (c_o) (Average) (Angstroms)	Probable Error (Angstroms, ±)
26	S1-2	As-deposited tube	6.8656	0.0065
27	S2-1	As-deposited tube	6.8646	0.0065
28	S2-2	As-deposited tube	6.8663	0.0070
29	2S-1	As-deposited tube	6.8671	0.0073
30	2S-2	As-deposited tube	6.8618	0.0063
31	S1-1	Heat treated tube	6.8637	0.0049
32	S2-1	Heat treated tube	6.8636	0.0044
33	2S-1	As-deposited, fragment	6.8645	0.0050
34	4S	Heat treated, fragment	6.8608	0.0038
35	P1	As-deposited tube	6.8636	0.0044
36	T1	As-deposited tube	6.8639	0.0044
37	H10	As-deposited fragment 71°F	6.8608	0.0036
38	H10	As-deposited fragment 96°F	6.8663	0.0038
39	H12	As-deposited tube 72°F	6.8644	0.0040
40	H12	As-deposited tube 96°F	6.8677	0.0045

TABLE VIII

MELTING POINTS OF REFRACTORY CARBIDE--GRAPHITE SYSTEMS

Material	Melting Temperature (°F)
Pyrolytic Graphite	$^{s}6600$
HfC	7028
HfC - Graphite eutectic	5882
HfO_2	5252
ZrC	6386
ZrC - Graphite eutectic	5288
ZrO_2	4868
TaC	7010
TaC - Graphite eutectic	5990
Ta_2O_5	3614
NbC	6332
NbC - Graphite eutectic	5702
Nb_2O_3	3221
TiC	5882
TiC - Graphite eutectic	5576
TiO_2	3367

s = Sublimation point

TABLE IX

IMPURITY CONTENT OF ZIRCONIUM AND HAFNIUM TETRACHLORIDE POWDERS

Element	$ZrCl_4$ (ppm)	$HfCl_4$ (ppm)
Al	135.0	175.0
B	0.4	< 0.2
Cb	<100.0	<100.0
Cd	< 0.3	< 1.0
Co	< 5.0	< 5.0
Cr	130.0	< 10.0
Cu	27.0	< 40.0
Fe	1900.0	< 50.0
Hf	41.0	--
Mg	120.0	< 10.0
Mn	52.0	< 10.0
Mo	< 12.0	< 10.0
Ni	46.0	< 10.0
Pb	25.0	< 5.0
Si	650.0	65.0
Sn	< 10.0	< 10.0
Ta	<200.0	< 20.0
Ti	26.0	50.0
V	< 5.0	< 5.0
W	25.0	< 50.0
Zn	< 50.0	--
Zr	--	3.0%

TABLE X

ANALYSIS OF C. P. METHANE

Constituent	Amount (Mole Fraction)
Methane	0.9905
Ethane	0.0012
Carbon dioxide	0.002
Nitrogen	0.006
Propane	0.0003

TABLE XI

RUPTURE TEST DATA FOR ZrC-C TUBES

	Tube MZ-2	Tube MZ-4
Alloy composition	2 Weight % Zr	12 Weight % Zr
Wall thickness, inches	0.036	0.036
Inside radius, inches	1.007	1.112
Pressure at rupture, psig	230	395
Residual hoop stress, psi (Inside surface)	4,700	5,000 (Approx.)
Pressure stress at rupture, psi	6,600	12,400
Tensile strength, psi	11,300	17,400

UNCLASSIFIED

TABLE XII

RUPTURE TEST DATA FOR ZrC-C TUBES

Alloy Composition (Wt. % Zr)	Tube MZ-9					Tube HR-63Z		
	5.4	6.9	8.9	9.3	9.7	2.1	3.0	5.1
Specimen location (inches from bottom)	3	5	6 1/2	8	10	3	6 1/2	10
Inside radius, inches	1.149	1.141	1.142	1.142	1.143	1.150	1.133	1.130
Wall thickness, inches (At gage)	0.033	0.037	0.044	0.037	0.039	0.040	0.052	0.055
Modulus of elasticity (10^6 psi)	7.2	5.1	5.5	5.3	5.6	5.4	5.0	5.2
Poisson's ratio	0.07	0.11	0.10	0.04	--	--	--	--
Pressure at rupture, psig	375	575	425	485	650	400	320	385
Residual hoop stress, psi (Inside surface)	3,950	3,520	2,960	3,520	3,340	1,200	920	870
Pressure stress at rupture, psi	13,600	18,600	11,600	15,700	19,900	11,800	7,200	8,100
Tensile strength, psi	17,500	22,100	14,600	19,200	23,200	13,000	8,100	9,000

THE Marquardt CORPORATION
VAN NUYS, CALIFORNIA
REPORT 6086

TABLE XIII

RUPTURE TEST DATA FOR ZrC-C TUBE MZ-20

	Specimen Location (inches from bottom)		
	3	6 1/2	10
Alloy composition (Weight % Zr)	Neg.	Neg.	Neg.
Inside radius, inches	1.145	1.130	1.130
Wall thickness, inches (At gage)	0.039	0.053	0.053
Density (gm/cc)	2.19	2.19	2.19
Modulus of elasticity (10^6 psi)	4.2	4.5	4.4
Pressure at rupture (psig)	400	665	615
Residual hoop stress, psi (Inside surface)	2,560	2,560	2,560
Pressure stress at rupture, psi	11,600	14,600	13,400
Tensile strength, psi	14,200	17,200	16,000

TABLE XIV

RESIDUAL STRESS DATA FOR ZrC-C

Run No.	Ring Separated from Tube and Severed	Gage Isolated from Thickness	Comments
MZ-16 Position 4	σ_t = 8200 psi σ_ℓ = -3310 psi	σ_t = 5800 psi σ_ℓ = -4870 psi	Isolated from 0.038 to 0.010 in.
MZ-16 Position 9 1/2	σ_t = 3580 psi σ_ℓ = 2900 psi	σ_t = -6300 psi σ_ℓ = 2160 psi	Isolated from 0.048 to 0.011 in.
MH-4* Position 6 1/2	σ_t = -1630 psi σ_ℓ = 1450 psi	σ_t = -3700 psi σ_ℓ = 1310 psi	Isolated from 0.045 to 0.017 in.

* The stresses presented for Tube MH-4 are principal stresses which are 12.4° from the axial and transverse directions

σ_t = Transverse stress

σ_ℓ = Longitudinal stress

TMC A673

TABLE XV

DATA SUMMARY FOR STOICHIOMETRIC ZrC

Microstructure	Fine grained
Density	6.5 g/cc
Flexural strength	46,500 psi at room temperature
Thermal expansion	$6.8/°C \times 10^{-6}$ at 0° to 1075°C
Zirconium content	88.4 weight percent

TABLE XVI

DATA SUMMARY FOR TUBE MZ-7
(6 Weight % Zr)

Microstructure	Fine grained
Density	2.3 g/cc
Flexural strength	39,700 psi at room temperature 24,800 psi at 1800°C
Elastic modulus	2×10^6 psi at room temperature
Thermal expansion	2×10^{-6}/°C at 0° to 1075°C

TABLE XVII

FLEXURAL STRENGTH FOR TUBE MH-3

(22 weight % Hf)

Test Temperature (°C)	Sample Number	Flexural Strength (x 10^3 psi)
20	1	51.3
20	2	56.6
20	3	46.7
20	4	43.9
		Average 49,700 psi
1800	4	70,000
1800	6	50,100
1800	7	60,300
		Average 60,100 psi

TABLE XVIII

FLEXURAL STRENGTHS FOR TUBES MZ-9, MZ-16, MZ-17, AND MH-4

Tube No.	Sample Number	σ_{ult} (x 10^3 psi)	Density (gm/cc)
MZ-9 (6 weight % Zr)	1 2 3 4 5 6	29.7 25.9 27.8 24.1 25.3 28.2 Average 26,800 psi	2.25
MZ-16 (3 weight % Zr)	1 2 3 4 5	35.1 37.9 37.8 40.3 42.5 Average 41,000 psi	2.19
MZ-17 (3.5 weight % Zr)	1 2 3 4 5	40.4 40.1 47.4 39.7 36.4 Average 41,000 psi	2.19
MH-4 (3.5 weight % Hf)	1 2 3 4 5	23.8 43.7 33.6 34.3 28.1 Average 32,300 psi	2.26

TMC A673

TABLE XIX

SUMMARY OF OXIDATION TESTS OF PYROLYTIC NOZZLE MATERIALS WITH ARC PLASMA HEATED AIR

Run No.	Material	Surface Temperature (Corrected) (°F)	Test Duration (sec)	Erosion Rate (mils/sec)	Remarks
33	PG	5310	26.	5.4	
34	20% ZrC-PG	5060	17.7	5.0	Oxide melted
37	78.6% HfC-PG	5270	15.2	13.3	Oxide melted
40	PG	5130	12.7	4.2	
41	PG	5470	19.5	5.3	
47	PG	4250	30.6	2.6	
49	PG	4150	13.4	2.8	
50	ZrC-PG	4410	30.2	0.6	Oxide discolored
51	78.6% HfC-PG	4400	30.4	0.6	Oxide discolored
54	20% ZrC-PG	4660	58.5	0.6	
58	MTC-XVII-H	4700	15.8	1.8	
60	75% HfC-PG	5240	16.0	0.6	
61	75% HfC-PG	4930	14.8	0.6	

TMC A673

TABLE XX

SUMMARY OF TESTS OF TAPERED, FREE STANDING PYROLYTIC NOZZLES

Nozzle Number	Vendor	Material	Nozzle Expansion Ratio	Wall Thickness at Throat (in.)	Proof Test (psig)	Previous Test Experience (Reference 1)	Test Firing Results with O_2/H_2 (P_c = 100 psia)
1	Berylco	PG	1.38	0.050	100	Total test firing 43 sec. Chipped exit. Low C*	Ruptured before test firing
2	Berylco	PG	1.38	0.050	100	Total test firing 40 sec. Low C*	Ruptured at ignition
3	Berylco	PG	1.38	0.050	--	Ruptured at 90 psig proof.	
4	Berylco	PG	1.38	0.050	150		Two 3 sec performance runs. Ruptured at ignition on this run.
5	Berylco	PG	1.47	0.030	85		Ruptured at ignition
6	Berylco	PG	1.47	0.030	85		None
7	Berylco	PG	1.47	0.030	--		Ruptured after 1.1 sec
8	Berylco	PG	40.			None	None
28-VI	Raytheon	ZrC-PG	1.8	0.067	35		Ruptured at ignition
MTC-XV-Z	Raytheon	ZrC-PG					None
MTC-XVI-H	Raytheon	HfC-PG	2.6	--	--		Tested on mandrel for 30 sec. Erosion rate = 0.2 mil/sec
MTC-XVII-H	Raytheon	HfC-PG	--	--	--		None

PRESSURE TEST FIXTURE FOR PYROLYTIC GRAPHITE TUBES

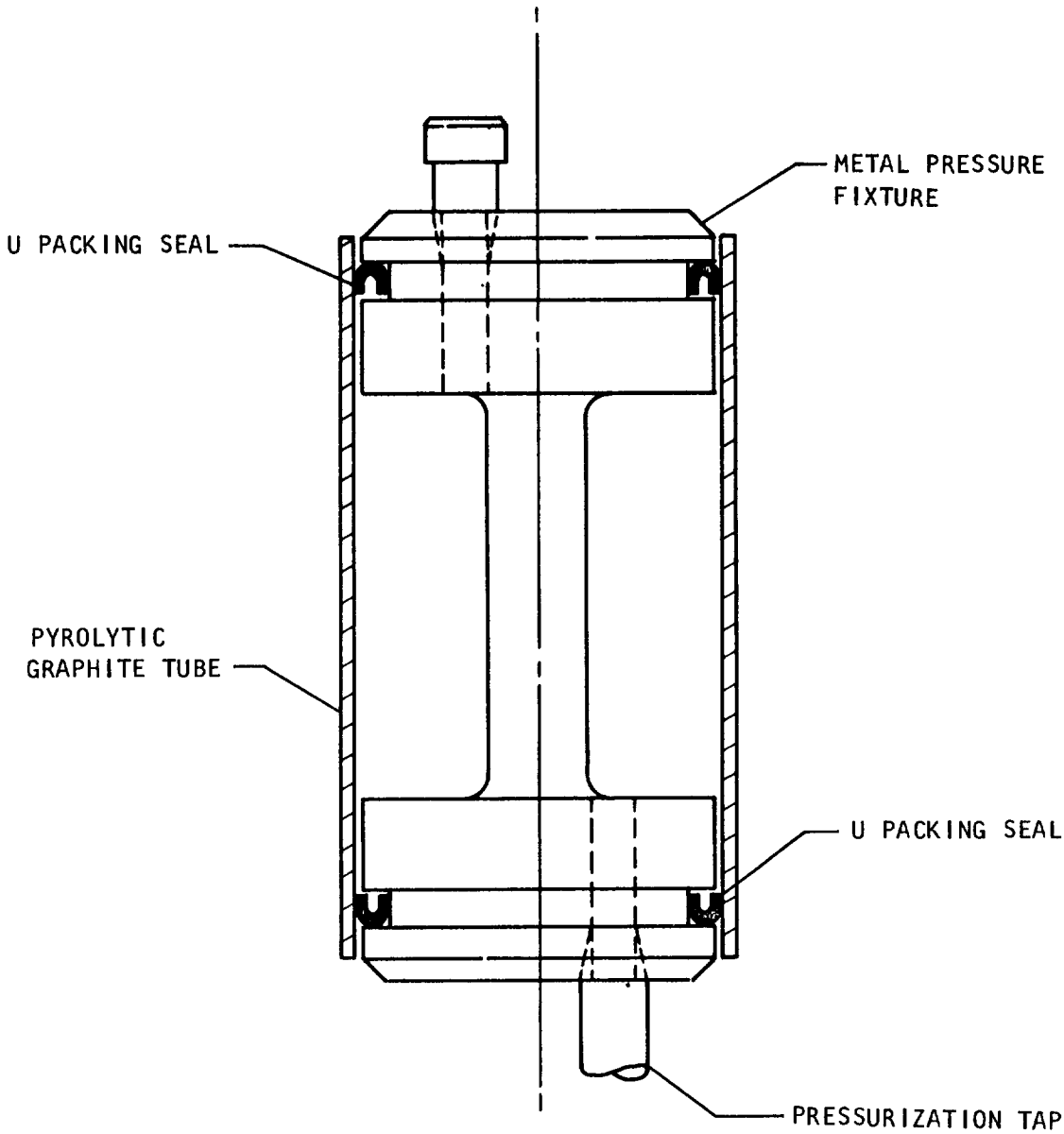

TMC A 673

FIGURE 1

VARIATION OF MAXIMUM NODULE DIAMETER WITH RUPTURE PRESSURE FOR PG TUBES, LOTS 1 & 2

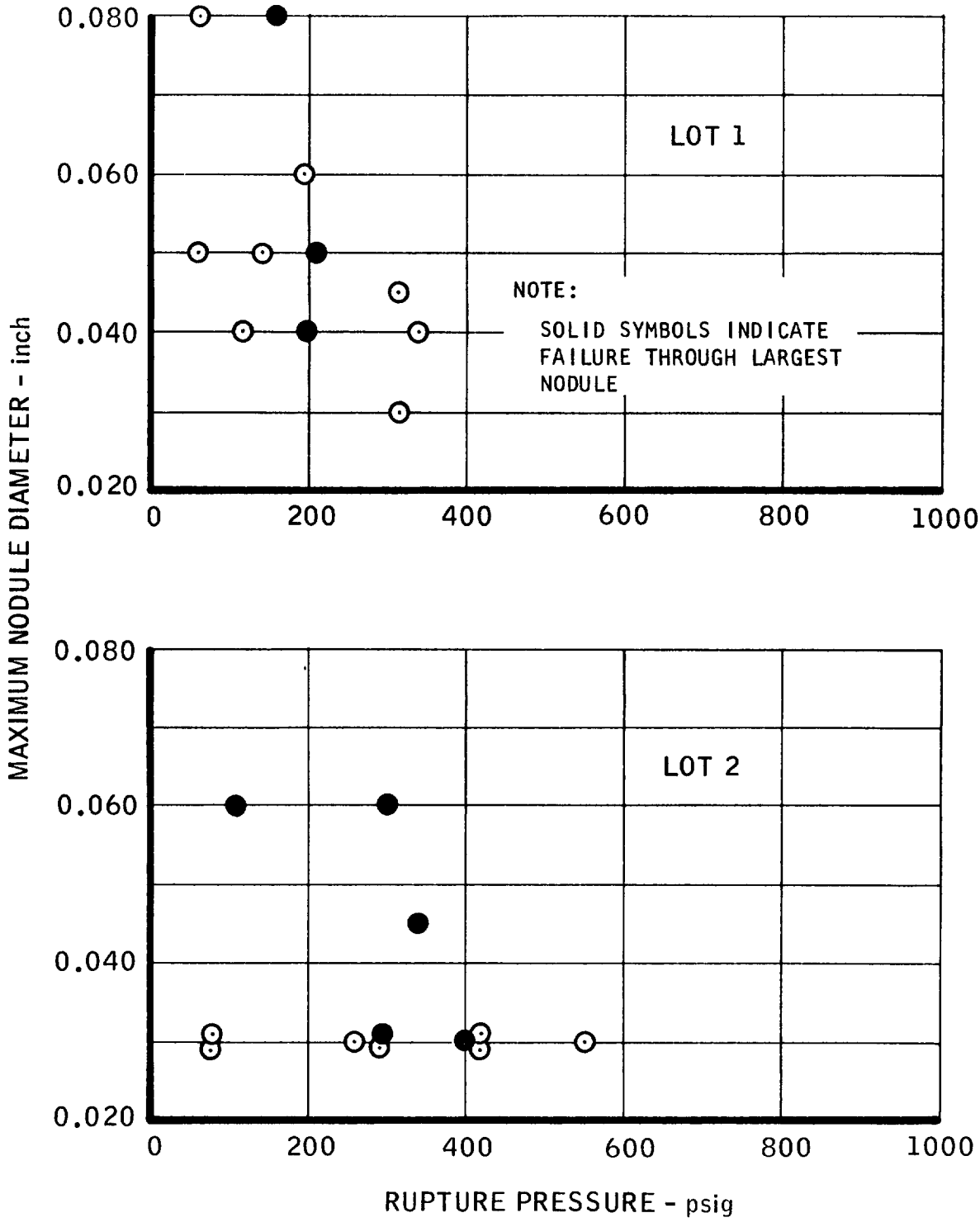

TMC A673

FIGURE 2

VARIATION OF MAXIMUM NODULE DIAMETER WITH RUPTURE PRESSURE FOR PG TUBES LOTS 3 & 4

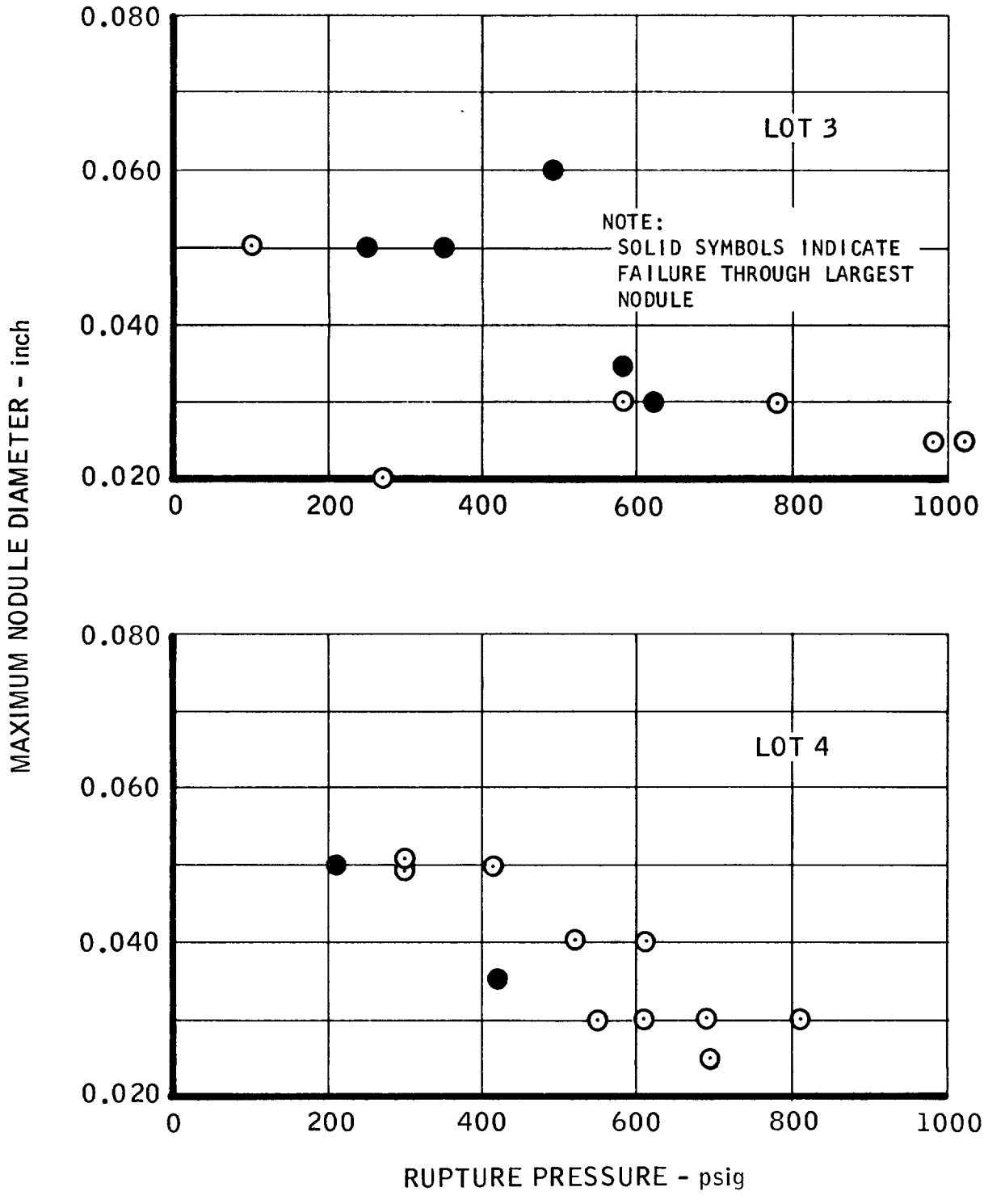

TMC A 673

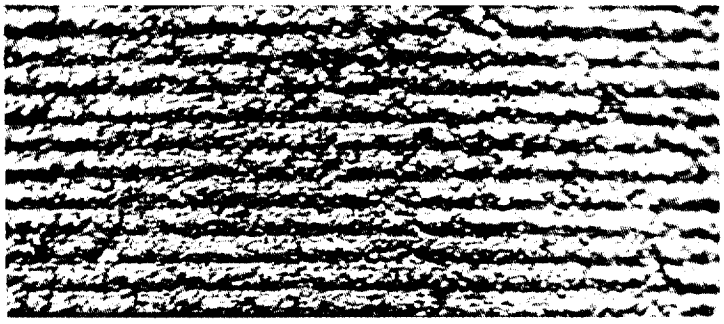

A. OD Surface (10X)

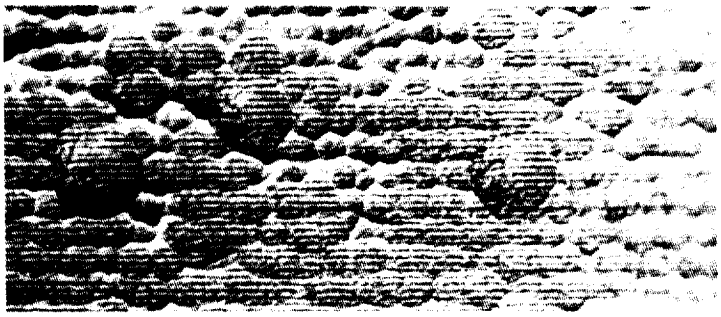

B. ID Surface (10X)

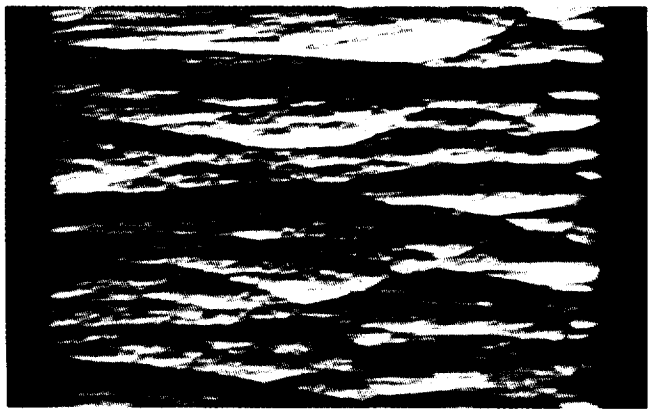

C. Cross Section (50X)

FIGURE 4. Microstructure of PG Tube 23, Lot 1
(Rupture Pressure = 70 psig)

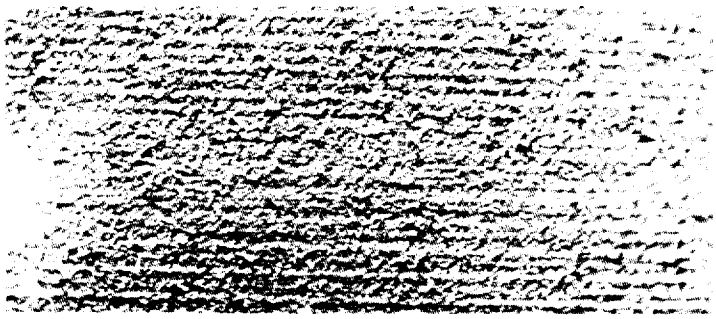

A. OD Surface (10X)

B. ID Surface (10X)

C. Cross Section (50X)

FIGURE 5. Microstructure of Tube H5, Lot 2
(Rupture Pressure = 420 psig)

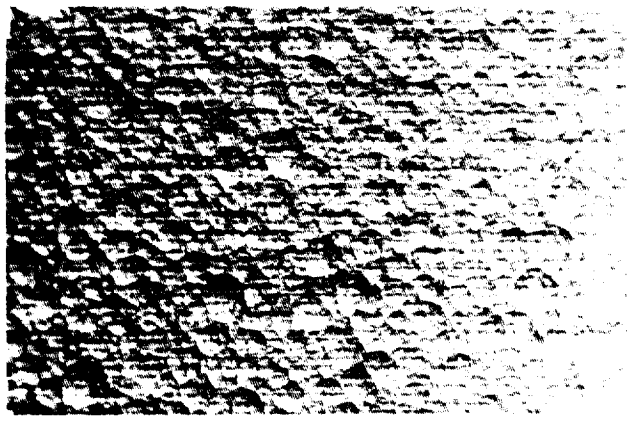

A. (10X)

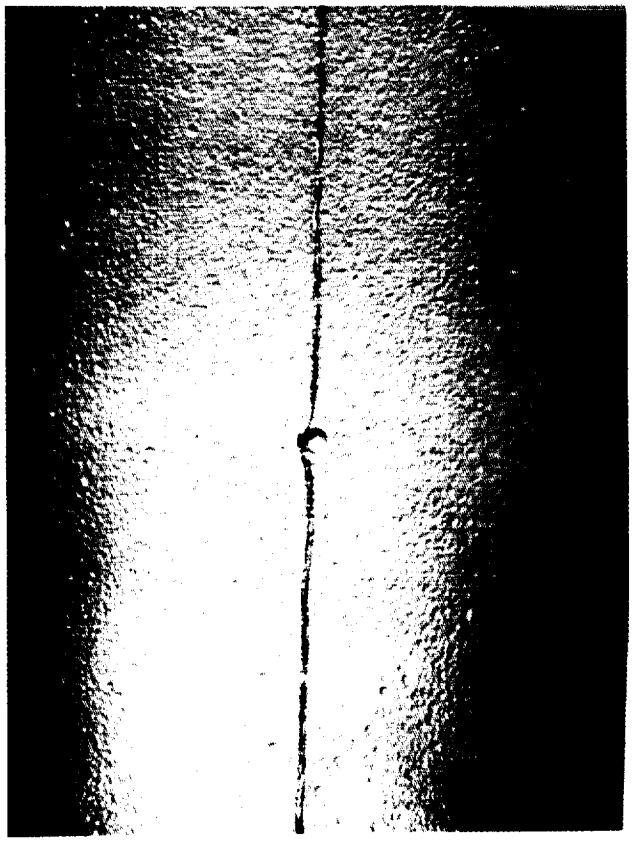

B. (2X)

FIGURE 6. Inside Surface of PG Tube H11, Lot 2
(Rupture Pressure = 110 psig)

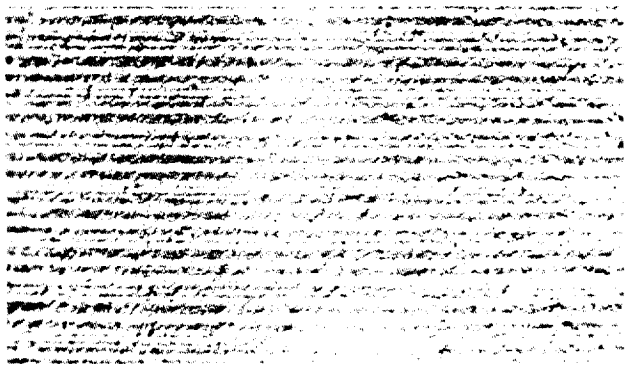

A. OD Surface (10X)

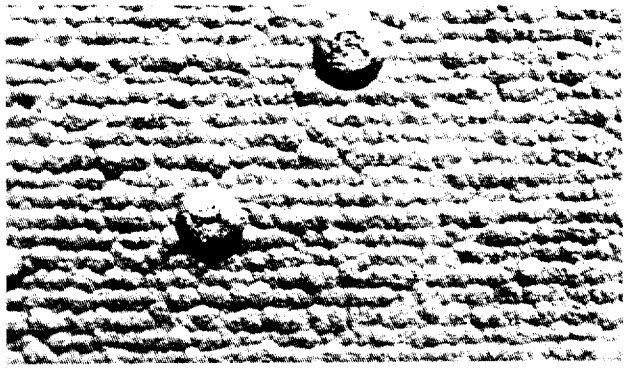

B. ID Surface (10X)

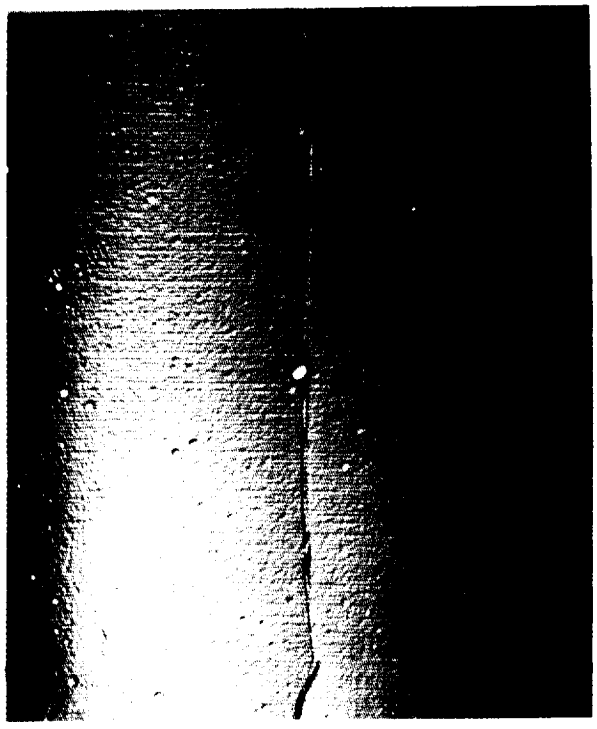

C. ID Surface (2X)

FIGURE 7. Surfaces of PG Tube S11 Lot 3
(Rupture Pressure = 250 psig)

TMC A673

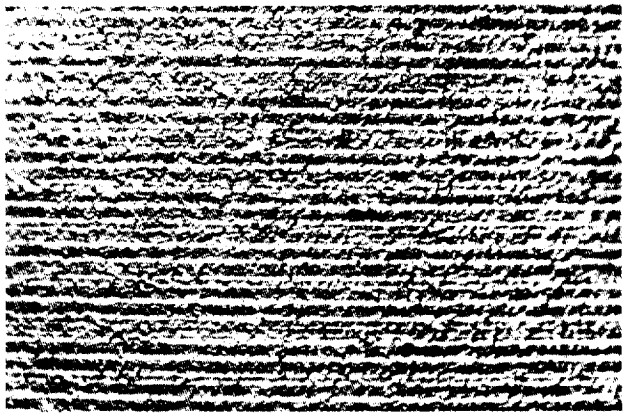

A. OD Surface (10X)

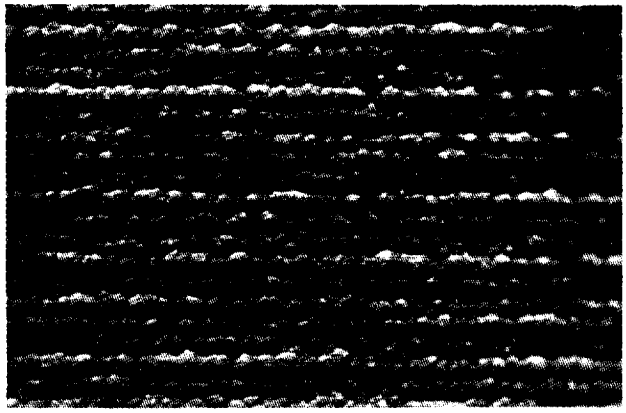

B. ID Surface (10X)

FIGURE 8. Surfaces of PG Tube S14, Lot 3
(Rupture Pressure = 1020 psig)

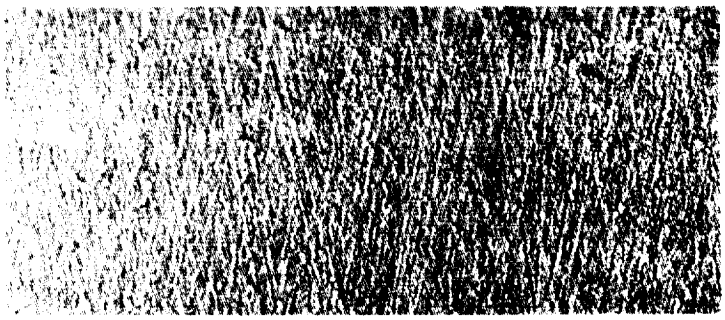

A. OD Surface (10X)

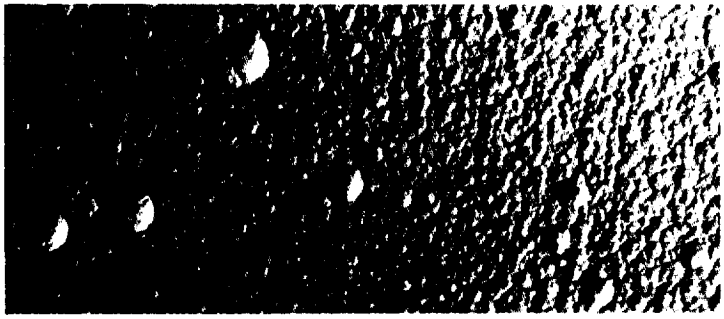

B. ID Surface (10X)

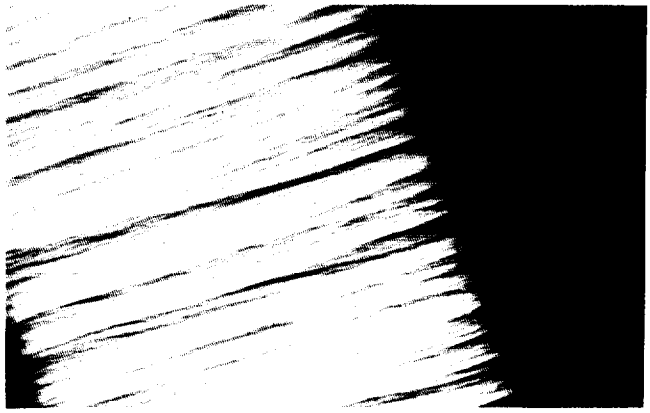

C. Cross Section (50X)

FIGURE 9. Microstructure of PG Tube 1S, Lot 4
(Rupture Pressure = 210 psig)

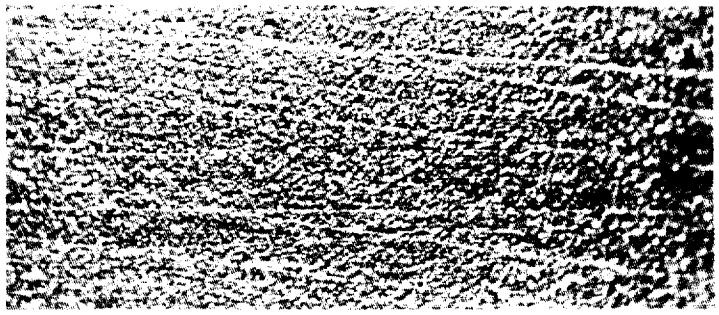

A. OD Surface (10X)

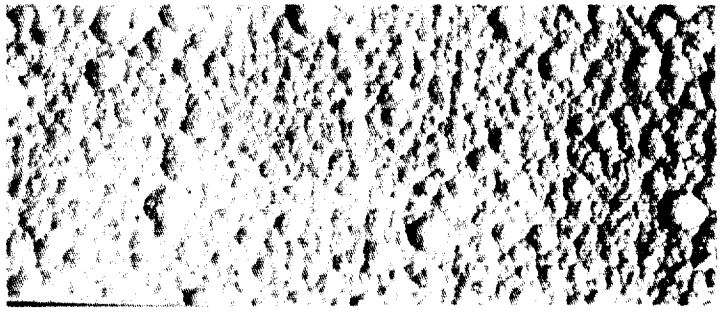

B. ID Surface (10X)

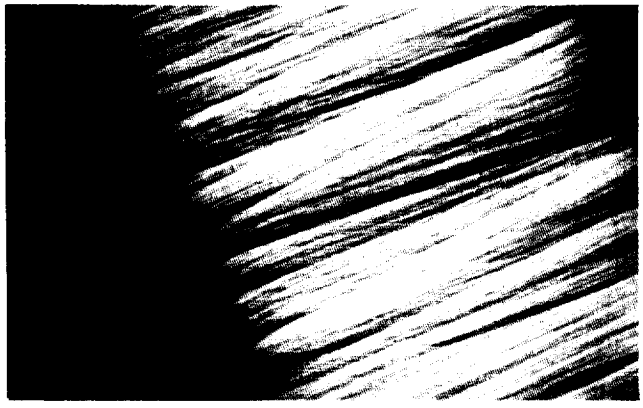

C. Cross Section (50X)

FIGURE 10. Microstructure of Tube 3S, Lot 4
(Rupture Pressure = 810 psig)

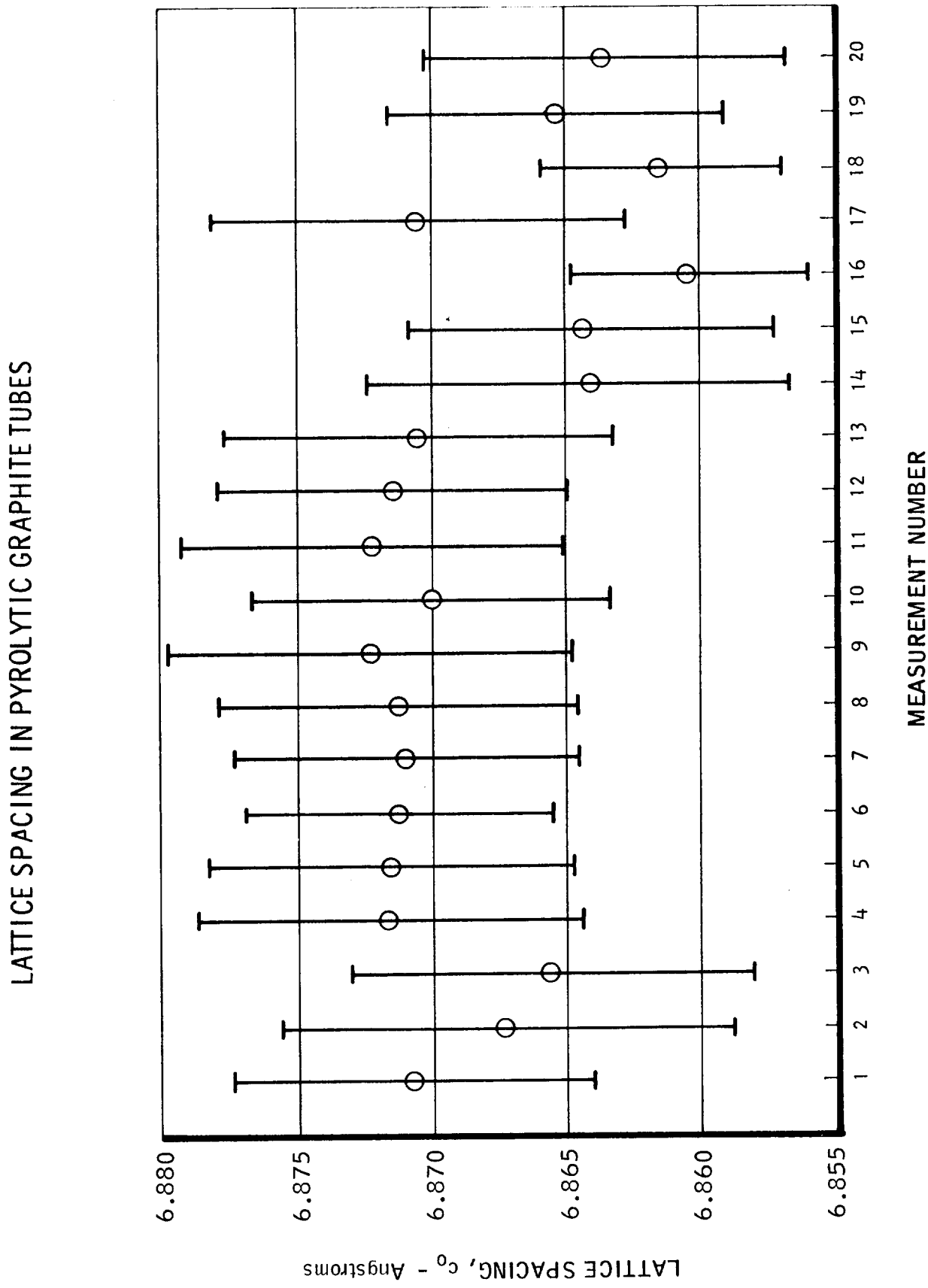
LATTICE SPACING IN PYROLYTIC GRAPHITE TUBES
LATTICE SPACING, c_o - Angstroms
6.880
6.875
6.870
6.865
6.860
6.855
MEASUREMENT NUMBER
1
2
3
4
5
6
7
8
9
10
11
12
13
14
15
16
17
18
19
20

TMC A673

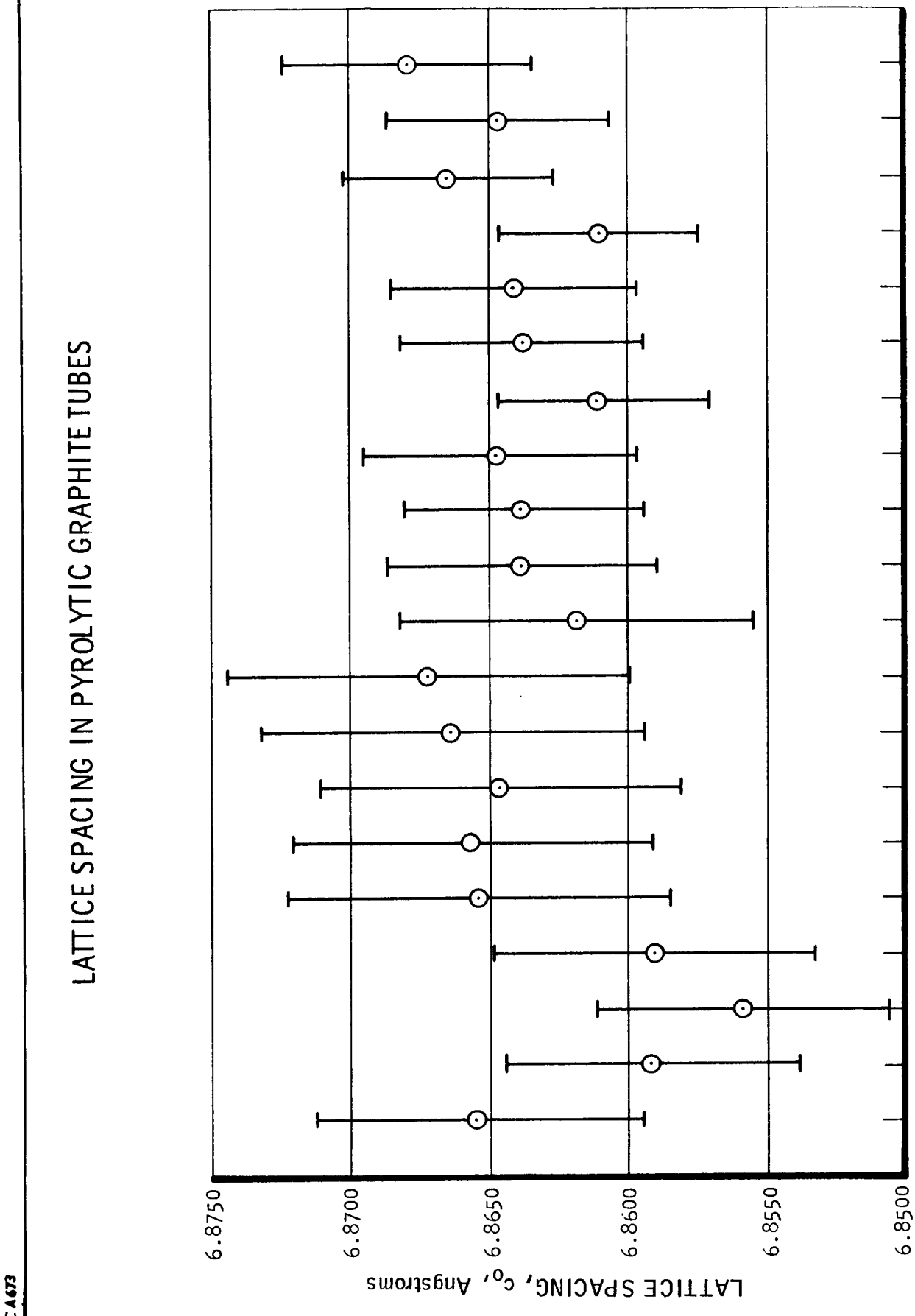

TMC A673

FIGURE 12

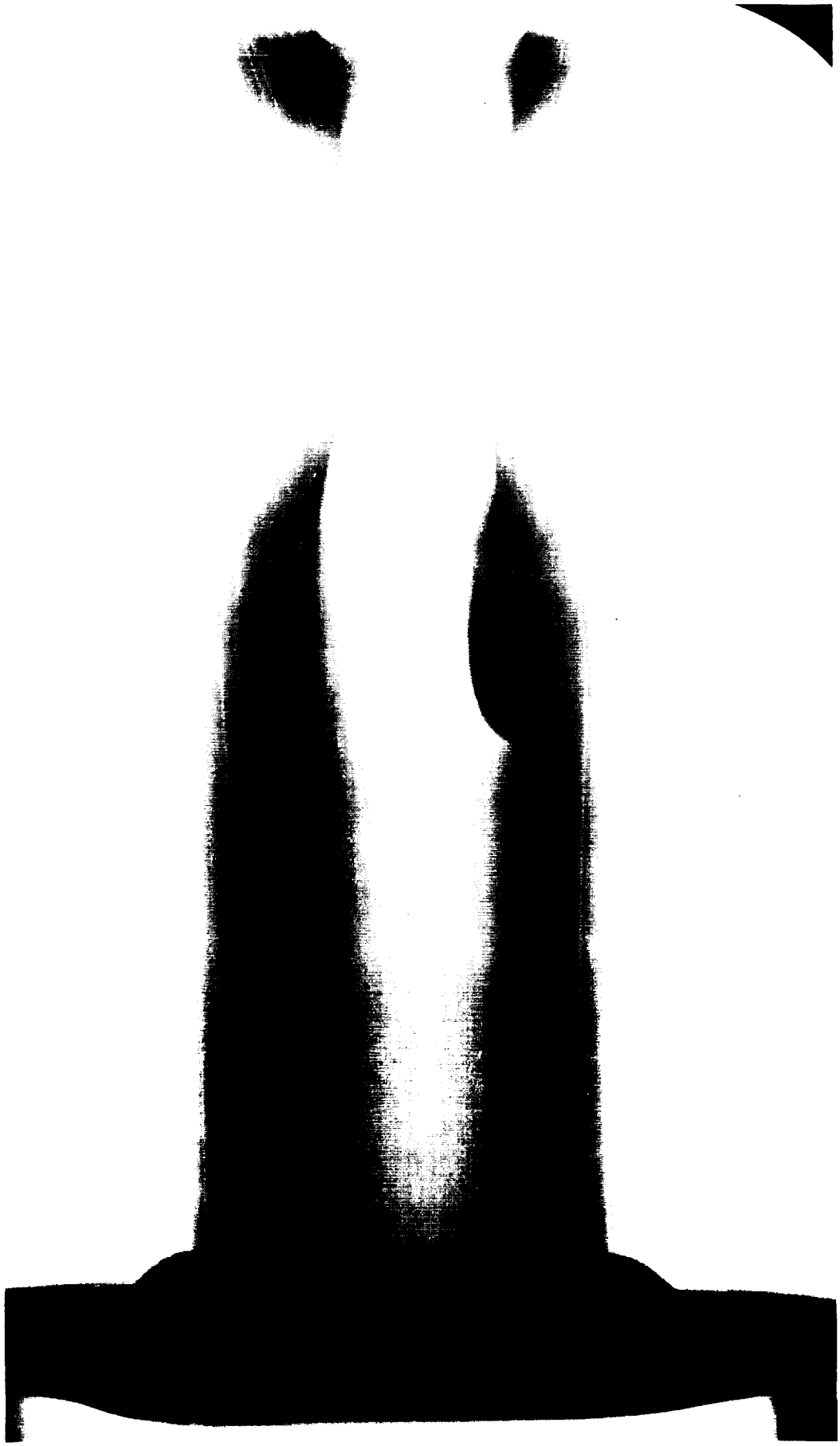

FIGURE 13. X-Ray Photograph of Pyroid Thrust Chamber

TMC A673

6152-3

FIGURE 14. Pyroid Thrust Chamber after Machining

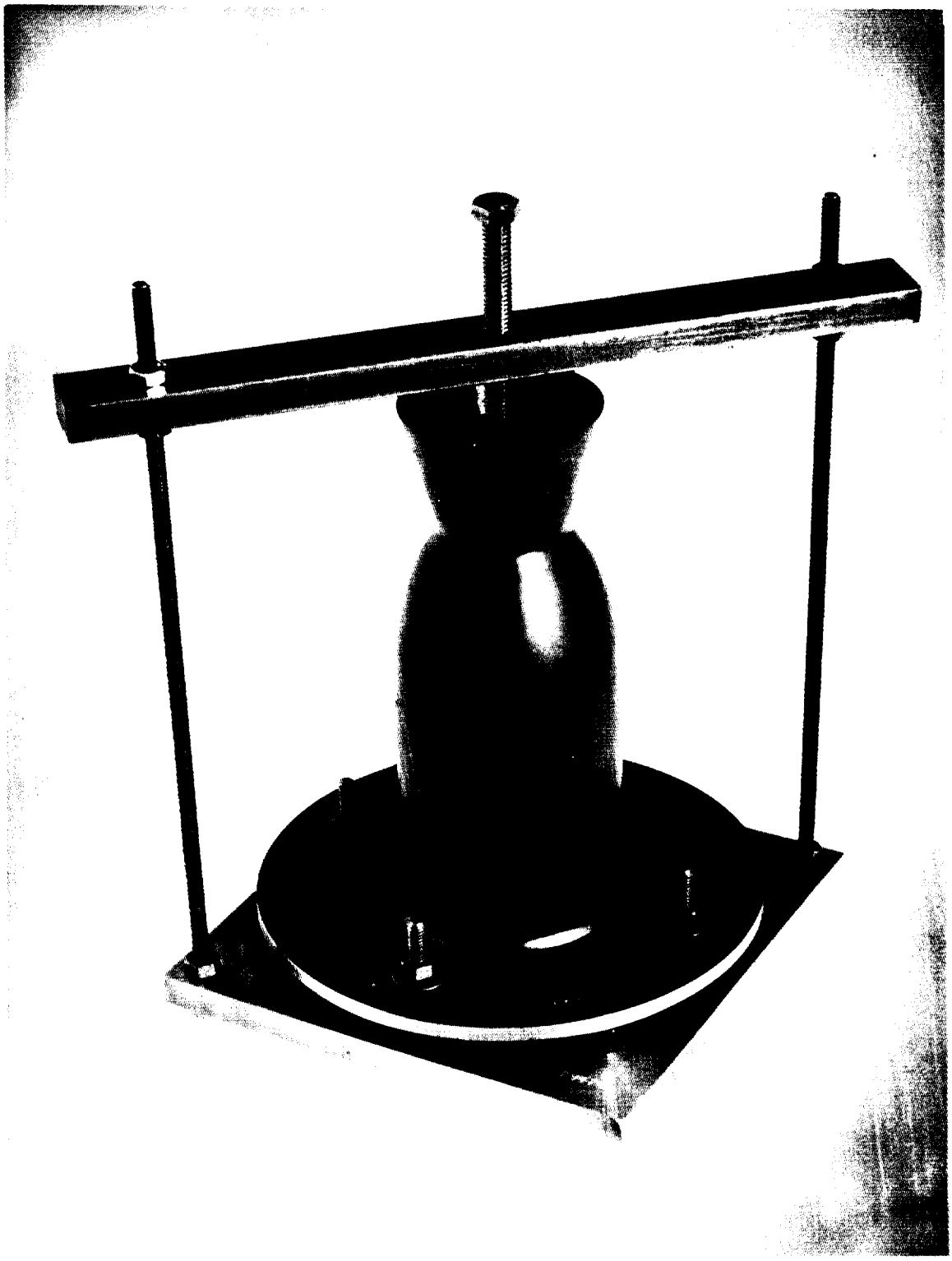

6152-2

FIGURE 15. Pressure [illegible] for Hybrid Thrust Chamber

PROVISIONAL PHASE DIAGRAM OF THE Zr-C SYSTEM

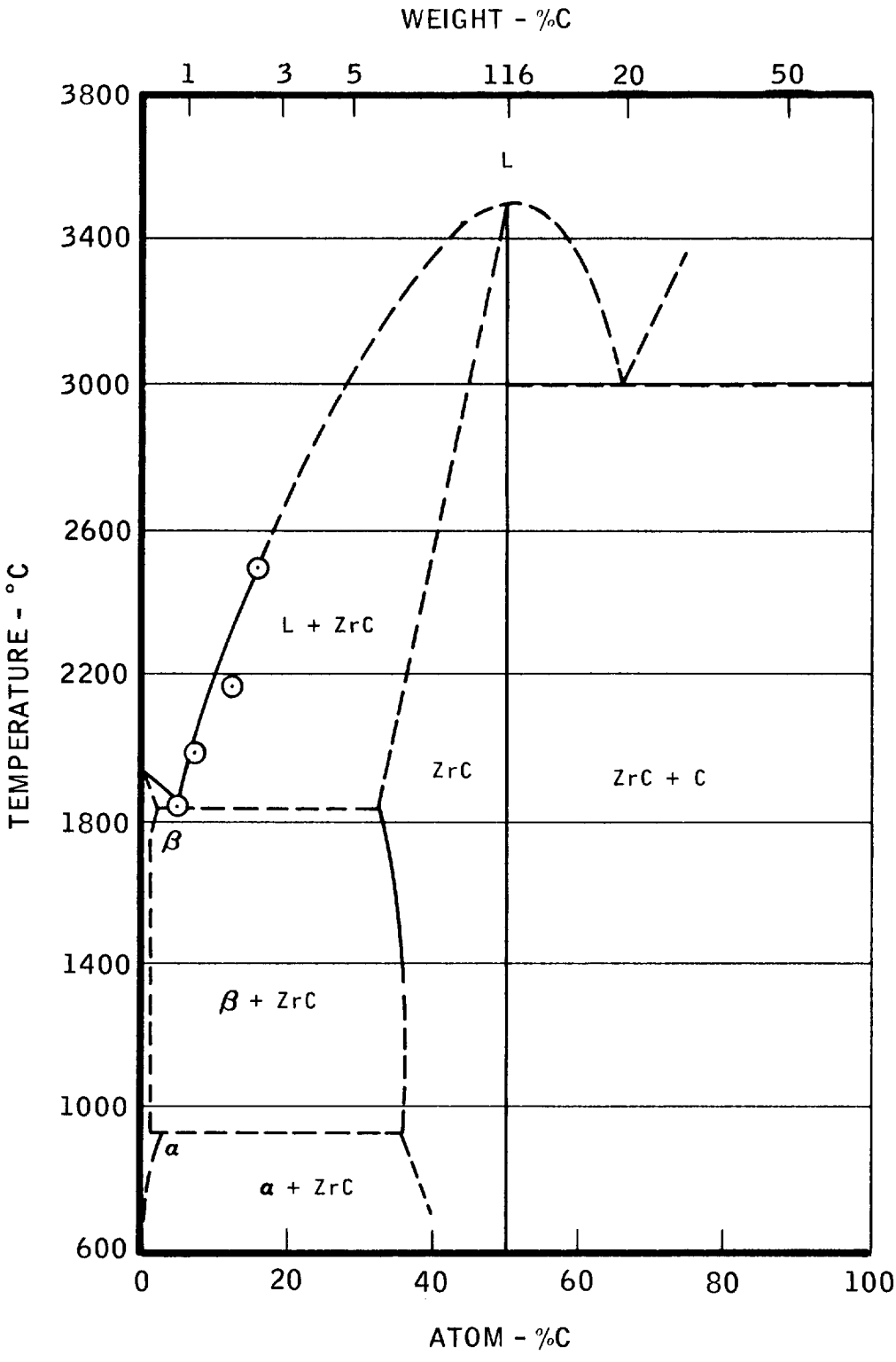

TMC A673

FIGURE 16

FLEXURAL STRENGTH OF ZrC-PG ALLOY

(a-Direction)

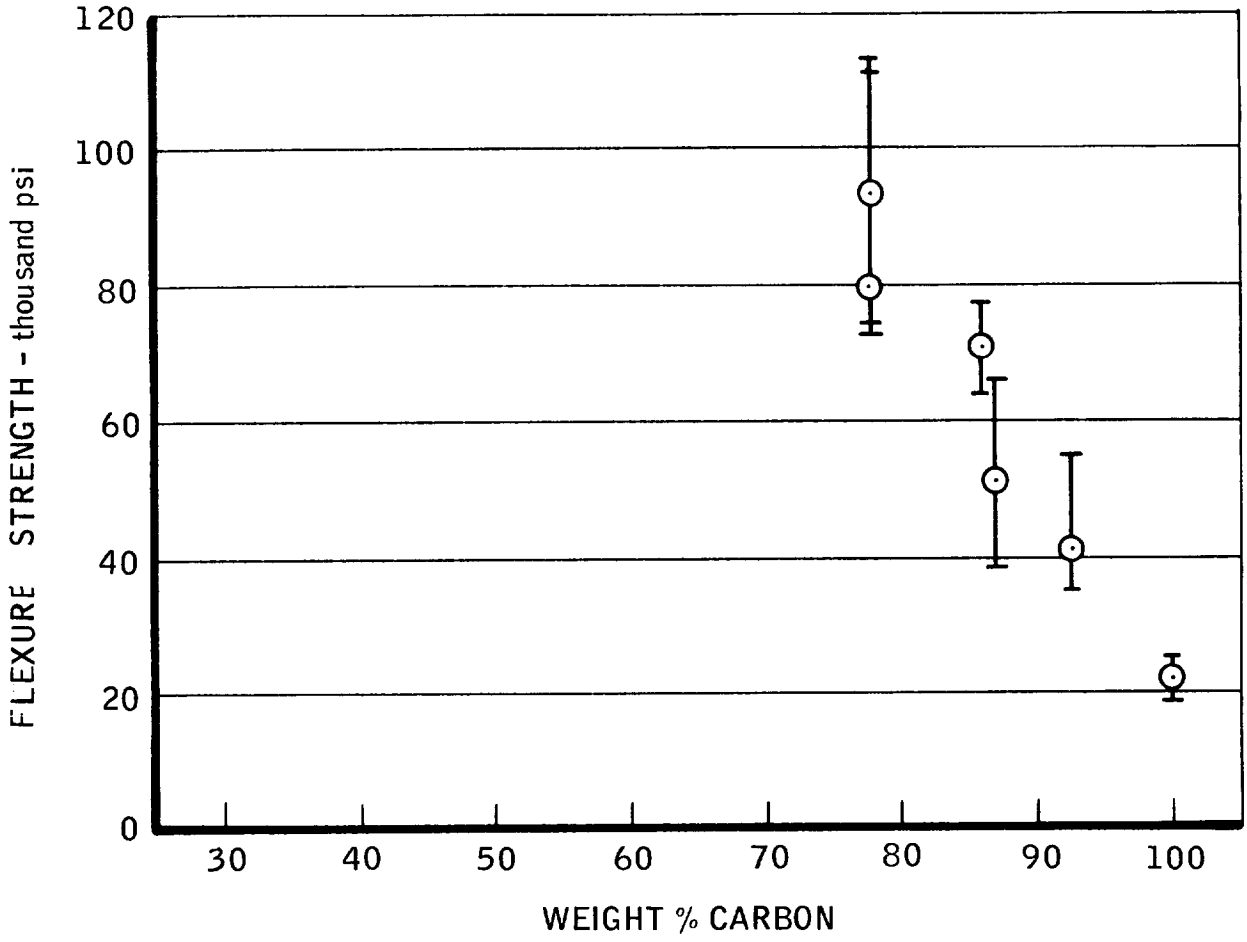

TMC A673

EDGE ORIENTED NOZZLE DESIGN

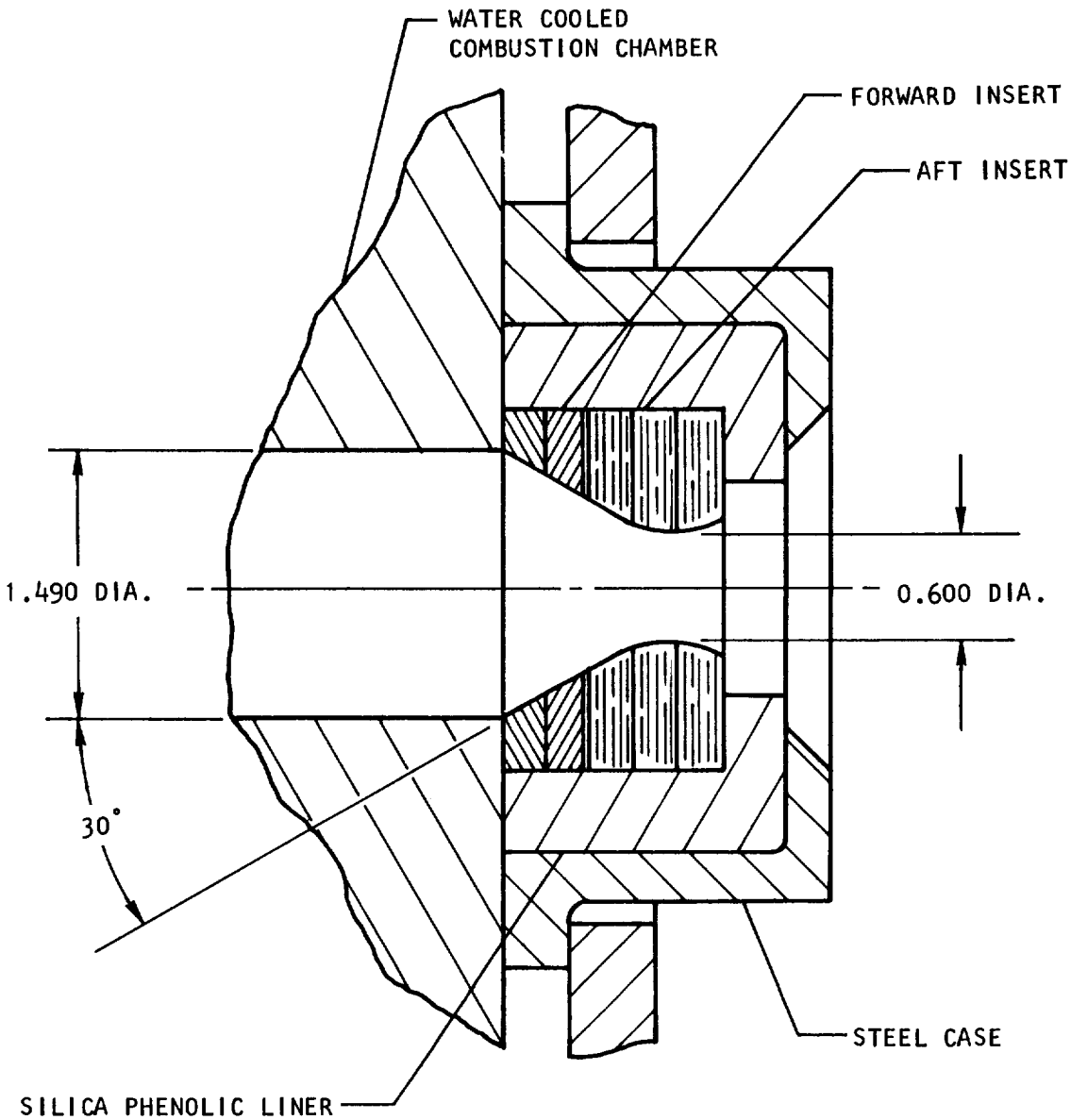

TMC A673

FIGURE 18

TAPERED PYROLYTIC GRAPHITE MOTOR DESIGN

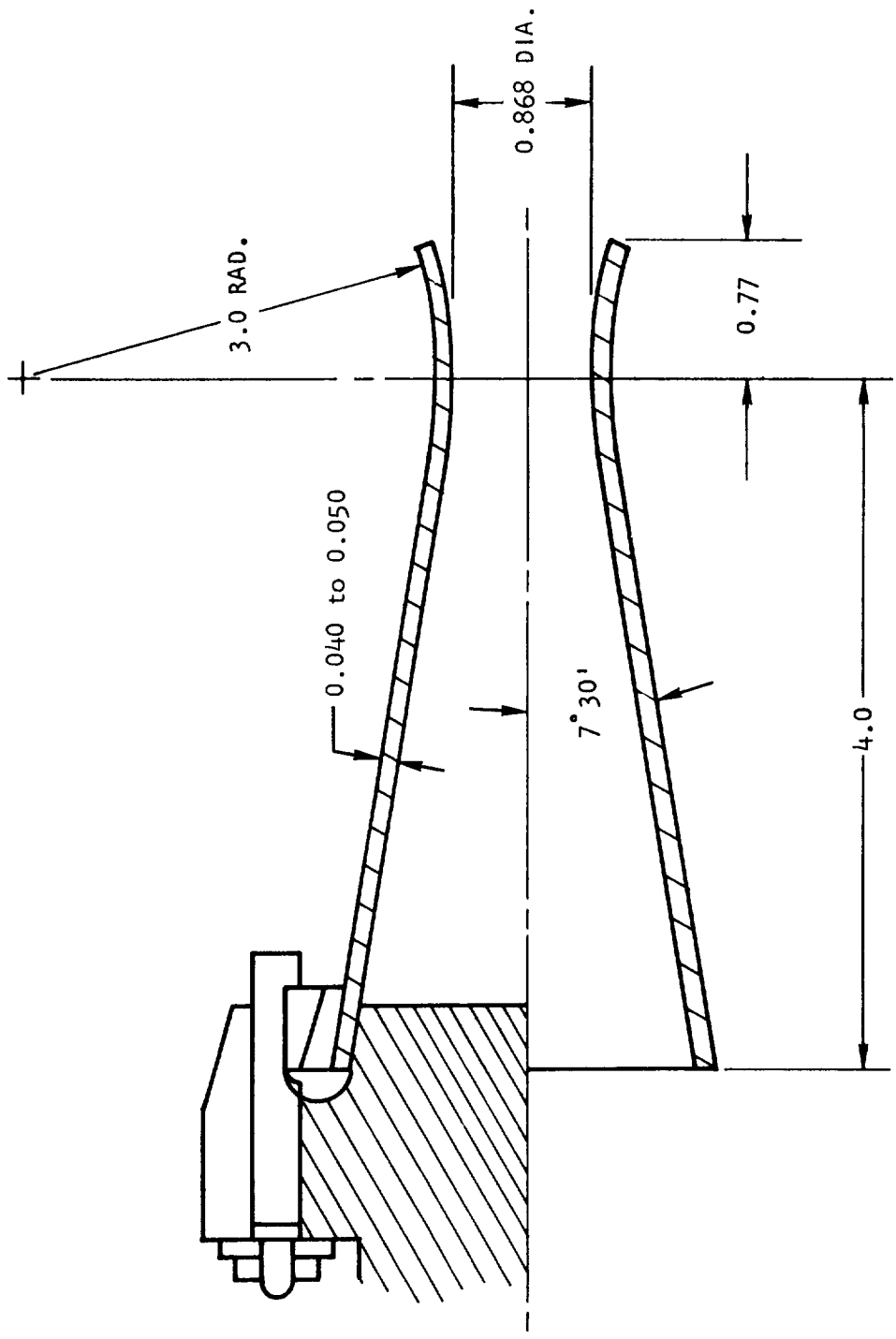

TMC A 673

THERMAL EXPANSION OF ALLOYED AND UNALLOYED PYROLYTIC GRAPHITE PARALLEL TO THE DEPOSITION PLANE

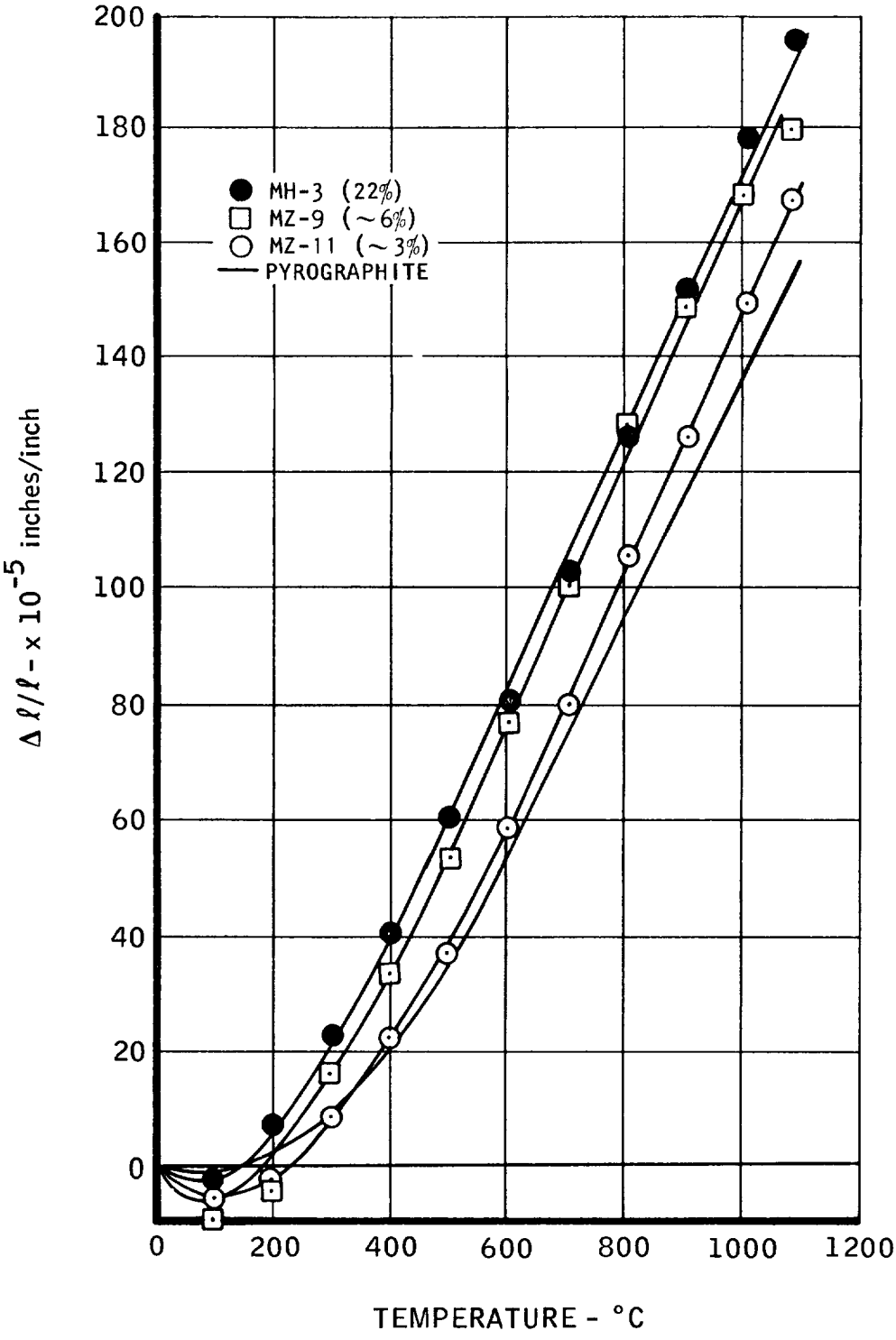

TMC A673

THERMAL EXPANSION FROM RUNS MZ-17 AND MH-4

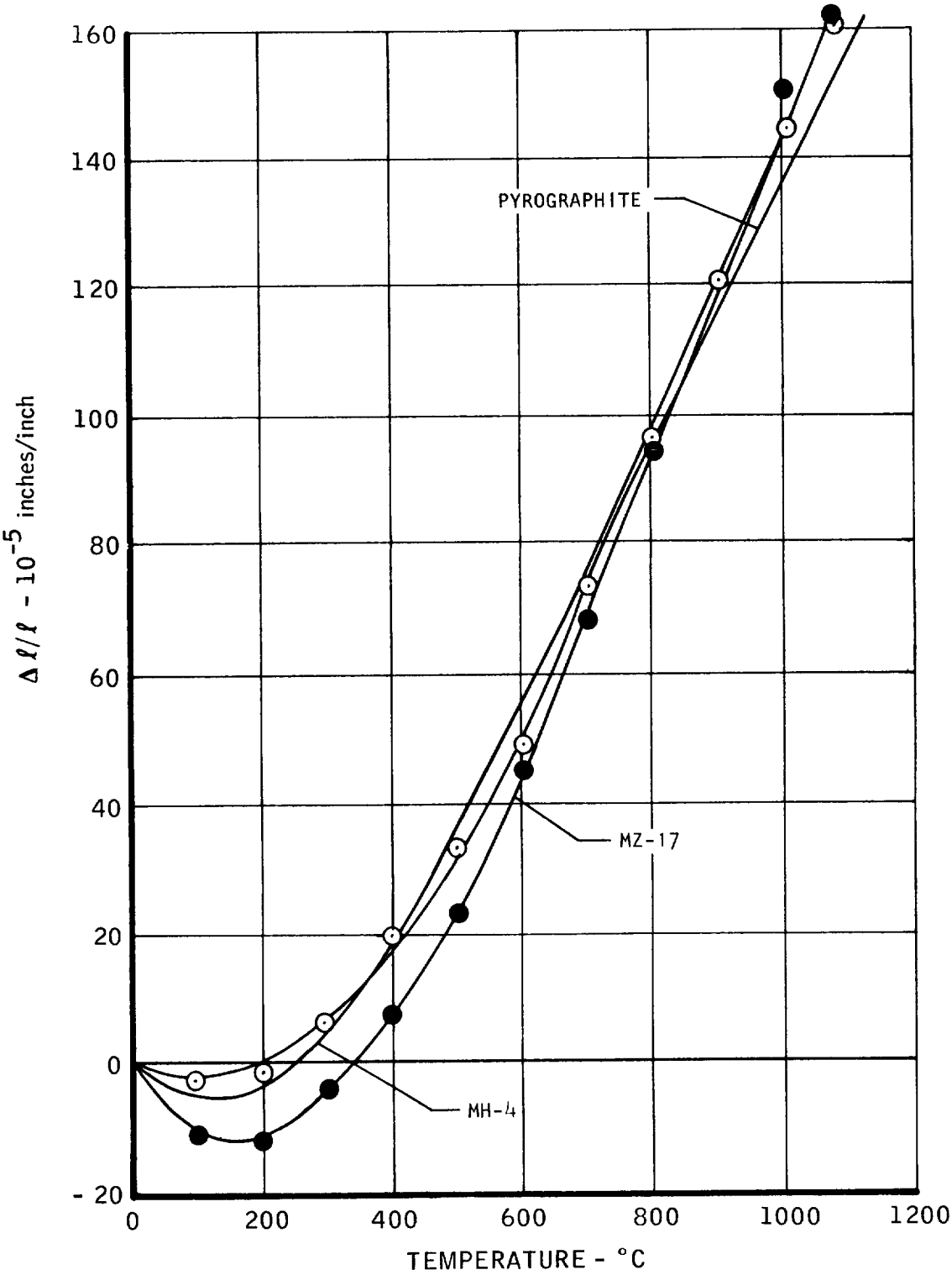

TMC A673

THERMAL EXPANSION FROM RUN MZ-16

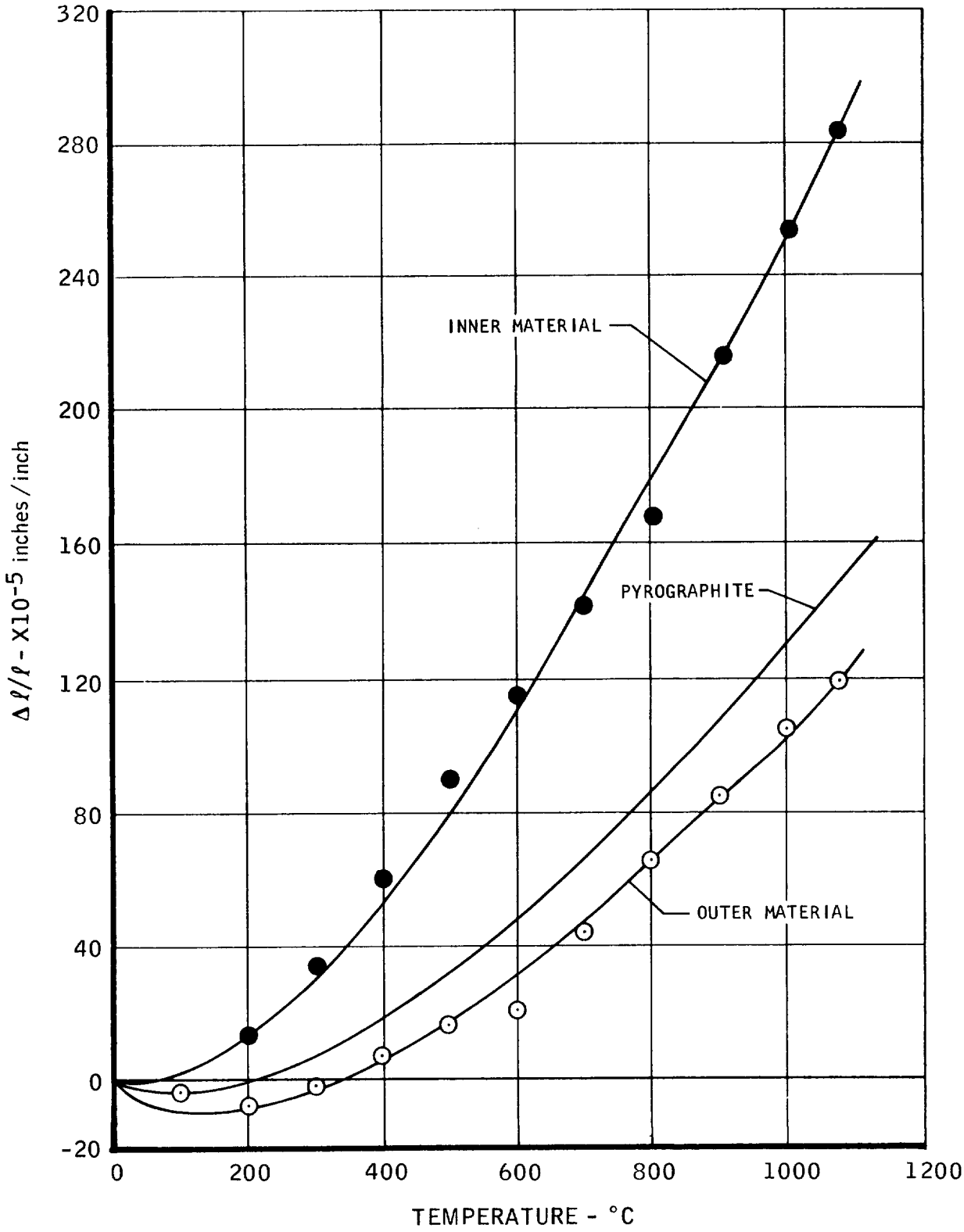

TMC A673

MZ-9

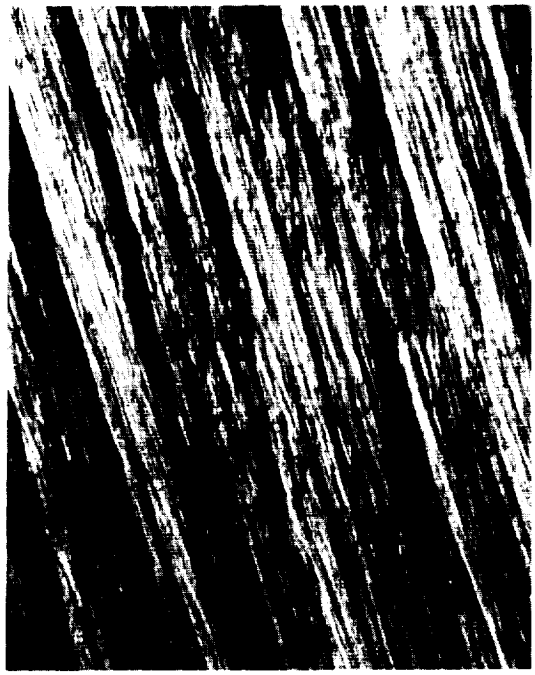

MZ-11

FIGURE 23. Microstructure of MZ-9 and MZ-11 Tube Sections (100X)

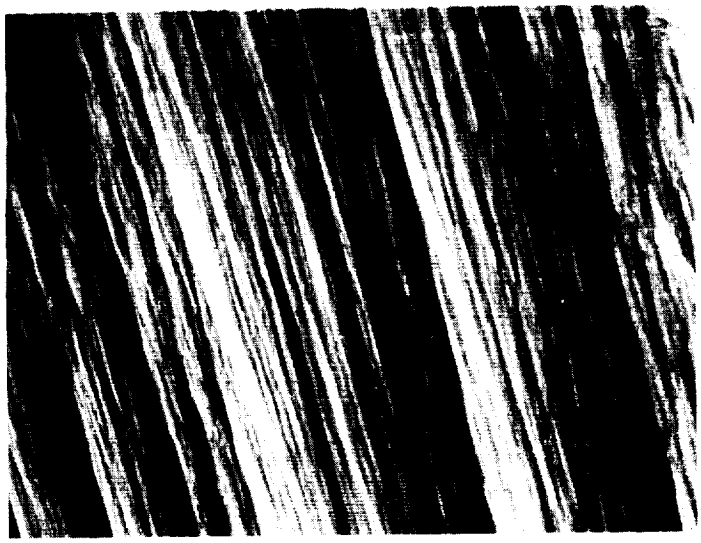

MF-3

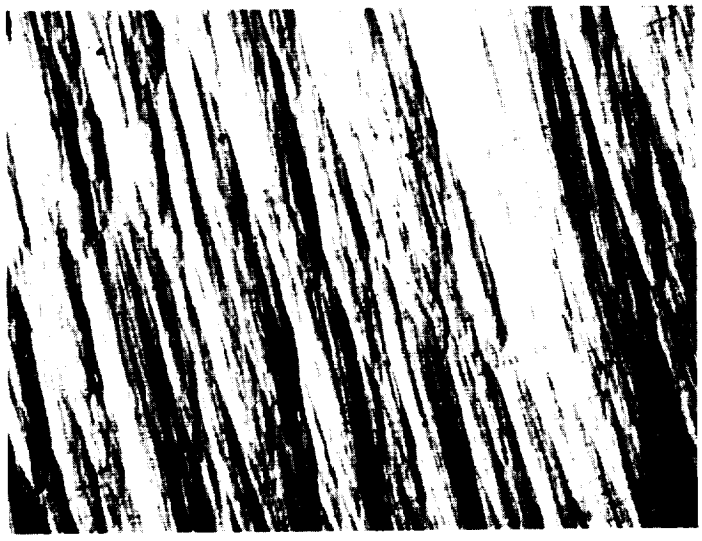

HR63Z

FIGURE 24. Microstructure of MF-3 and HR63Z Tube Sections (100X)

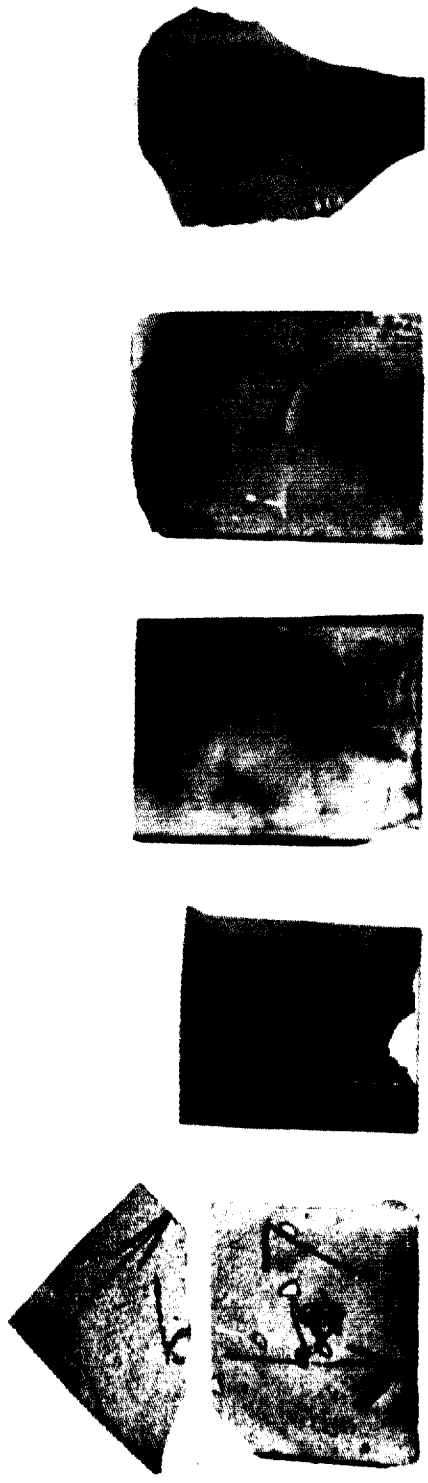

6275-3

FIGURE 25. Top Surfaces of ZrC-PG Samples for Oxidation Testing

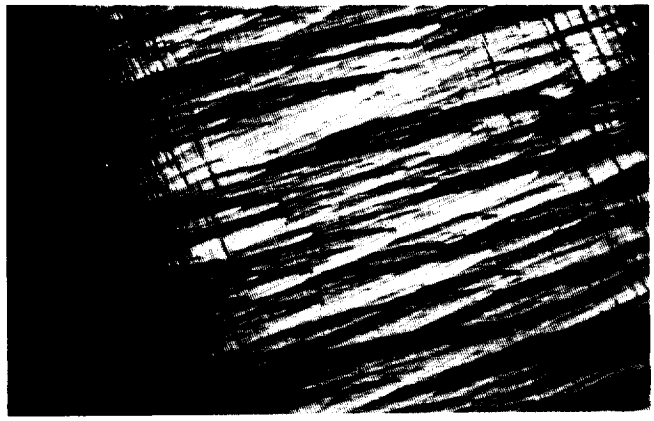

A ZrC-P5 (Current Contract)
20 weight % Zr

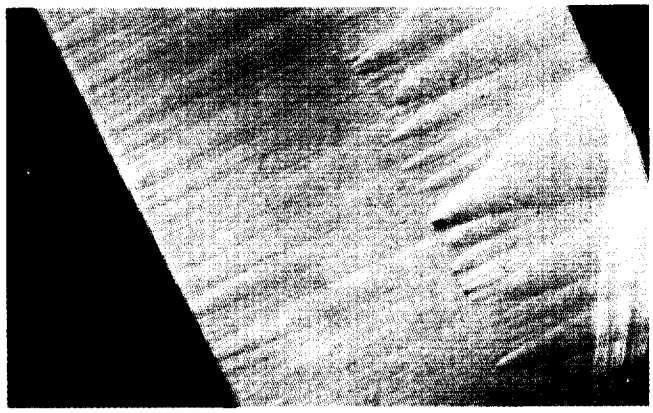

B ZrC-P4 (Previous Contract)
20 weight % Zr

FIGURE 26. Comparison of Microstructures of ZrC-P4 Oxidation Samples (50X)

TMC A673

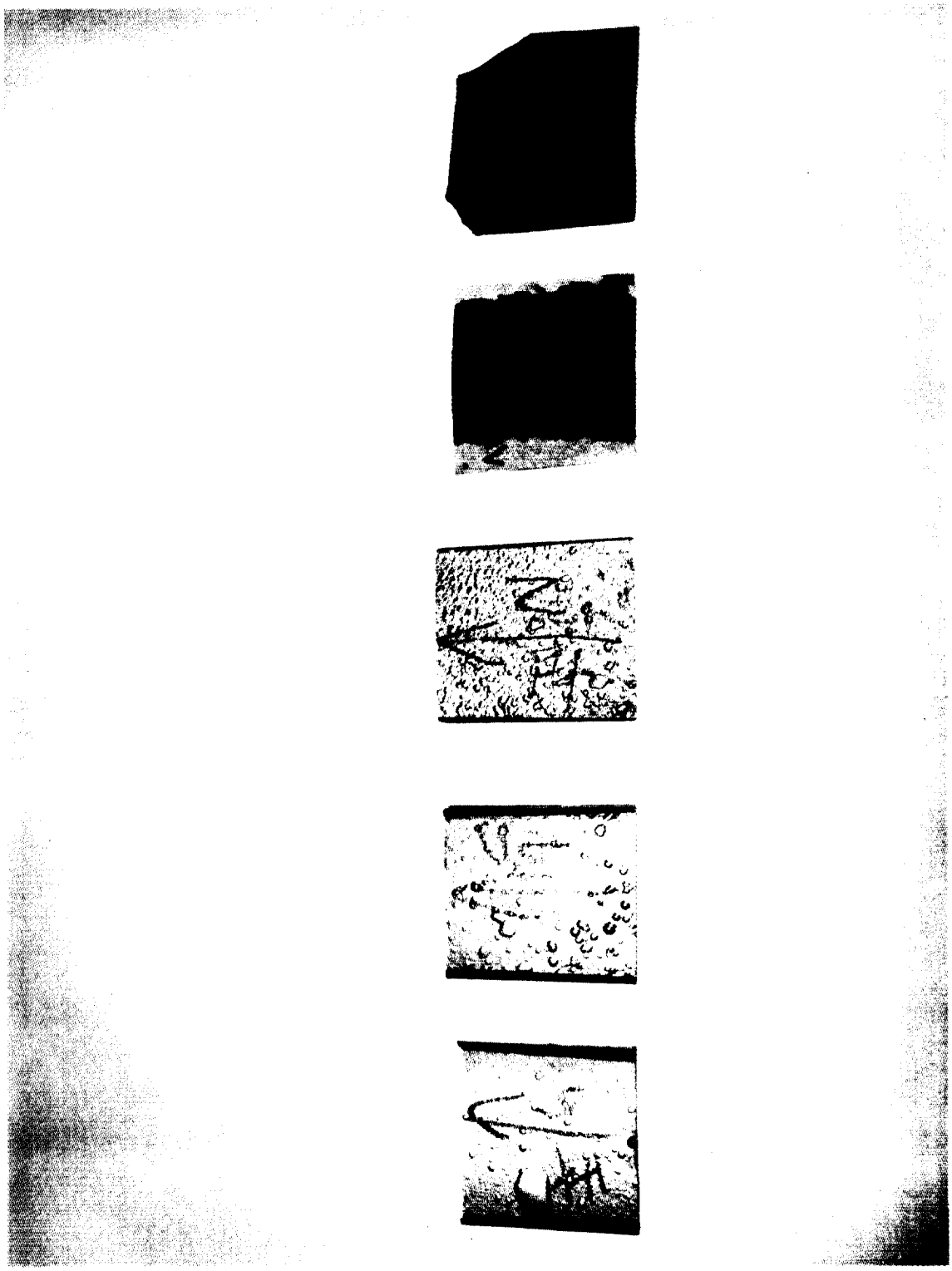

6275-5

FIGURE 27. Top Surfaces of HfC-PG Samples for Oxidation Testing

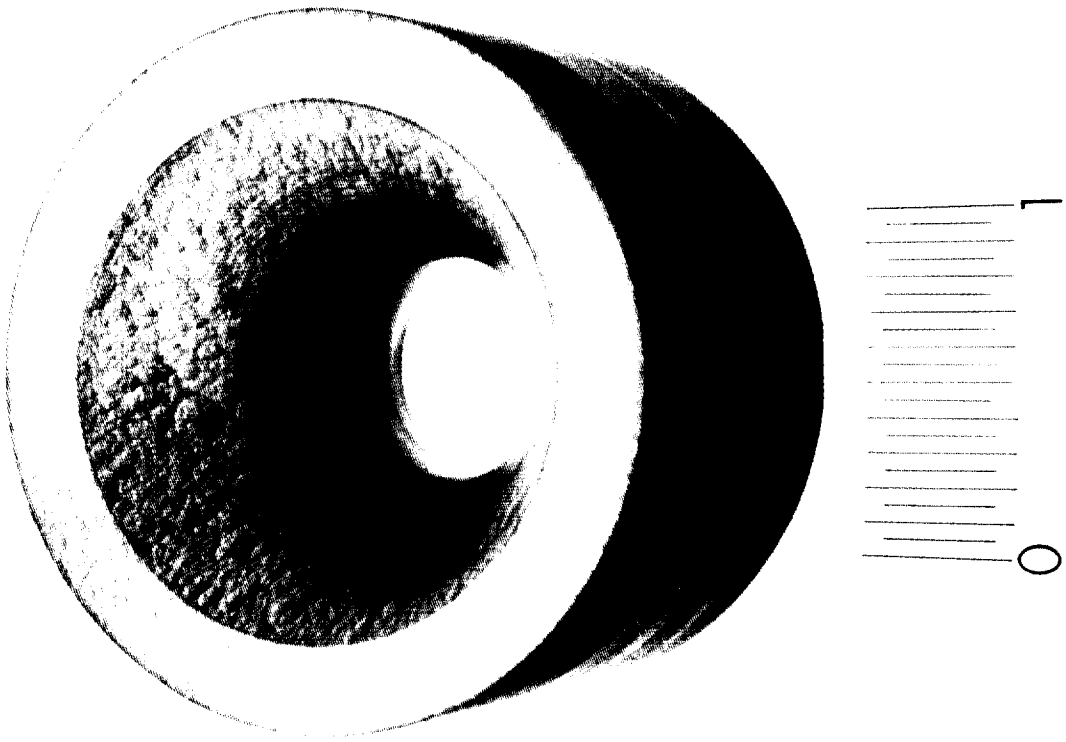

FIGURE 28. Edge Oriented ZrC-PG Nozzle Insert for Motor Testing

6275-1

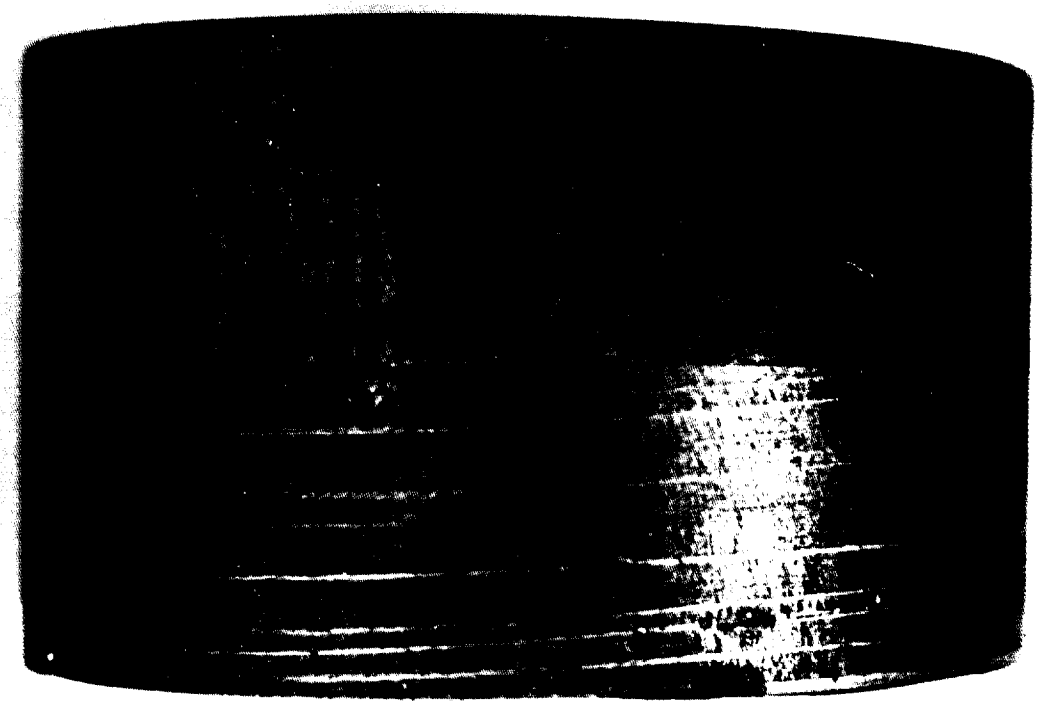

FIGURE 29. Side View of Edge Oriented HfC-PG Nozzle Insert

T3198-2

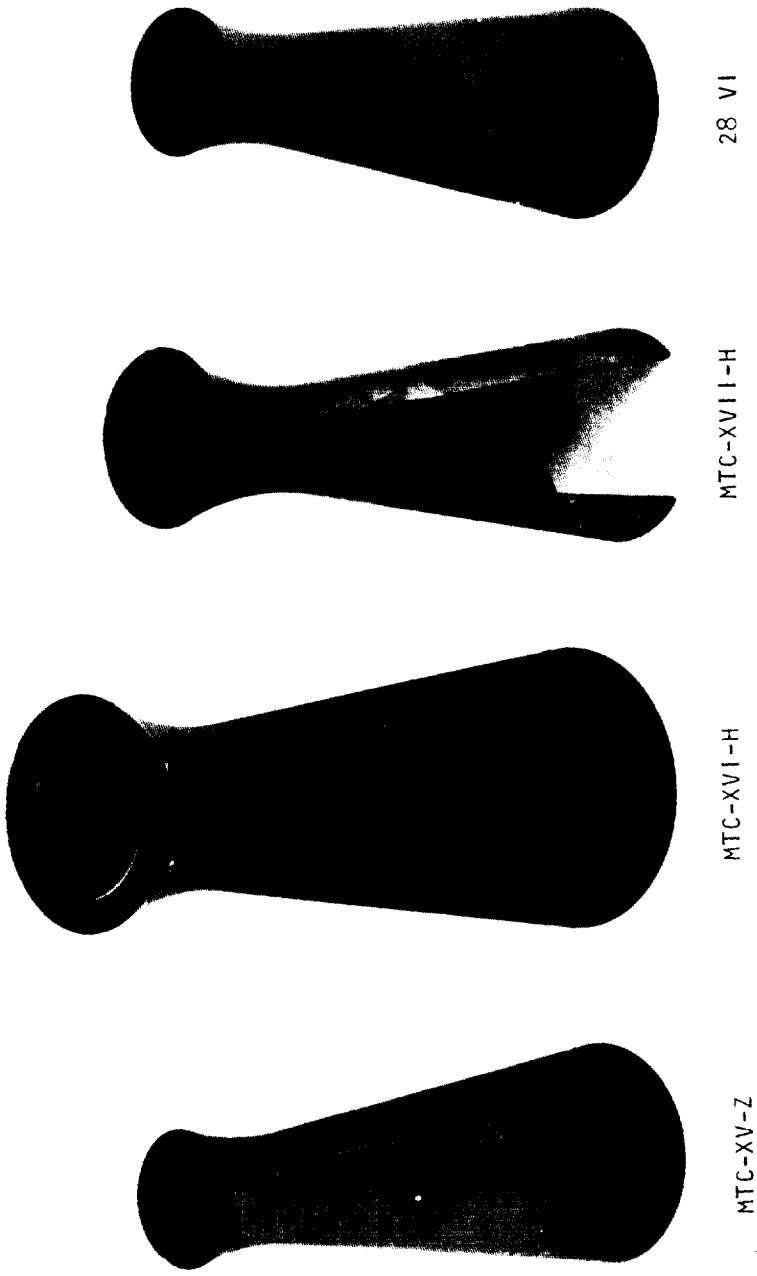

T3198-16
FIGURE 30. Tapered Pyrolytic Graphite Alloy Thrust Chambers Delivered by Raytheon

TMC A673

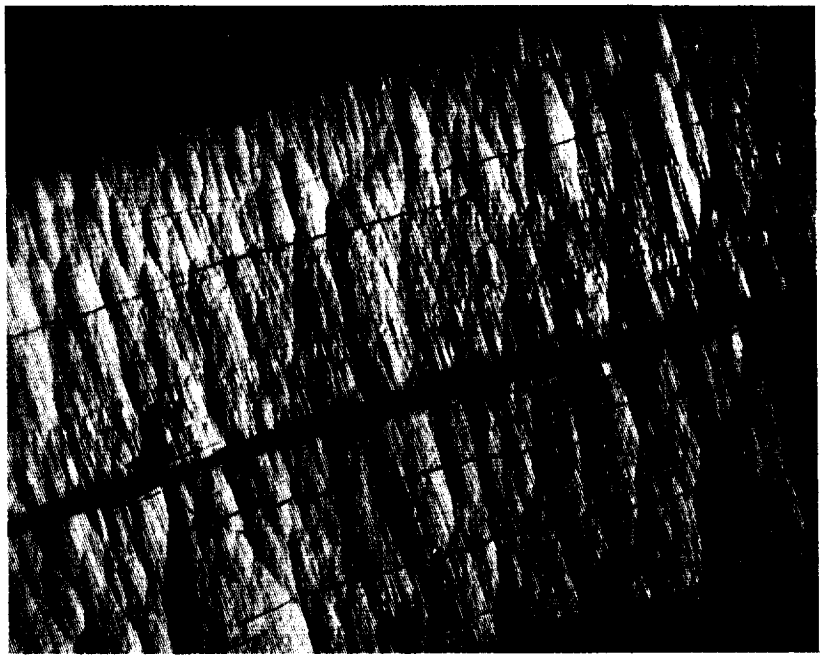

A [illegible]

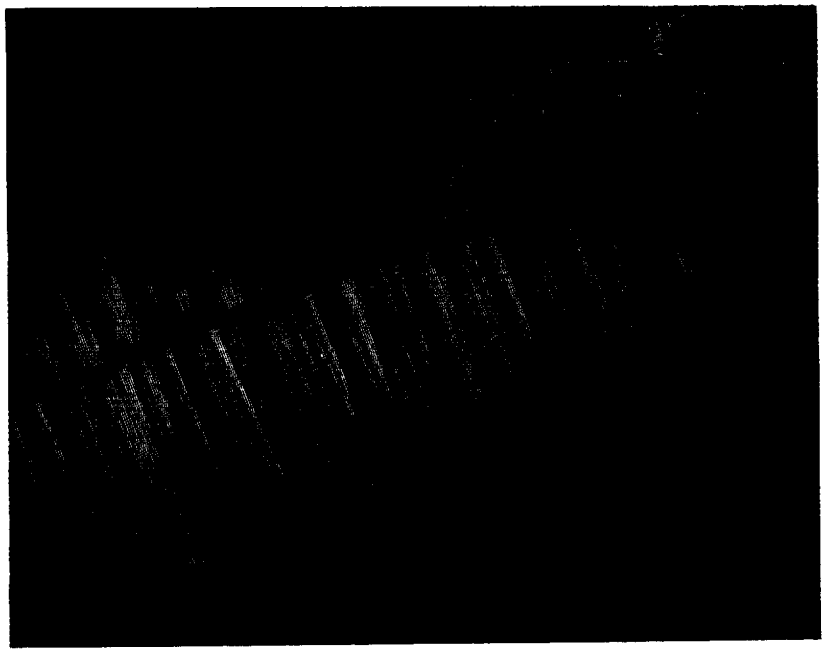

B [illegible]

FIGURE 31. Comparison of [illegible]

EXPERIMENTAL EROSION RATES FROM OXIDATION TESTS OF PG, ZrC-PG, AND HfC-PG WITH ARC PLASMA HEATED AIR

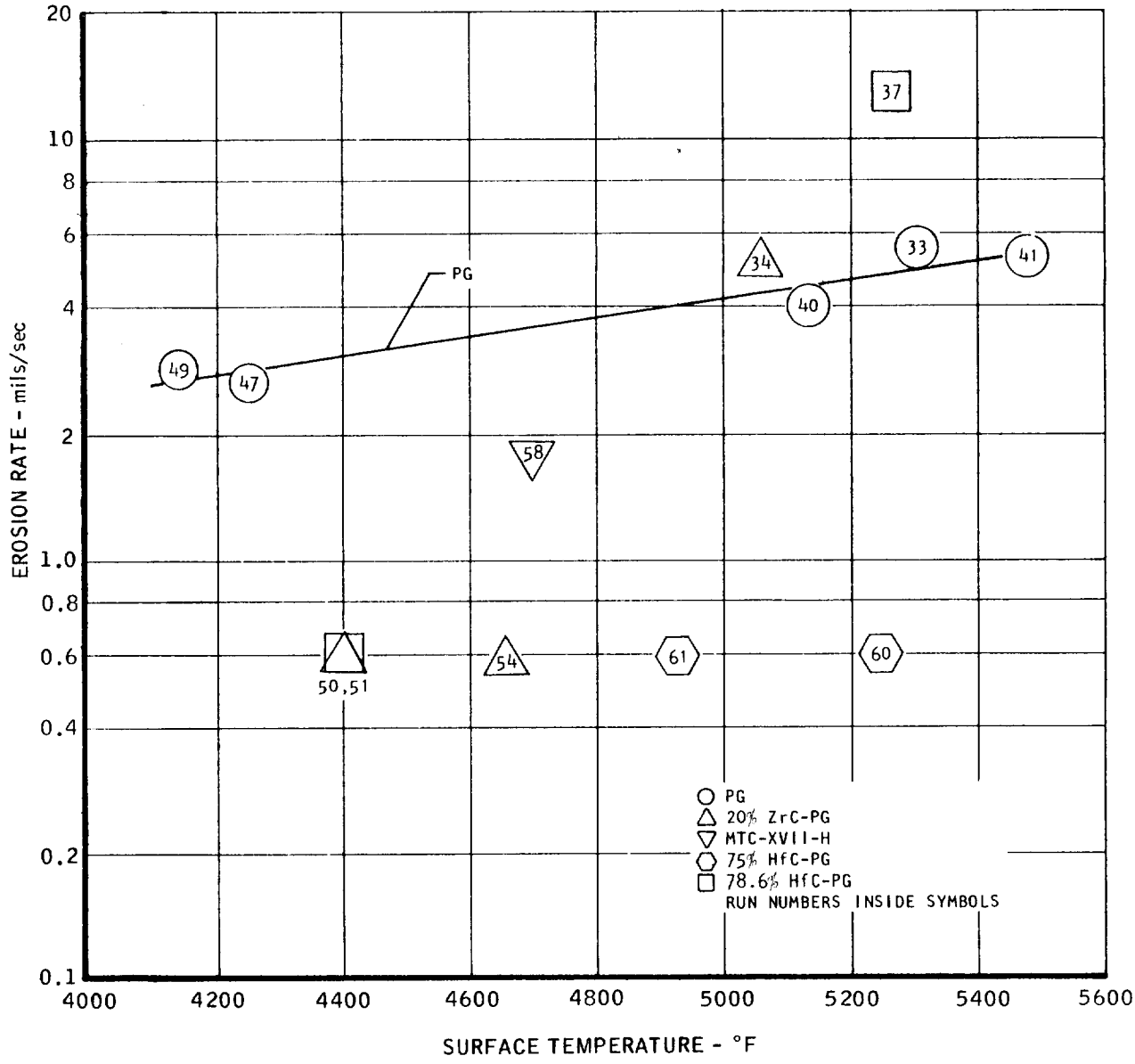

TMC A673

FIGURE 32

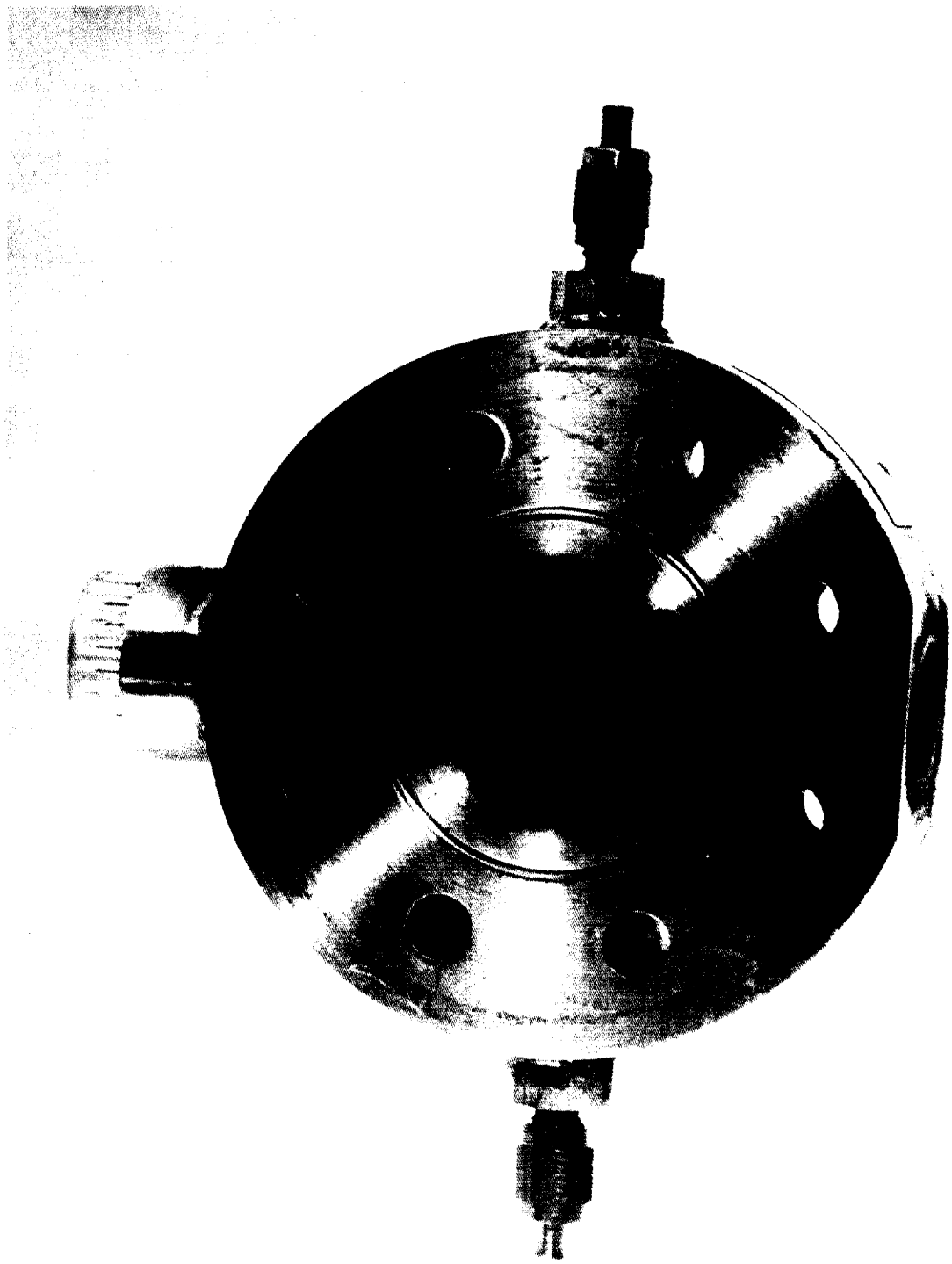

FIGURE 33. Astrosystems Injector after Firing

6452-1

STEEL NOZZLE DESIGN

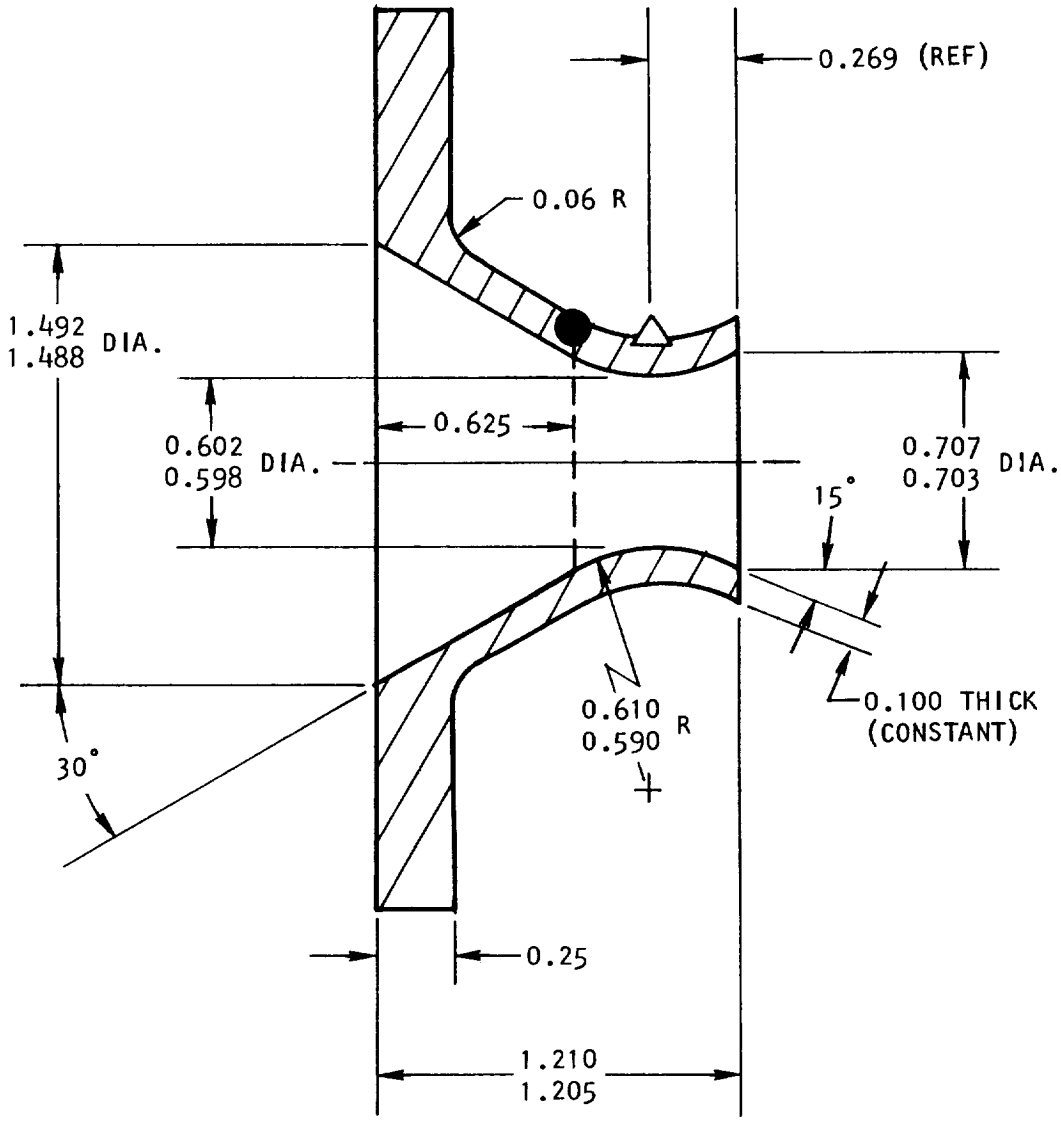

TMC A673

FIGURE 34

HEATING PATTERN IN STEEL NOZZLE WITH ASTROSYSTEMS 201291-1 INJECTOR

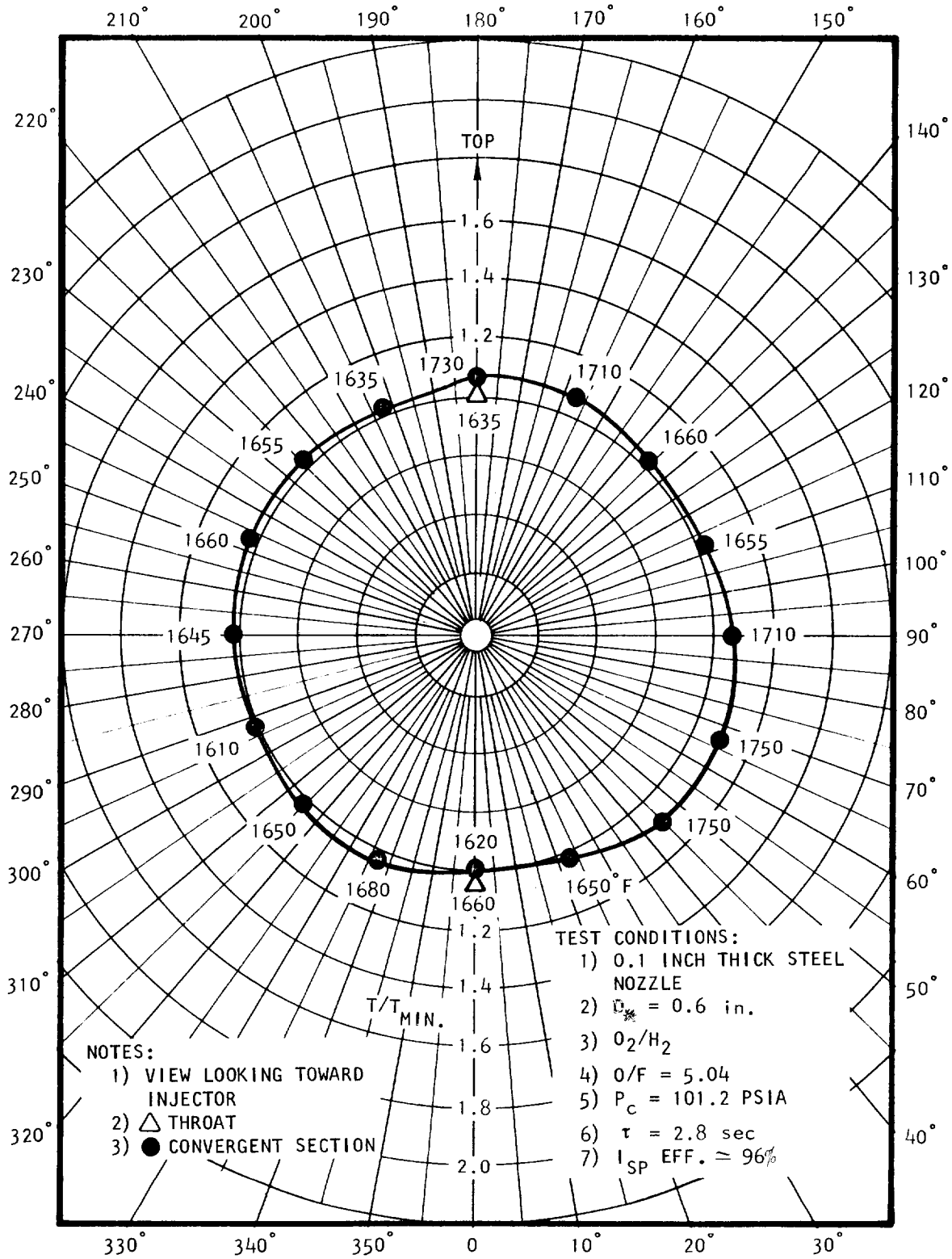

TMC A673

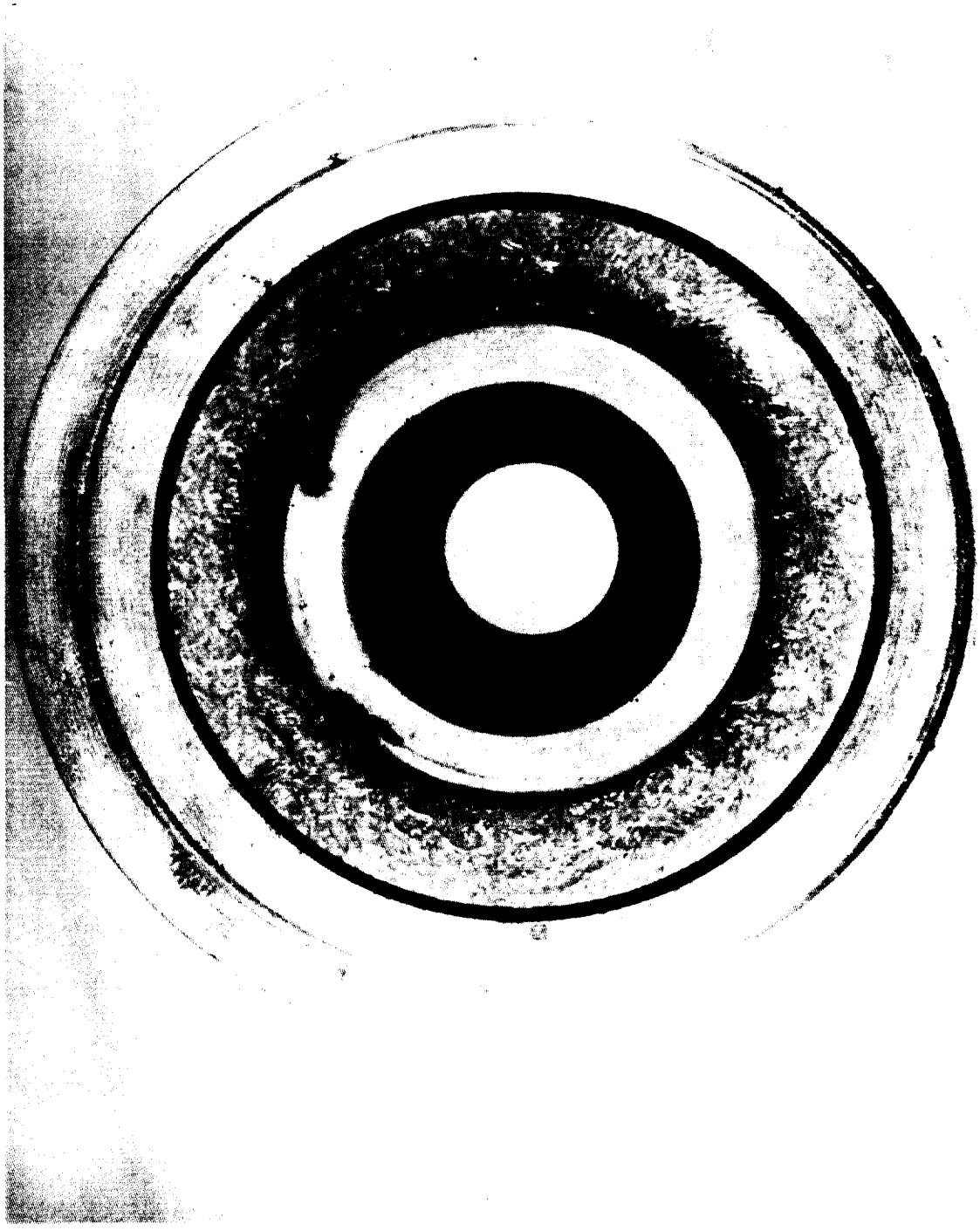

FIGURE 36. ATJ Graphite Nozzle after Run 10

T3198-22

MOTOR FIRING TEST SETUP FOR EDGE ORIENTED NOZZLES

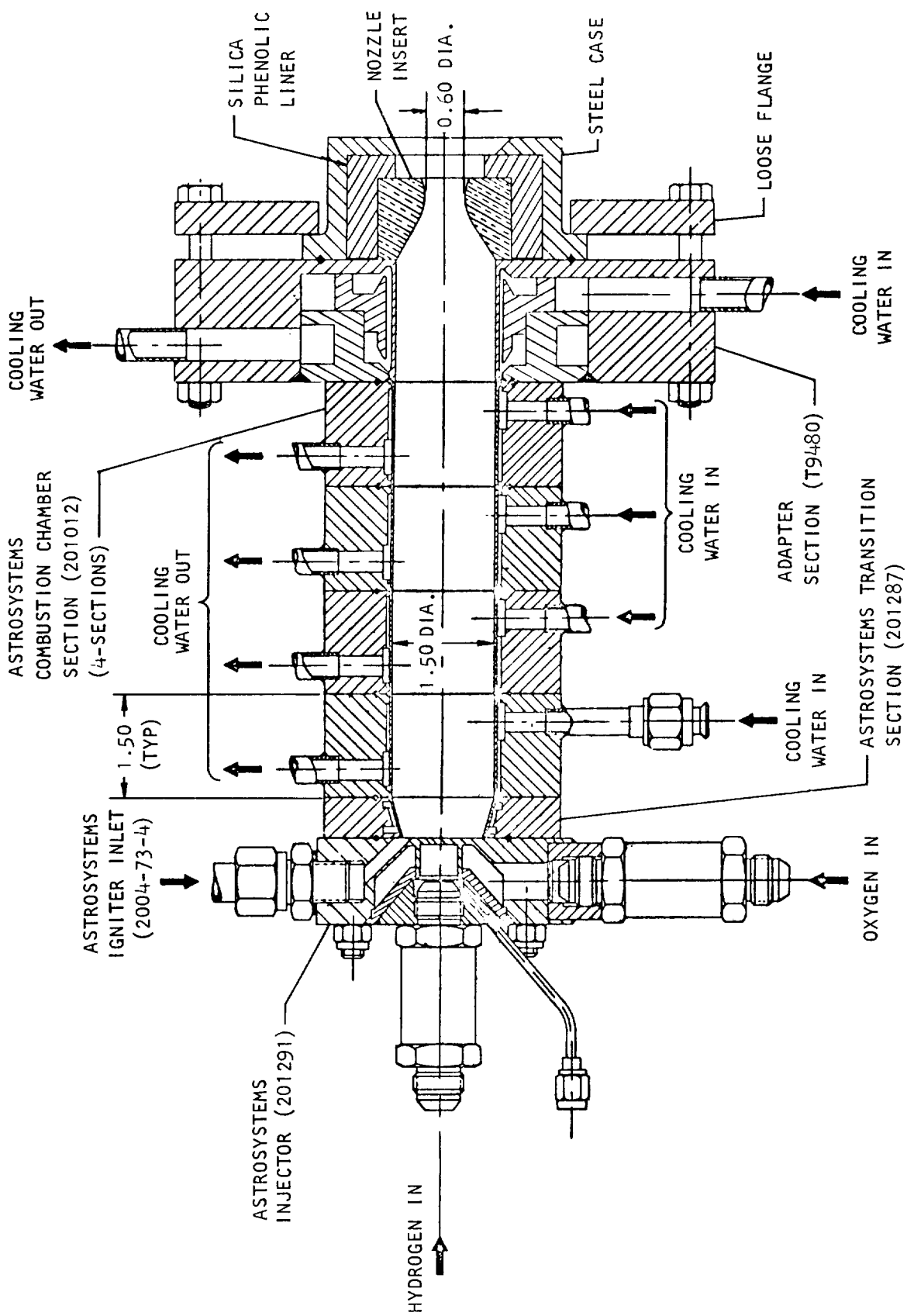

TMC A673

FIGURE 37

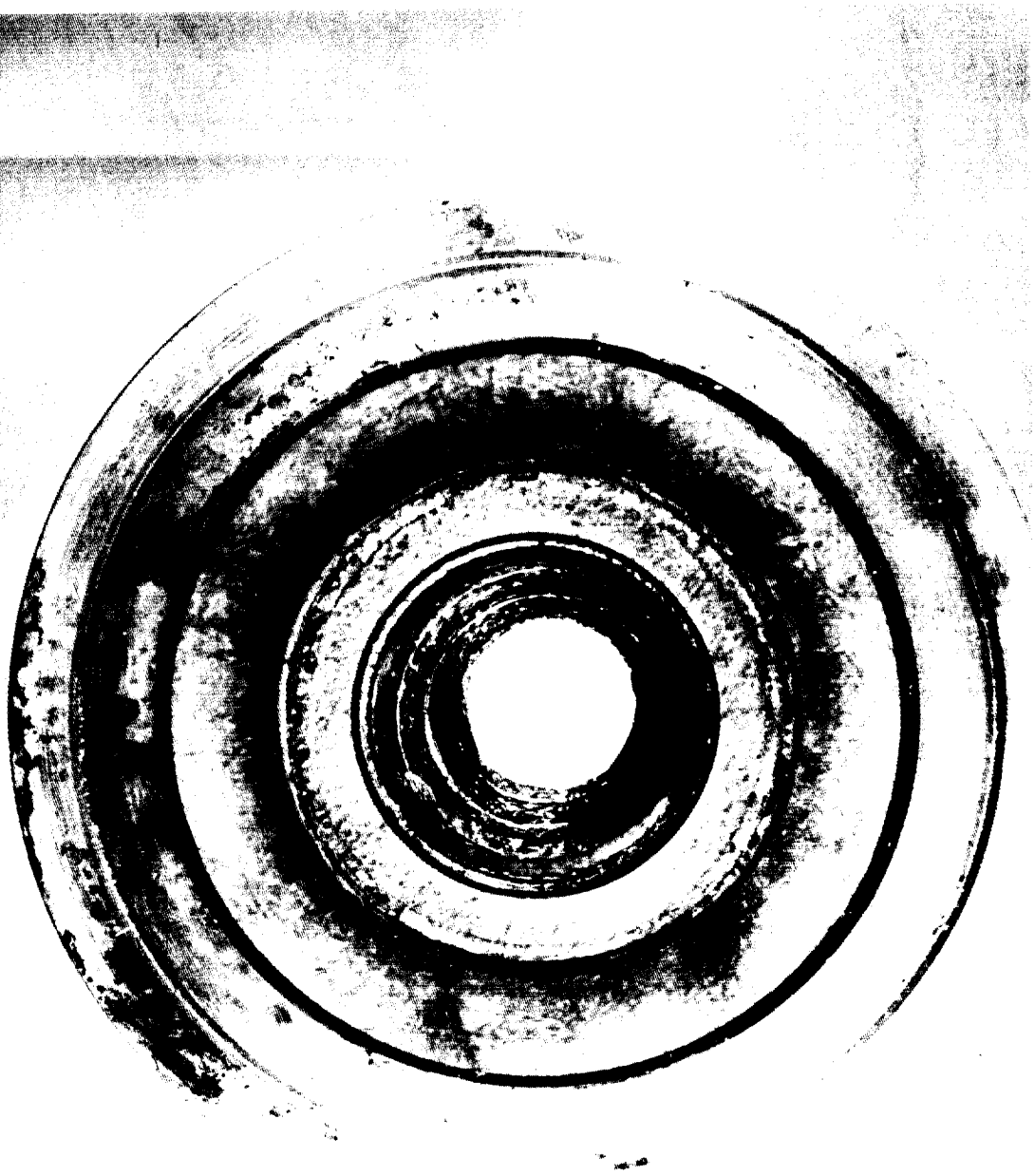

FIGURE 38. Pyrolytic Graphite Nozzle after Run 14

T3198-23

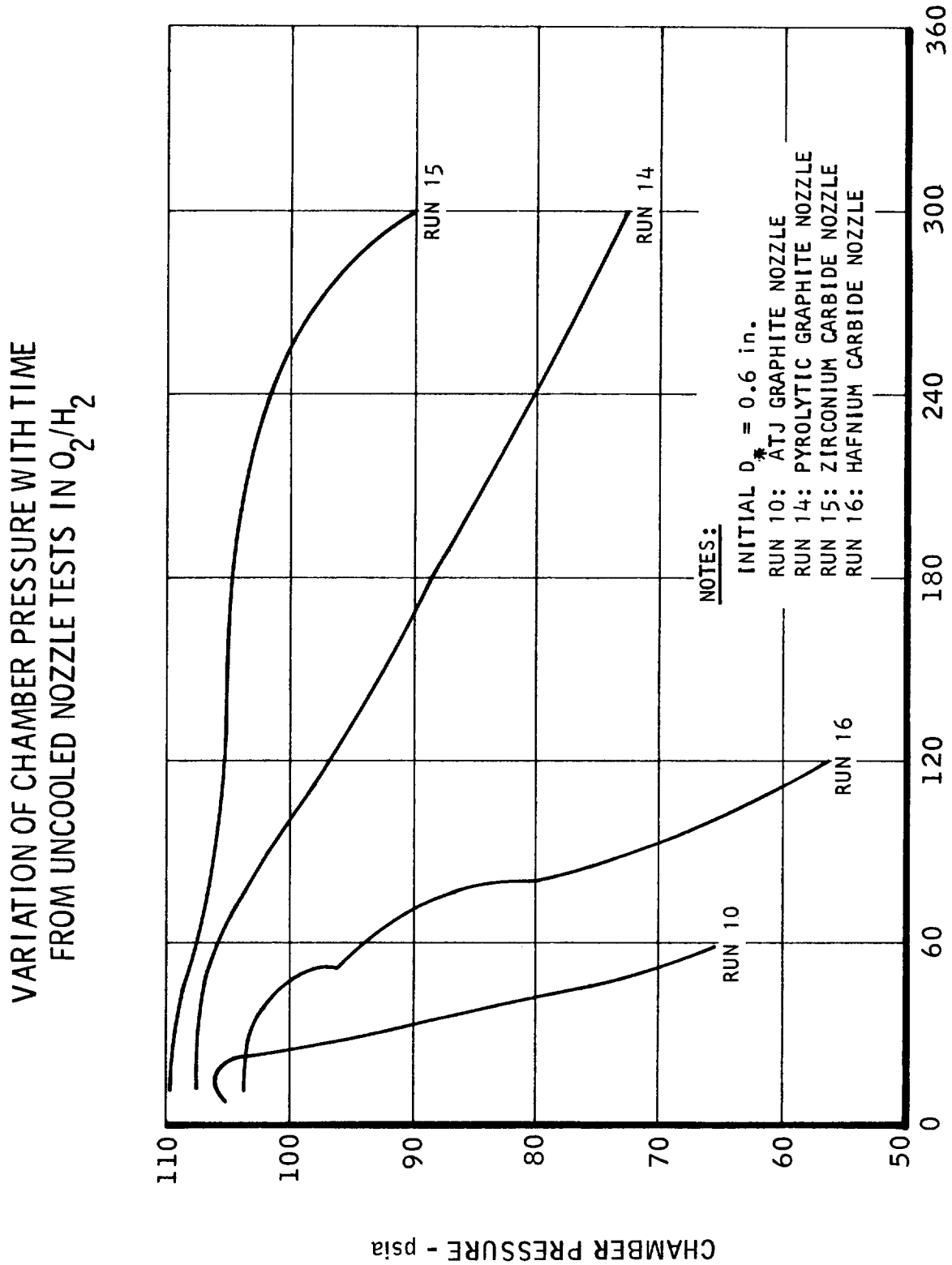
VARIATION OF CHAMBER PRESSURE WITH TIME
FROM UNCOOLED NOZZLE TESTS IN O_2/H_2
CHAMBER PRESSURE - psia
110
100
90
80
70
60
50
TIME - seconds
0
60
120
180
240
300
360
RUN 15
RUN 14
RUN 16
RUN 10
NOTES:
INITIAL D_* = 0.6 in.
RUN 10: ATJ GRAPHITE NOZZLE
RUN 14: PYROLYTIC GRAPHITE NOZZLE
RUN 15: ZIRCONIUM CARBIDE NOZZLE
RUN 16: HAFNIUM CARBIDE NOZZLE

TMC A673

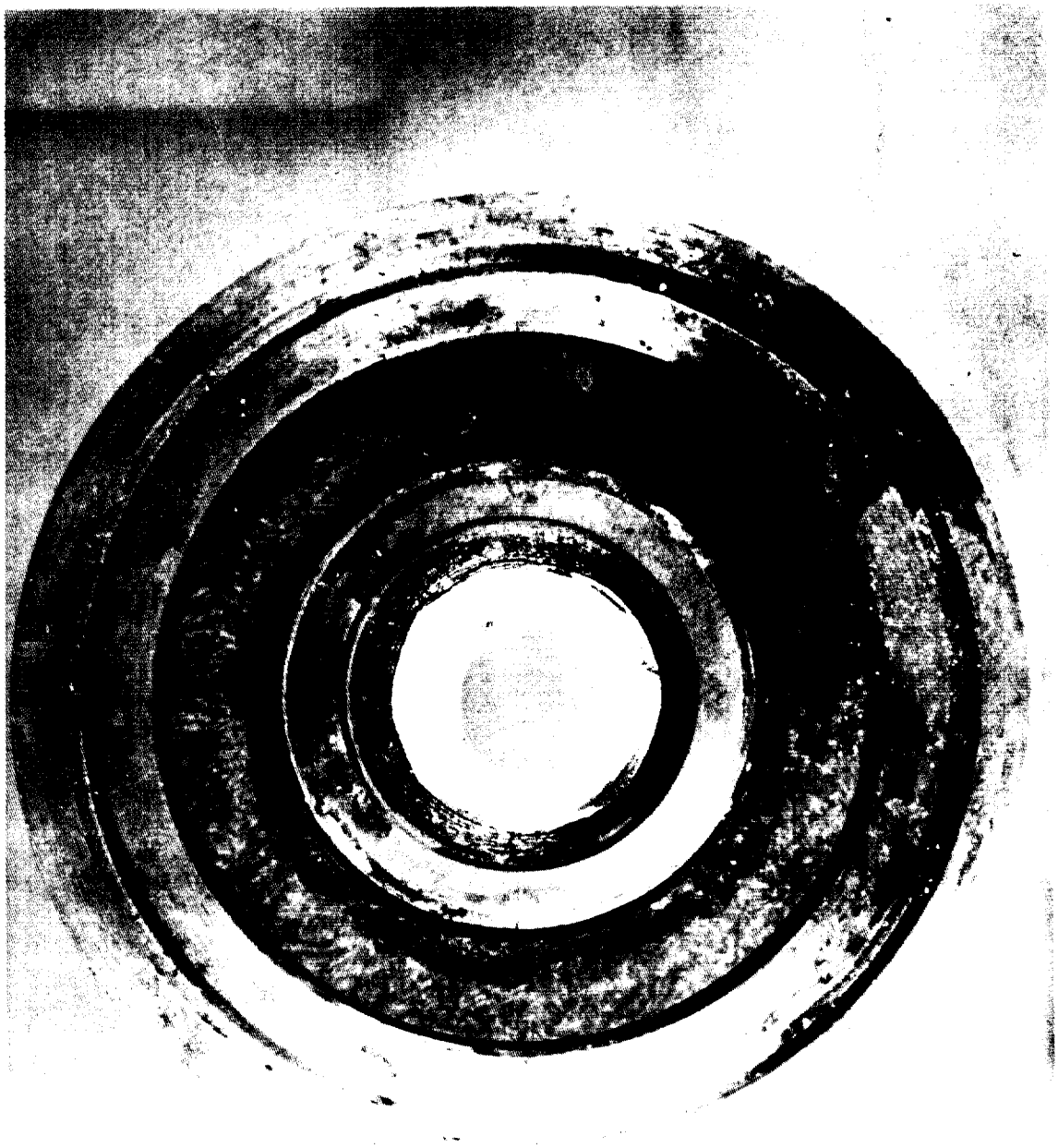

T3198-24
FIGURE 40. Convergent Section of Edge Oriented ZrC-PG Throat Insert after Run 15

TMC A673

13198-8

FIGURE 41. Exit End of Edge Oriented ZrC-PG Throat Insert after Run 15

CONTOURS OF PG AND ZrC-PG EDGE ORIENTED NOZZLES AFTER 300 second FIRING RUNS

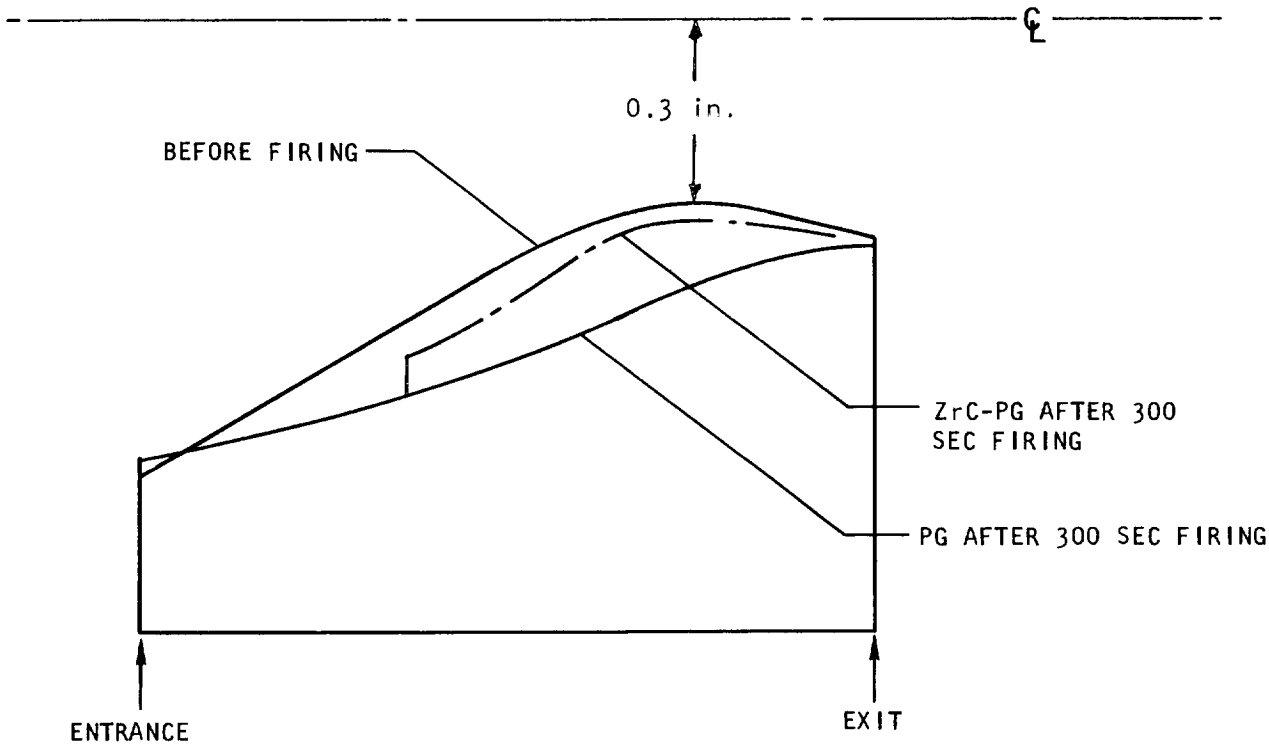

TMC A673

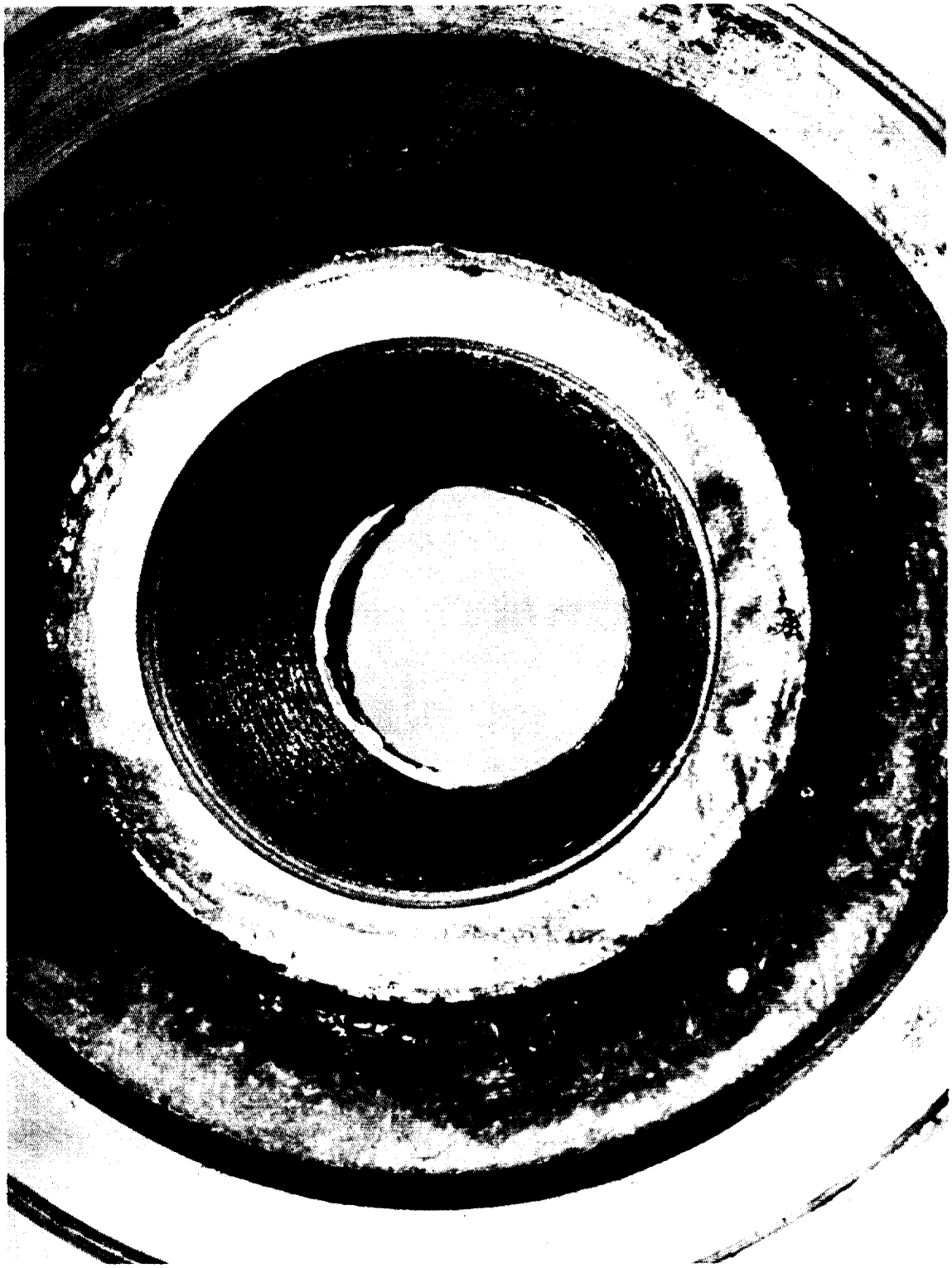

F3198-10

FIGURE 43. Convergent Section of Edge Oriented HfC-PG Throat Insert after Run 16

T3198-11

FIGURE 44. Exit End of Edge Oriented HfC-PG Throat Insert after Run 16

TMC A673

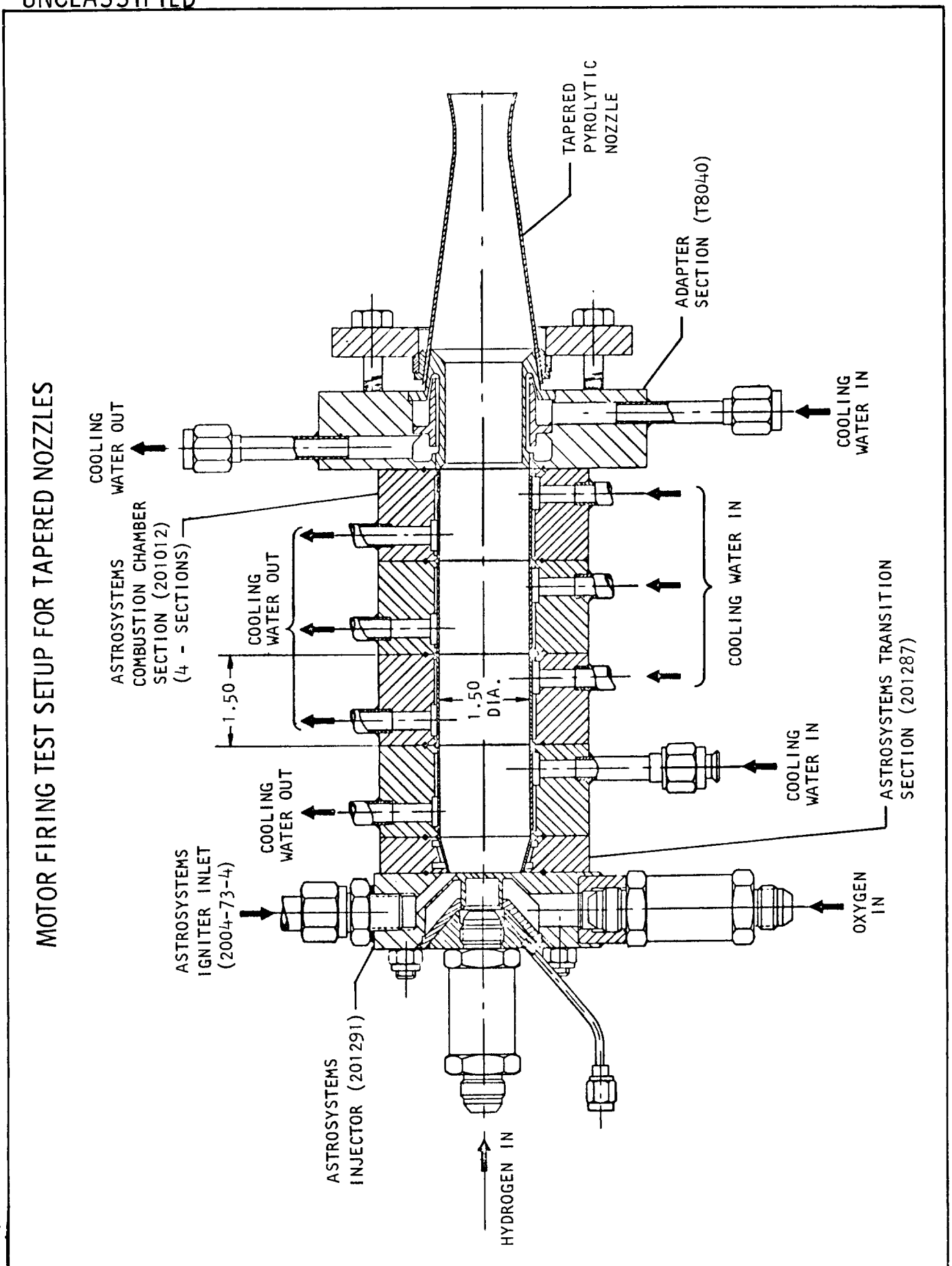

TMC A673

FIGURE 45

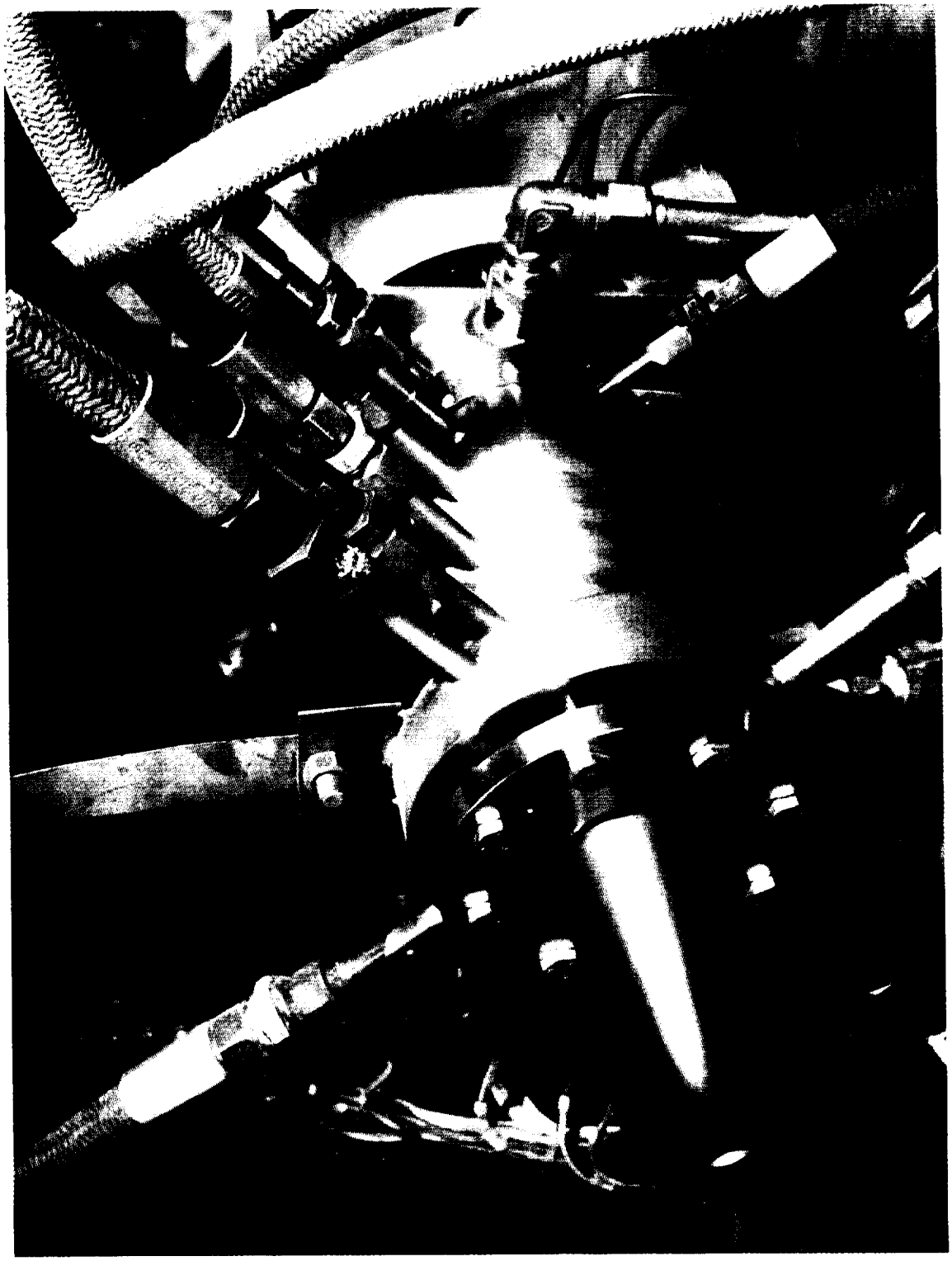

T3198-12

FIGURE 46. Tapered Pyrolytic Graphite Nozzle Set Up for Motor Firing Test

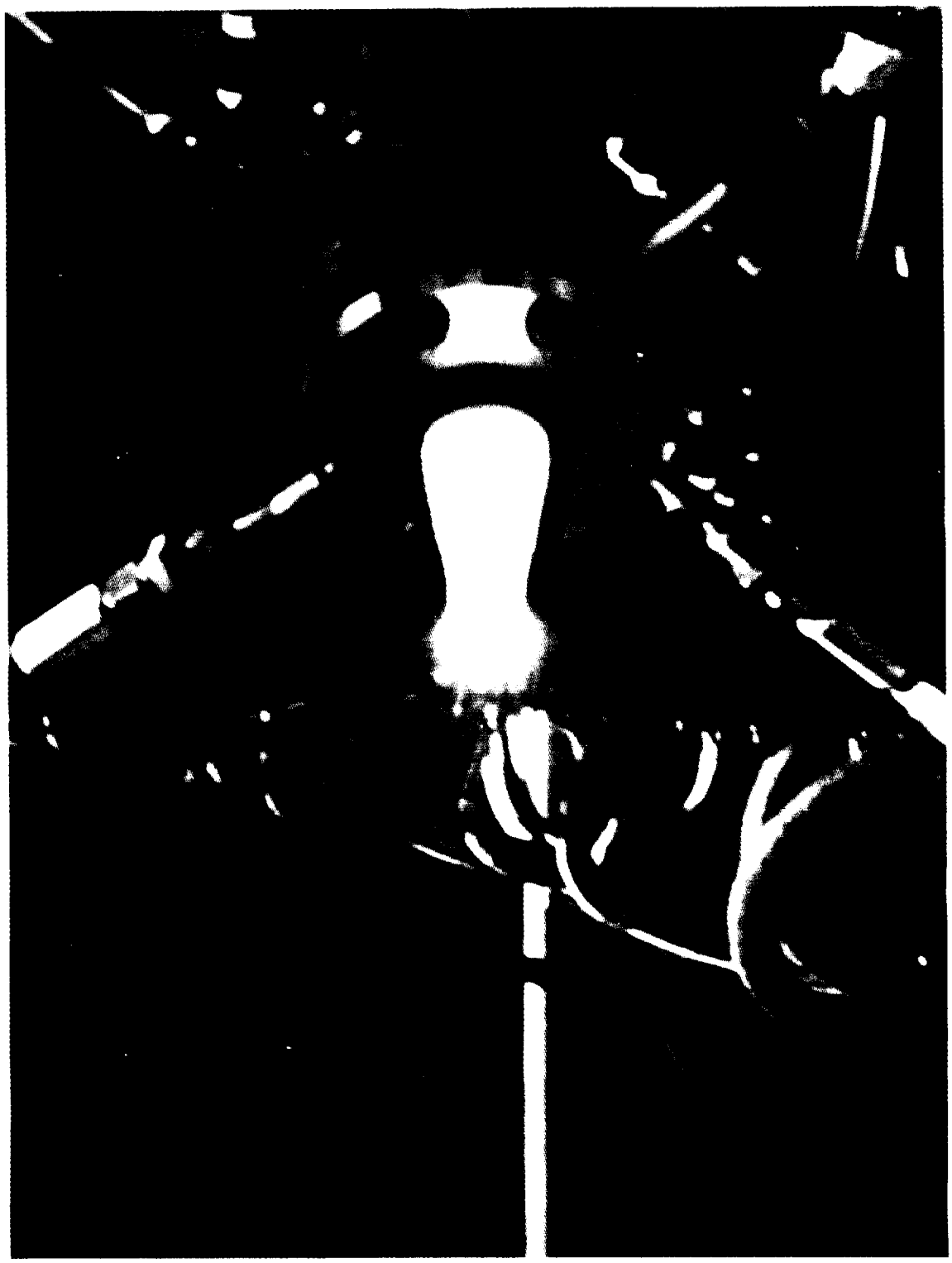

CI3198-17

FIGURE 47. Test Firing of Tapered Pyrolytic Graphite Nozzle No. 4

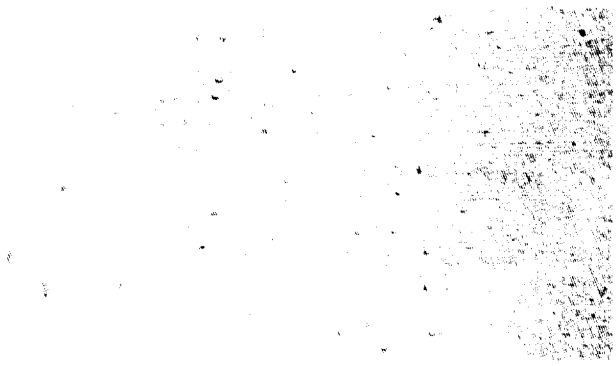

A. OD Surface (10X)

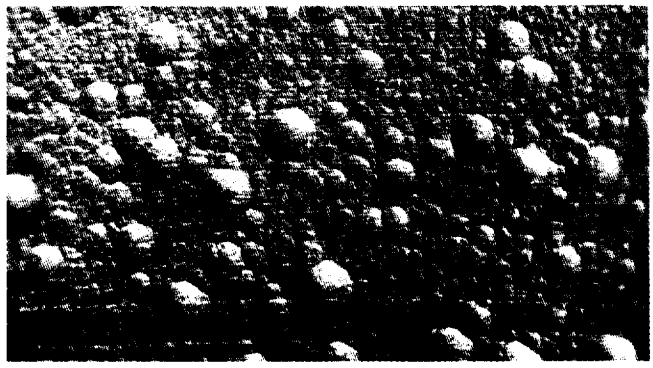

B. ID Surface (10X)

C. Cross Section (50X)

FIGURE 48. Microstructure of Tapered Pyrolytic Graphite Nozzle No. 3

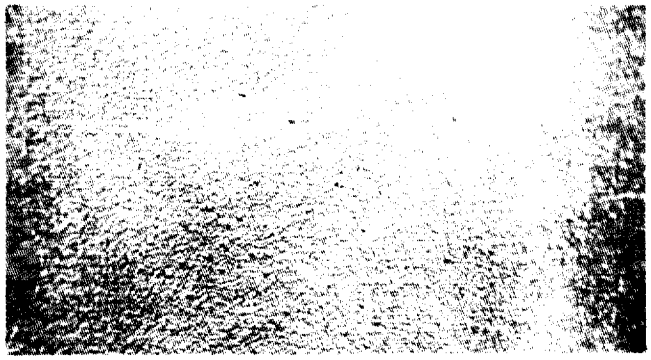

A. OD Surface (10X)

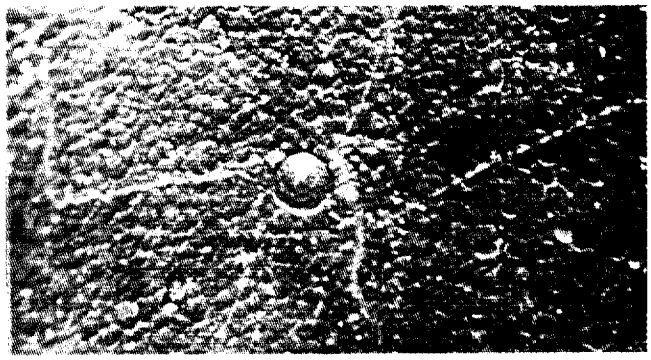

B. ID Surface (10X)

C. Cross Section (50X)

FIGURE 49. Microstructure of Tapered Pyrolytic Graphite Nozzle No. 4

TMC A673

A. OD Surface (10X)

B. ID Surface (10X)

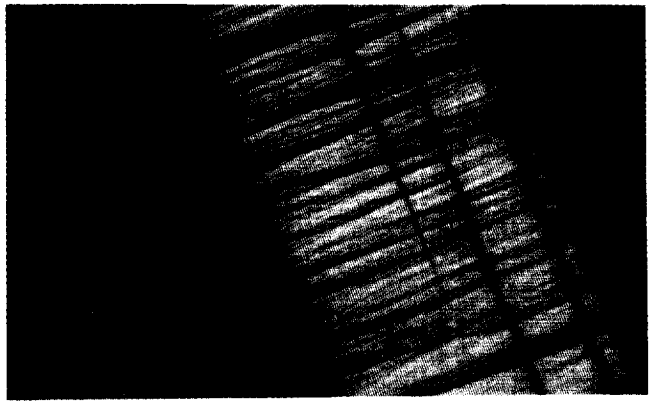

C. Cross Section (50X)

FIGURE 50. Microstructure of Tapered Pyrolytic Graphite Nozzle No. 7

TMC A673

CT3198-20

FIGURE 51. Test Firing of Tapered HfC-PG Nozzle MTC-XVI-H

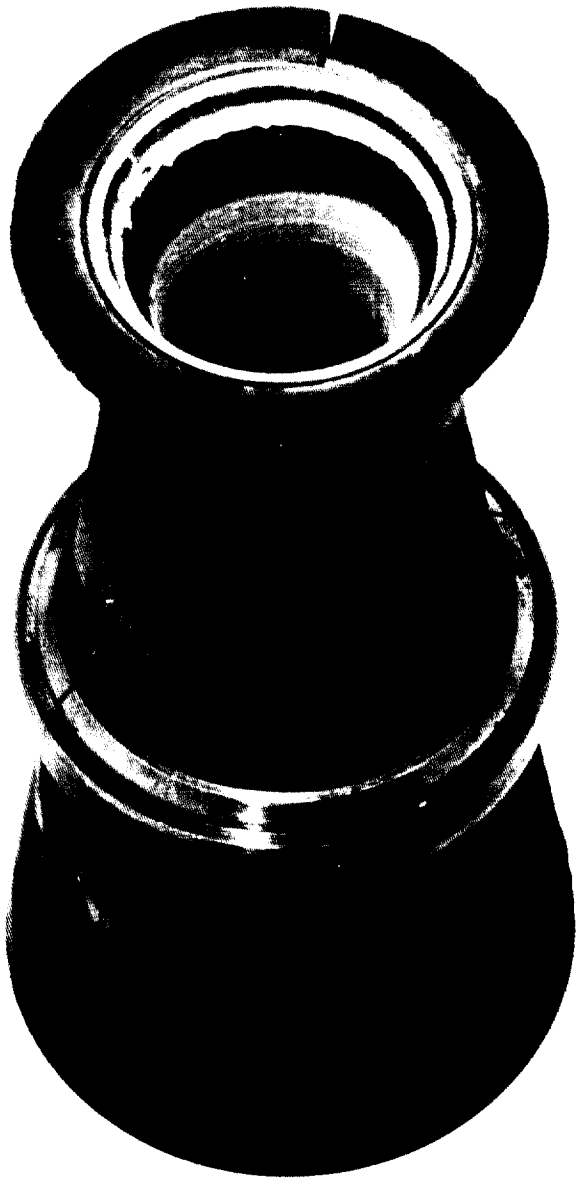

T3198-19

FIGURE 52. Exit of Tapered HfC-PG Nozzle MTC-XVI-H after Test Firing

APPENDIX A

PROCUREMENT SPECIFICATIONS FOR FREE STANDING PYROLYTIC GRAPHITE

A. Recommended Procurement Specification for Free Standing Pyrolytic Graphite

A-1. Super-Temp Corporation Specification for Pyrolytic Graphite

A-2. General Electric Company Specification for Pyrolytic Graphite Plate

A-3. Suggested Vendor's Process Questionnaire for Free Standing Pyrolytic Graphite Components

APPENDIX A

A. RECOMMENDED PROCUREMENT SPECIFICATION FOR FREE STANDING PYROLYTIC GRAPHITE

There are at least three approaches which might be considered in specifying PG component quality. These three approaches are as follows:

1. Specify nondestructive inspection criteria for acceptance. These criteria might include
   a. Proof pressure test
   b. Nodule size
   c. Matrix grain size
   d. Substrate or continuously nucleated microstructure
   e. Growth cone angle
2. Specify physical properties of each batch of material, such as
   a. Tensile strength
   b. Modulus of elasticity
   c. Coefficients of thermal expansion
3. Specify all process parameters from mandrel design to post-deposition cooling rate and surface machining.

The best method of procuring high quality pyrolytic graphite components is probably a combination of these three approaches. The exact content of such specifications will depend on the end use of the component.

For free standing thrust chambers, the most pertinent inspection technique is undoubtedly a proof test, since this simulates one of the most severe operating conditions.

The relationship between rupture strength and the process parameters has not been studied systematically. Most of the previous studies of process parameters have had the objectives of increasing production yield, reducing residual stresses and achieving greater values of the thickness/radius ratio. However, it was shown in Reference 1 that although residual stresses are an important limitation on the feasibility of free standing PG thrust chambers, an even greater

APPENDIX A (Continued)

limitation is the low tensile strength of PG in axisymmetric shapes. The recent work presented in this report shows again that high strength tubes do not have significantly different residual stresses than do low strength tubes. Instead, it seems that localized stress concentrations at large nodules are much more important than residual stresses.

It is also shown in Reference 1 that an optimum thickness/radius ratio for free standing thrust chambers is not simply the thickest that can be produced, since such a chamber would probably have such high residual stresses that it might be unable to carry much internal pressure unless the tensile strength were also increased.

Two vendors supplying PG tubes for the present study were asked to supply process and inspection information listed in the Vendor's Process Questionnaire (Appendix A-3). Their replies showed that some aspects of their deposition techniques were different, indicating either that the differences are unimportant or that the effect of the various parameters of PG quality has not been established. Much of the vendor's deposition processes are considered proprietary and they therefore cannot be revealed. Both vendors used ATJ graphite for the mandrels with similar techniques for cleaning the mandrel after machining. However, as described in the body of this report, a close examination of the tubes produced by the various vendors shows small differences in the mandrel machining techniques which may be important.

In time, many of the process parameters and microstructure features may be systematically evaluated as to their effect on rupture strength. In the interim, some iterative procedure will be necessary, involving the testing of prototype PG components produced by the vendors techniques, and later specifying that vendor or vendor process which produces the optimum PG, both from a quality and an economic standpoint.

It is recommended that a questionnaire such as that in Appendix A-3 be furnished by each vendor with each free standing PG part supplied. In addition, the standard specifications presently used by the vendors (Appendixes A-1 and A-2) should also be used, with modifications as indicated by further experience. As higher quality parts are supplied by the vendors, then more of these process specifications should become part of the specifications for the delivered chambers.

Specification of physical properties for the material in a specific PG component would require semi-destructive inspection techniques, and the correlations between these physical properties and PG component quality is unknown.

Therefore, the only quantities which can be specified at the present time are a proof pressure capability and the maximum nodule size.

APPENDIX A (Continued)

The relationship between rupture pressure and the size of the largest nodule on the tube was presented in Figures 2 and 3 in the main body of this report. Although the absence of large nodules does not guarantee high strength, the presence of large nodules almost certainly precludes very high strength tubes or free standing thrust chambers. Therefore, one of the critical entries in the specification of free standing PG thrust chambers will be a maximum nodule diameter anywhere in the chamber or throat.

Thermal, vibration, and pressurization stresses in a free standing PG chamber will vary throughout various portions of the chamber, and a specification of nodule size would ideally be tailored to the different strength requirements of the combustion chamber, throat region, and expansion nozzle. However, the role of nodule size in thermal or vibration stresses is speculative at present, and further study of the effects of nodules is required.

Residual hoop stresses are maximum at the inside surface, and the total of hoop residual and pressurization stresses during a rupture test is also maximum at the inside surface. Therefore, the correlation between maximum nodule size and rupture pressure (Figures 2 and 3 above) is probably pertinent only for circumferential stresses at the inside surface.

Stresses in a free standing PG chamber during motor operation are usually maximum at the outside surface and the role of nodules in this situation is not known. However, nodules in free standing PG have a very small diameter at the outer surface and will probably have less of an effect there than they do at the inside surface where they reach maximum size.

It now seems reasonable to at least establish a specification for regions of high pressurization stress such as the combustion chamber and throat region, as follows:

Maximum Nodule Size.-No nodule or cluster of nodules shall be larger in diameter than one-half the wall thickness of the free standing shape.

Proof Pressure.-Free standing shapes shall pass a proof test according to the following schedule:

t/r	Proof Pressure (psig)
0.04	450
0.06	500
0.08	425
0.10	230

TMC A673

APPENDIX A (Continued)

A maximum nodule diameter of one-half the wall thickness corresponds to 0.030 inch for the tubes used in this program, which had a wall thickness of about 0.060 inch and a t/r ratio of 0.06.

When one examines the burst pressure of all tubes with a maximum nodule size of 0.030 inch (Figures 2 and 3 above), it is observed that the burst pressure variation still ranges from 70 to 1000 psig. If a proof pressure acceptance test at 500 psig had been imposed on these tubes meeting the nodule size requirement all but one tube in Lots Nos. 3 and 4 would have been accepted while only one tube in Lot No. 2 would have been accepted. Also, it may be noted that only two tubes from any lots with nodule sizes greater than 0.03 inch could have passed the 500 psig acceptance test. In applying this approach to accepting a free standing PG thrust chamber, it is recommended that both criteria be applied to the thrust chamber up to the throat (i.e., maximum nodule size and proof pressure) with exact numbers specified according to the intended design requirements. The exit expansion cone could then be accepted on the basis of nodule size plus the other visual inspection criteria which were established.

The detailed stress distribution near a nodule is not known at present, but is undoubtedly very complex. The specification of the maximum nodule size as a fraction of the wall thickness is arbitrary and would have to be confirmed by a comparison of maximum nodule size and rupture pressure for a number of PG tubes of other dimensions than those used in the present program.

A proof test of 500 psig will impose a total circumferential stress, pressure plus residual stress, of 11,800 psi on a tube with a t/r ratio of 0.06. The average tensile strength of the Lot No. 4 tubes was 11,800 psi, hence such a proof test specification is a reasonable objective.

The proof pressure specification for other values of the t/r ratio is based on the same tensile strength (11,800 psi) but it also considers the variation of residual stress with t/r as presented in Reference 1. Much more data are required to clearly establish the residual stresses at t/r ratios other than 0.06, but the above specification illustrates the decreased pressure carrying capacity of thicker walled PG components. The proof test should be conducted so as to apply only hoop pressure stresses unless otherwise specified.

It might appear that the specification of maximum nodule size is superfluous if a proof test is also required. However, the present evidence is so strong that large nodules are danger points in PG that it is thought best to avoid them even though the proof test is satisfied, since they may well be objectionable under vibration stresses not simulated by a proof test.

APPENDIX A (Continued)

It is probable that free standing chambers will be designed for use in the as-deposited condition without machining, except for attach areas. Therefore, the dimensional tolerances, axially and circumferentially, should be consistent with the fabrication technique. One approach to dimensional tolerances is to have a graded specification which would vary both with the number of chambers produced to a given design and the end use of the part (e.g., research, development, flight test, or man rated mission). A preproduction agreement on chamber price as a function of variation from a given dimensional and microstructure specification would provide an incentive for achieving the highest quality chambers while also providing a procedure for accepting lower quality chambers suitable for certain research and development tests. This approach to PG chamber production is attractive because of the special fabrication technique involved. A single furnace run to produce a free standing chamber may run in excess of 100 hours and there is no way to correct the imperfections or dimensional variations once the process has begun. There is no satisfactory way to determine before the end of the run whether or not a chamber will meet the required specifications. However, it is often possible to determine that a run has been ruined by unscheduled process variations due to a furnace leak, pressure surge, power failure, etc. Only by repeated furnace runs and by fabricating a number of chambers, can dimensional control and repeatability be assured.

APPENDIX A-1

Super-Temp Corporation

2.05 PYROLYTIC GRAPHITE SPECIFICATIONS

Specification #101-B, Revised August 15, 1964

MATERIAL

Pyrolytic graphite is a vapor-deposited form of carbon having a high degree of preferred crystalline orientation. The material is produced by the thermal decomposition of a hydrocarbon gas on a hot surface and deposits so that the direction of high strength and high thermal conductivity is always parallel to the deposition surface.

TECHNICAL AND QUALITY REQUIREMENTS

Unless otherwise specified and agreed to between Super-Temp Corporation and the customer, only the following physical tests and quality measurements will be performed; should looser or tighter tolerances be desired, special arrangements on quality and price can be arranged:

2.05.10 PLATE

Flat plate or machined shapes produced from plate.

.11 Density gr/cc @ 77°F ±5 — 2.20 ±.02
(as determined by differential weighing in air and CP carbon tetrachloride)

.12 Nodules (Conical Growth Defects)

The following nodule sizes and distribution will be considered the maximum allowable in plate material

MAXIMUM NODULE SIZE ALLOWABLE

Size–Round or Square	Thickness 1/8"	1/4"	3/8"	1/2"	5/8"
Up to 2"	.062	.125	.187	.250	.312
2" to 4"	.094	.156	.250	.312	.406
4" to 6"	.125	.203	.312	.406	.500
6" to 8"	.156	.250	.375	.500	.500
8" to 10"	.203	.312	.437	.500	.500
10" to 12"	.250	.375	.500	.500	.500

MINIMUM DISTANCE BETWEEN EDGES OF NODULES OF MAXIMUM SIZE

Size–Round or Square	Thickness 1/8"	1/4"	3/8"	1/2"	5/8"
Up to 2"	1	1	1	1	1
2" to 4"	7/8	7/8	15/16	1	1
4" to 6"	13/16	13/16	15/16	1	1
6" to 8"	3/4	3/4	7/8	1	1
8" to 10"	5/8	5/8	13/16	1	1
10" to 12"	1/2	1/2	3/4	1	1

PYROLYTIC MATERIALS 2.0-4 NEW 7/64

.13 Surface Flaws: The exposed surfaces of the plate parallel to the "a" direction shall be free of cracks when examined visually, and shall not be visibly marked (grooved or gouged) by measuring instruments. Final inspection for cracks shall be made by a penetrant dye check after finish machining according to the appropriate Military Specifications.

.14 Delaminations: The exposed surfaces of the plates parallel to the "c" direction shall be free of major delaminations when examined visually; and shall not be visibly marked (grooved or gouged) by the measuring instruments. No delaminations shall extend more than one-fourth the length of the size on which it appears. There shall be no more than two delaminations through the thickness in any material up to ¼" in thickness, and no more than three through the thickness in material between ¼" and ½" thick. Final inspection for delaminations shall be made by a penetrant dye check after final machining according to the appropriate Military Specifications.

Bow in Plate as Deposited:

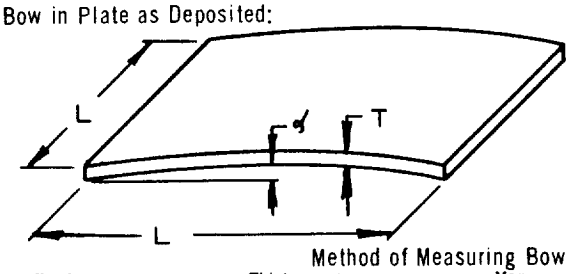

Method of Measuring Bow

For L	Thickness t	Max.
Up to 4"	Up to 3/8"	1°
4" to 8"	Up to 1/2"	2°
8" and above	Up to 1/2"	4°

For thicknesses above 1/2" maximum, L will be 5° unless special arrangements are made with Super-Temp Corp.

.15 Purity – Total ash content by combustion – 0.01% max. – 0.005% typ.

.16 Minimum flexural strength "a" direction – 12,000 psi (loaded parallel to the surface of deposition min. at RT)

2.05.20 CYLINDERS

Hollow cylinders and closely related shapes such as ovals, cones, etc.

.21 Density gr/cc @ 77°F ±5 — 2.20 ± .02
(as determined by differential weighing in air and CP carbon tetrachloride)

TMC A673

APPENDIX A-1 Continued)

Super-Temp Corporation

.22 Nodules (Conical Growth Defects) – No nodule or cluster of nodules (nodules touching each other) shall be larger in diameter than equal to the cylinder wall thickness for all thicknesses up to and including ½" material. For cylinders with wall thicknesses greater than ½" the nodule size and distribution shall be agreed upon between Super-Temp Corp. and the customer. Nodule distribution shall be such that no more than two nodules of the maximum size shall be closer than 1" apart.

.23 Surface Flaws: The exposed surfaces of cylinder parallel to the "a" directions shall be free of cracks when examined visually; and shall not be visibly marked (grooved or gouged) by measuring instruments. Final inspection for cracks shall be made by a penetrant dye check after finish machining according to the appropriate Military Specifications.

.24 Delaminations: Due to the anisotropy of thermal expansion of pyrolytic graphite, it is extremely difficult to produce all sizes of pyrolytic graphite cylinders which are free of delaminations and cracks. At present cylinders free of cracks and delaminations can be produced if the wall thickness-to-radius ratio does not exceed .06 and if the length is not greater than three times the diameter. Final inspection for delaminations shall be made by a penetrant dye check after final machining according to Military Specifications. For cylinders which exceed these limits, delaminations and/or cracks can be a serious problem and special quality control arrangements between Super-Temp Corp. and the customer are required.

.25 Purity: Total ash content by combustions – 0.01% max. – 0.005% typ.

2.05.30 By mutual agreement between Super-Temp Corp. and the customer, the material will be tested to see that it conforms to the following specifications in whole or part:

.31 Tensile Strength "a" direction 10,000 psi
(pulled in the plane parallel to the surface of deposition min. at RT)

.32 Compressive Strength min. at RT — parallel to "a" dir. 10,000 psi; parallel to "c" dir. 45,000 psi

.33 Thermal Expansion ($\times 10^{-6}$ in/in/°F at 1000°F) — parallel to "a" dir. 0.1 ± 0.3; parallel to "c" dir. 15.0 ± 3.0

.34 Thermal conductivity BTU-ft-ft^{-2} hr^{-1} °F^{-1} — parallel to "a" dir. 100 ± 50; parallel to "c" dir. 1.0 + 0.5

.35 Elastic Modulus min. at RT 3 x 10^6 psi Plate only

.36 Minimum Flexural Strength "a" direction – 12,000 psi Cylinders Only
(loaded parallel to the surface of deposition min. at RT)

.37 Internal Residual Stress – inner fiber bending stress psi maximum – 5,000 Cylinders Only
(A 7/8 inch wide ring from one end of each cylinder shall be provided for measuring internal residual stress before machining. The internal residual stress is a function of the thickness-to-radius ratio.)

.38 Out-of-Roundness, difference in diameters 90° apart after machining in., ±.003 to .005 – Cylinders Only.

2.05.40 Special Testing

Super-Temp Corp. will perform other property and quality control tests such as radiographic and ultrasonic inspection as agreed to mutually with the customer. Tests can also be specially designed to meet certain customer requirements and to insure a closer control over properties. Super-Temp Corp. will be glad to work with the customer in establishing the test procedures and performing the required measurement.

2.05.50 Dimensional Measurements

The dimensions and tolerances, including surface finish, will be held according to the customer's engineering drawings and agreed to by Super-Temp Corp. by acceptance of the purchase order.

2.05.60 Certification

Three copies of a Certificate of Test will be furnished upon request stating that the product conforms to the requirements of our standard tests and any other tests agreed upon mutually by Super-Temp Corp. and the customer. This report will include the purchase order

APPENDIX A-1 (Continued)

Super-Temp Corporation

number, furnace run number, form or part number, quantity, and dimensional measurements. Where agreed to mutually between Super-Temp Corp. and the customer, process data including furnace cycle times and temperatures, and types of gases used will be furnished. Detailed drawings or sketches of the furnace hardware will not be provided.

2.05.70 Identification

All parts will be clearly marked to show part number, lot number, etc. in such a way that the marking does not in any way remove or displace the parent material of the part.

2.05.80 Packaging

Packaging shall be accomplished to such a manner as to insure the product during shipment and storage will be protected against damage from exposure to weather or any normal hazard.

PYROLYTIC
MATERIALS
2.0-6
NEW 7/64

TMC A673

APPENDIX A-2

METALLURGICAL PRODUCTS DEPARTMENT

GENERAL ELECTRIC COMPANY

MAT'L. SPEC. (TENT) SA-24-1

Effective May 1, 1964

GENERAL ELECTRIC MATERIAL SPECIFICATION (TENTATIVE)
TITLE: PYROLYTIC GRAPHITE PLATE

1. *SCOPE.*

1-1. Application. This specification covers the manufacture, properties, acceptance standards, grades, certificates, packaging, and definitions for unalloyed pyrolytic graphite plate manufactured by the General Electric Company.

1-2. Manufacture. Pyrolytic graphite plate is a polycrystalline form of carbon having a high degree of anisotropy and purity. Material applicable to this specification shall be produced by the deposition of carbon from the vapor phase onto a substrate at an elevated temperature and under reduced pressure.

2. *PROPERTIES.*

2-1. General. The plate material supplied in accordance with this specification has the following *average, typical* property values:

2-1-1. Physical properties.

Density (75±5°F)	2.21 gm cm^{-3}
Ash (% by wgt.)	0.004%

2-1-2. Mechanical properties.

Tensile, ab (75±5°F)	18,500 lb in^{-2}
Young's modulus, aa (75±5°F)	4.4 x 10^6 lb in^{-2}
Flexural, perpendicular (75±5°F)	21,300 lb in^{-2}

2-1-3. Thermal properties.

Conductivity, ab (1000±25°F)	115 BTU-ft-hr-°F
Conductivity, ab (2000±25°F)	65 BTU-ft-hr-°F
Conductivity, c (1000±25°F)	0.6 BTU-ft-hr-°F
Conductivity, c (2000±25°F)	0.4 BTU-ft-hr-°F
Thermal expansion coefficient, ab (75-1000°F)	0.2 x 10^{-6} in in^{-1} $°F^{-1}$
Thermal expansion coefficient, c (75-1000°F)	12.6 x 10^{-6} in in^{-1} $°F^{-1}$

2-2. Test methods. Accumulated test data are published in the *General Electric Pyrolytic Graphite Engineering Handbook* (hereinafter referred to as the *Handbook)* and constitute the bases for the above given average, typical property values. These values, and those determined for *Certificates of Test,* are obtained by the following methods:

2-2-1. Density. Differential weighing by Method A of ASTM D 792-60 T, using distilled water as the immersion fluid.

2-2-2. Ash. Muffle oxidation in air *(see Handbook).*

2-2-3. Ultimate tensile strength. Modification of standard method adapted for brittle materials *(see Handbook).*

2-2-4. Young's modulus. Modification of standard strain gauge method (*see Handbook).*

2-2-5. Ultimate flexural strength. Conditioned at proposed test temperature and tested by Method A of ASTM D 790-61, using a cross-head speed of 0.01 in min^{-1}.

2-2-6. Thermal conductivity. Standard, published procedures of the Southern Research Institute (Birmingham, Alabama).

2-2-7. Thermal expansion coefficient. Modification of standard method adapted for highly anisotropic materials *(see Handbook).*

2-3. Specific property tests. Charges for material and testing for specific property values, which includes the submission of *Certificates of Test,* are subject to customer-General Electric negotiation. Such negotiation must be accomplished prior to order acceptance by the General Electric Company.

TMC A673

APPENDIX A-2 (Continued)

3. *ACCEPTANCE STANDARDS.*

3-1. Cracks and delaminations.

3-1-1. Visual inspection. General Electric pyrolytic graphite plate material supplied under this specification shall be free from visible cracks and delaminations and shall display the characteristics of good workmanship.

3-1-2. Penetrant inspection. Normally, dye penetrant inspection per Military Specification MIL-I-6866, Type II, is performed. At the specific request of the customer at the time of order placement, either of the following penetrant inspection procedures may be substituted without additional cost:

3-1-2-1. Black light inspection per Navy Specification OD 19488.

3-1-2-2. Fluorescent inspection per Military Specification MIL-I-6866, Type I.

3-2. Nodules. Nodule size and distribution is used in this specification and in the General Electric Company as the basis for grade designation for unalloyed pyrolytic graphite plate. Wherever the term "nodules" is used in this subparagraph, read "individual nodules or clusters of nodules." All measurements are to be made on the last deposited surface and those relating to minimum separations are to be made from the nearest boundaries of adjacent nodules in the cluster.

3-2-1. General Electric grade PG75. The maximum allowable size of nodules shall not exceed 75% of the thickness of the plate material. The average distribution of such maximum sized nodules shall not exceed 2 per square inch and the minimum separation shall not be less than 1/8 inch.

3-2-2. General Electric grade PG50-1. The maximum allowable size of nodules shall not exceed 50% of the thickness of the plate material. The average distribution of such maximum sized nodules shall not exceed 2 per square inch and the minimum separation shall not be less than 1/2 inch.

3-2-3. General Electric grade PG50-2. The maximum allowable size of nodules shall not exceed 50% of the thickness of the plate material. The average distribution of such maximum sized nodules shall not exceed 1 per square inch and the minimum separation shall not be less than 1 inch.

4. *CERTIFICATION*

4-1. Certificate of Conformity. The General Electric Company shall furnish a *Certificate of Conformity,* in quadruplicate, with each shipment of pyrolytic graphite plate material supplied under this specification. This certificate will state that the material supplied was manufactured by standard General Electric production procedures.

4-2. Certificate of Test. Upon specific customer request prior to order acceptance by the General Electric Company and subject to prior customer-General Electric test material and testing charges negotiation, the General Electric Company shall furnish a notarized *Certificate of Test,* in quadruplicate.

5. *PACKAGING.* Packaging shall be accomplished to insure that the material, during shipment and under normal conditions, will not be damaged by normal handling and will be protected against damage from exposure to weather or any other normal hazard.

6. *DEFINITIONS.*

6-1. Lot. A *lot* is defined as the product of a single pyrolytic graphite plate furnace run.

6-2. Crack. A *crack* is defined as any material separation other than a delamination. Surface scratches not exceeding 0.005 inches in depth shall be disregarded.

6-3. Delamination. A *delamination* is defined as a material separation parallel to the plane of deposition, except where limited to a single grain.

6-4. Nodule. A *nodule* is defined as a single grain growth significantly larger in size than the surrounding matrix, appearing on the last deposited surface. A *cluster of nodules* is defined as a group of nodules, touching one another, each of which is significantly larger in size than the surrounding matrix.

Attachments: Specimen *Certificate of Conformity.*
Specimen *Certificate of Test.*

APPENDIX A-3

SUGGESTED VENDOR'S PROCESS QUESTIONNAIRE FOR FREE STANDING PYROLYTIC GRAPHITE COMPONENTS

1. Customer _____
2. Part identification (P.O. No., etc) _____
3. Quantity delivered to this specification _____
4. Date or period of manufacture _____
5. Nominal dimensions _____ OD _____ Length _____ Wall t _____
6. Mandrel material _____
7. Mandrel wall thickness _____
8. Mandrel finish process (Tool, steel wool, file, etc.) _____
9. Mandrel cleaning _____
10. Inspection technique (Surface finish specification, etc.) _____

    _____
11. Extra processes considered critical _____

    _____

Deposition Process

12. Gas, composition _____
13. Gas, purity, dilution, tolerances _____
14. Furnace size _____
15. Furnace space for each part _____
16. Furnace pressure and tolerance _____
17. Furnace temperature and tolerance _____
18. Heat up time _____
19. Gas flow rate, gas velocity _____
20. Cool down schedule _____

TMC A673

APPENDIX A-3 (Continued)

21. Postdeposition soaking at temperature _____

22. Mandrel breakaway technique _____

23. Part cutoff technique _____

24. Procedures affecting microstructure

    a. Deposition rate (etc.)

    b. _____

    c. _____

    d. _____

25. Procedures affecting residual stress

    a. t/r (etc.)

    b. _____

    c. _____

    d. _____

Inspection and Quality Control

26. Nodule distribution specification _____

27. Nodule size criteria _____

28. Microstructure criteria _____

29. Current reject rate _____

    a. Versus time and quantity _____

    b. Versus geometry complexity _____

30. Thickness tolerance capability, circumferentially _____

31. Thickness tolerance capability, axially _____

APPENDIX A-3(Continued)

32. X-ray _____

33. Dye check _____

34. Density _____

35. Properties measured, if required _____

36. Properties controlled, if required _____

TMC A673

APPENDIX B

LATTICE SPACINGS

OF

PYROLYTIC GRAPHITE TUBES

APPENDIX B

Super-Temp Corporation
11008 So. Norwalk Blvd.
Santa Fe Springs, Calif.

LATTICE SPACINGS

OF

PYROLYTIC GRAPHITE TUBES

Work performed for:

MARQUARDT CORPORATION
Van Nuys, Calif.

MSL Report No. 1170
30 July 1964

Edward W. LaRocca
Technical Director
Metallurgical Services Laboratory

TMC A673

APPENDIX B (Continued)

LATTICE SPACINGS OF PYROLYTIC GRAPHITE TUBES

I. INTRODUCTION

The measurement of the c axis of hexagonal (pyrolytic) graphite was obtained for 15 tubes, using copper radiation and a Philips diffractometer. This work was performed for the Marquardt Corporation under purchase order 471044.

APPENDIX B (Continued)

II. EXPERIMENTAL METHOD

The measurement of the "c" axis of hexagonal graphite has been the subject of recent interest, in keeping with the increased number of applications for the material. A specific necessity for the study of this crystallographic parameter lies in the possible application of this dimension as an aid to quality control as well as a manufacturing specification so that more reproducible properties may be obtained.

Considerable care must be exercised in the interpretation of the lattice measurements in order to avoid misleading conclusions and yet derive useful data.

Considerable care must also be exercised in obtaining the values of "c" for a particular graphite sample. Accurate determination of the lattice constants of deposited pyrolytic graphite are difficult to achieve for two reasons. First, the spacings are so dependent on the time-temperature history of the graphite during nucleation and growth processes that a realistic "average" value is meaningless without a complete prior history of the material. Secondly, the structure of this form of graphite is such that very few strong lines are available for powder camera analysis. For example, the (00.2) reflection is the most intense, but the next strongest reflection (00.4) is less than 10% relative to it. The higher angle reflections, desirable from the standpoint of doublet-resolution for precision measurements, are extremely weak and essentially useless for this purpose.

APPENDIX B (Continued)

A previously employed method of determining the value of "c" has been to observe the (00.2) and the (00.4) reflections and calculate an average value based on these two readings. The method employed by the author has shown that a third value can be obtained by removing the nickel filter, usually inserted in the path from sample to counter to eliminate unwanted β wavelength, and actually employing the β radiation to produce a smaller angle reflection of the (00.2) planes. The result of this allows an averaging process derived on 3 readings instead of the previous 2 values, and permits a more accurate value of the spacing to be calculated.

The complete technique involves standardization of a Philips diffractometer using copper radiation, unfiltered. Curren and voltage are maintained constant throughout the sequence of measurements, and a proportional counter is used to detect reflections. Since the samples are generally of such high purity and do not contain appreciable "alloying" constituents, the peaks produced are symmetrical enough to completely warrant curve-fitting by a parabolic formula. The (00.2) reflection occurs at approximately 23.3° (two-theta value) for β radiation, and 25.9° for the α wavelength. The (00.4) reflection occurs at 53.4° approximately. Peaks near these value are recorded to bracket the peak angular value and the fixed count method, measuring time to count 10^5 or 10^6 counts, is utilized. Angular increments of 0.10° or 0.15° on each side of an arbitrarily selected apparent peak are selected; the goniometer locked at that particular value, and times-to-count are recorded.

TMC A673

APPENDIX B (Continued)

From these data, a 3-point parabolic curve-fitting formula is calculated. (The derivation of this method is shown in Transactions ASM, Vol. 51, 1959, p. 548-549)

A "c" value is calculated from each 2-theta measurement so obtained, yielding 3 independent measurements of "c" per sample. These 3 values are then averaged, statistically, to produce a "mean error", based on the 3 observations, and, finally, a "probable error" of the result of the 3 observations is computed. A tabulation of these calculated values is given in Table I. A sample calculation is shown in Appendix A. All values of "c" are in Angstrom units.

APPENDIX B (Continued)

III. ANALYSIS OF RESULTS

Table I is a tabulation of the results of 20 sets of measurements made on 15 separate tubes; tube #25 was examined in two different areas, H9 in 3 places, and 31-76-3 in 3 areas. These repeated measurements were made to establish the reproducibility of the technique and, in general, show excellent agreement except in the case of the sleeve numbered 31-76-3. In this case, 2 out of the 3 determinations are within $3X10^{-4}$ Angstroms, while the 3rd determination varies $4X10^{-3}$ Angstroms from the others.

As indicated earlier, the interpretation of these values must be done with considerable care. The actual value of the "c" spacing is related to:

1) purity of material,
2) percent of graphitization,
3) residual stresses in the material,
and 4) manufacturing technology.

It should be noted that the probable error is higher in those samples which were cracked or slotted. This is almost entirely due to preferential stress relief in various areas in the tube itself.

Another variable causing dispersion of data is that it is difficult to correlate these dimensions between lots of graphite produced by different manufacturers. For example, it appears that the cracked and slotted specimens show a slightly higher value than those "sound" cylinders identified by the 31-76 and 31-78 series. Whether this discrepancy is due to manufacturing variations between suppliers, or residual stresses, or actual graphitization percentages remains to be seen.

APPENDIX B (Continued)

TABLE I

Compilation of values of "c" and probable errors, based on 3 independent angular measurements. All values in Angstrom units.

Sample Identification	Average c	Error	Condition of Sample
#11	6.8708	± .0067	Slotted
#12	6.8673	± .0083	Cracked
#24	6.8656	± .0075	Slotted
#25-1	6.8716	± .0071	Cracked
#25-2	6.8715	± .0068	Cracked
#26	6.8712	± .0057	Slotted
H9-1	6.8709	± .0064	Sound
H9-2	6.8712	± .0066	Sound
H9-3	6.8722	± .0075	Sound
H10	6.8699	± .0066	Sound
H11	6.8721	± .0071	Sound
H12	6.8713	± .0065	Sound
H13	6.8704	± .0072	Sound
#31-76-3-1	6.8639	± .0063	Sound
#31-76-3-2	6.8642	± .0065	Sound
#31-76-3-3	6.8603	± .0044	Sound
#31-76-4	6.8704	± .0077	Sound
#31-76-5	6.8613	± .0044	Sound
#31-76-6	6.8652	± .0062	Sound
#31-78-1	6.8634	± .0067	Sound

APPENDIX B (Continued)

APPENDIX A

Typical calculation for the determination of the probable error of three observations:

Suppose the three observations are 6.7636, 6.7592, and 6.7543. The arithmetical average of these three determinations is 6.7590. The deviation of each value from the average is 4.6, 0.2, and 4.7 ($X10^{-3}$). The mean error of the result of the 3 observations is

$$M = \pm \frac{\sqrt{\Sigma(d^2)}}{n(n-1)}$$ where

d = each deviation,

n = number of observations.

In this case, $M = \pm 0.0039$

The probable error, P, is defined, for 3 observations as:

$$P = \pm 0.675\ M$$

In this case, $P = \pm 0.0027$

TMC A673

APPENDIX B (Continued)

LATTICE SPACINGS OF PYROLYTIC GRAPHITE TUBES

SERIES 2

I. INTRODUCTION

The measurement of the c axis of hexagonal (pyrolytic) graphite was obtained for 7 tubes, using copper radiation and a Philips diffractometer. This work is an extension of the analysis submitted on 30 July 1964 for the Marquardt Corporation, and was performed under purchase order 471346.

Technical details of the procedures have been previously recorded in MSL Report No. 1170 of 30 July 1964 and will not be repeated here.

APPENDIX B (Continued)

II. RESULTS

Table 1 is a tabulation of the results of 10 sets of measurements made on 7 different tubes. Parts marked S1, S2 and 2S were each measured in 2 different areas, opposite each other on one side of the sleeve.

Since each tube was not cracked or slotted, an improvement in consistency of readings was noted, and the average error was lower on this set of tubes than the previous set.

TABLE 1

Compilation of "C_o" Values and Probable Errors

All Values in Angstrom Units

Sample	Average C_o	Error
H-9	6.8653	± .0059
1-S	6.8591	± .0053
3-S	6.8558	± .0054
4-S	6.8590	± .0058
S1-1	6.8654	± .0069
S1-2	6.8656	± .0065
S2-1	6.8646	± .0065
S2-2	6.8663	± .0070
2S-1	6.8671	± .0073
2S-2	6.8618	± .0063

APPENDIX B (Continued)

LATTICE SPACINGS OF PYROLYTIC GRAPHITE TUBES

SERIES 3

I. INTRODUCTION

The measurement of the c axis of hexagonal (pyrolytic) graphite was obtained for 8 tubes, using copper radiation and a Philips diffractometer.

This work is an extension of the analysis submitted on 30 July and 9 October, 1964, for the Marquardt Corporation, and was performed under purchase order 471346.

Technical details of the procedures have been previously recorded in MSL Report No. 1170 of 30 July 1964, and will not be repeated here.

APPENDIX B (Continued)

II. RESULTS

Table I is a tabulation of the results of 10 sets of measurements made on 8 different tubes. Parts marked H-10 and H-12 were each measured twice, at two different temperatures.

An effort was made to adjust the temperature of the room in which the x-ray analysis is conducted, to provide as large a thermal difference as possible. Minimum temperature reached was 71°F, with a maximum of 96°F, giving a differential of 25°F.

Attention is called to the fact that 3 of the 8 samples were not complete cylinders, or sleeves, but were fragments of sleeves. This is important, since the fragments generally show different values because of stress relief.

In the case of sample marked H-10, there is an apparent increase in the c_o spacing of 0.0055 Angstrom units over a 25°F temperature differential, and an increase of 0.0033 Angstroms over a 24°F differential for specimen H-12.

APPENDIX B (Continued)

TABLE I

Compilation of c_o Values and Probable Errors

All Values in Angstrom Units

Sample	Condition	Test Temp.	Average c_o	Error
S-1	Whole	81°F	6.8637	± .0049
S-2	Whole	80°F	6.8636	± .0044
2-S	Fragment	82°F	6.8645	± .0050
4-S	Fragment	90°F	6.8608	± .0038
P-1	Whole	94°F	6.8636	± .0044
T-1	Whole	94°F	6.8639	± .0044
H-10	Fragment	71°F	6.8608	± .0036
H-10	Fragment	96°F	6.8663	± .0038
H-12	Whole	72°F	6.8644	± .0040
H-12	Whole	96°F	6.8677	± .0045